UNCLASSIFIED

AD NUMBER
AD008348
CLASSIFICATION CHANGES
TO: unclassified
FROM: confidential
LIMITATION CHANGES
TO: Approved for public release, distribution unlimited
FROM: Distribution authorized to U.S. Gov't. agencies only; Administrative/Operational Use; MAY 1952. Other requests shall be referred to Office of Naval Research, Ballston Center Tower One, Code ONR 06 Rm 215, 800 North Quincy St., Arlington, VA 22217-5660.
AUTHORITY
dept of the navy ltr, 10 sep 1954; onr via ltr dtd nov 9, 1977

THIS PAGE IS UNCLASSIFIED

THIS REPORT HAS BEEN DELIMITED
AND CLEARED FOR PUBLIC RELEASE
UNDER DOD DIRECTIVE 5200.20 AND
NO RESTRICTIONS ARE IMPOSED UPON
ITS USE AND DISCLOSURE.

DISTRIBUTION STATEMENT A

APPROVED FOR PUBLIC RELEASE;
DISTRIBUTION UNLIMITED.

UNCLASSIFIED

AD 83 48

Armed Services Technical Information Agency

Reproduced by

DOCUMENT SERVICE CENTER

KNOTT BUILDING, DAYTON, 2, OHIO

This document is the property of the United States Government. It is furnished for the duration of the contract and shall be returned when no longer required, or upon recall by ASTIA to the following address: Armed Services Technical Information Agency, Document Service Center, Knott Building, Dayton 2, Ohio.

CLASSIFICATION CHANGED TO UNCLASSIFIED

BY AUTHORITY OF ASTIA RECLASS. C | U | Ltr. fr. Dept. of Navy dtd. 10 Sep 54

Date 12 Dec. 1957 Signed Richard L. Eely

OFFICE SECURITY ADVISOR

Reclassification Bulletin No. 3

UNCLASSIFIED

gency

the du-
ASTIA
ency,

ED

Dept. of
10 Sep 54

SOR

D

AD NO. 22418
ASTIA FILE COPY

EXPERIMENTAL TOWING TANK

[redacted]
SECURITY
Report
May

LIFT AND DRAG OF HYDROFOIL
APPLICATION OF THEORY ON
TO
EXPERIMENTAL RESULTS

by

B.V. Korvin-K
and
Robert J. W

Experimental Towing Tank
Stevens Institute of Technology
Hoboken, New Jersey

Copy N
SECURITY [redacted]

[redacted]
SECURITY INFORMATION

EXPERIMENTAL TOWING TANK
STEVENS INSTITUTE OF TECHNOLOGY
HOBOKEN, NEW JERSEY

LIFT AND DRAG OF HYDROFOILS:

APPLICATION OF THEORY TO EXPERIMENTAL RESULTS

by

B.V. Korvin-Kroukovsky
and
Robert J. Wernick

PREPARED UNDER
CONTRACT Nonr 263-01
U.S. NAVY
OFFICE OF NAVAL RESEARCH
(E.T.T. PROJECT DZ1407)

May 1952

Report N

[redacted]
SECURITY INFORMATION

[redacted]
SECURITY INFORMATION

EXPERIMENTAL TOWING TANK
STEVENS INSTITUTE OF TECHNOLOGY
HOBOKEN, NEW JERSEY

LIFT AND DRAG OF HYDROFOILS:

APPLICATION OF THEORY
TO
EXPERIMENTAL RESULTS

by

B.V. Korvin-Kroukovsky
and
Robert J. Wernick

PREPARED UNDER
CONTRACT Nonr 263-01
U.S. NAVY
OFFICE OF NAVAL RESEARCH
(E.T.T. PROJECT DZ1407)

May 1952 Report No. 438

[redacted]
SECURITY [redacted]

[redacted]
SECURITY INFORMATION

TABLE OF CONTENTS

	Page
Summary	1
Introduction	3
Symbols	5
Hydrofoil Theory	7
Induced Drag	7
Critical Velocity	11
Wave-Making Drag Theories	11
Relation between Lift Coefficient and Angle of Attack	19
Analysis of Experimental Results	21
Description of Models and Sources of Test Data	21
Determination of Profile Drag	21
Model Ia	21
Model Ib	23
Model II	24
Results and Discussion	25
Variation of Profile Drag with Lift Coefficient and Depth	25
Dependence of Profile Drag on Reynolds Number	26
Slope of Lift Coefficient with Angle of Attack	26
Concluding Remarks	28
References	30
Tables I - III	32
Figures 1 - 18	

[redacted] SECURITY INFORMATION

[redacted]

ACKNOWLEDGEMENT

This report has been prepared by the Staff of the Experimental Towing Tank, Stevens Institute of Technology, in connection with Office of Naval Research Contract No. Nonr 263-01.

[redacted]

SUMMARY

A hydrofoil moving at a given angle of attack near the surface of a fluid experiences a resistance which can be broken down into the following components: a wave-making drag caused by bound vortices in proximity to the surface, an induced drag caused by trailing vortices resulting from a finite span, and a profile drag consisting of the frictional and eddy-making drag of the hydrofoil.

It is found in the present report that the induced drag of a hydrofoil of aspect ratio $\geqslant 6$ (the smallest investigated) can be computed with sufficient accuracy by a procedure similar to that used for airfoils in an infinite medium.

The several methods for computing the wave-making drag of a hydrofoil in media of finite or infinite depth are compared and discussed. In shallow water, there is a maximum velocity for the propagation of waves, termed the critical velocity. If the hydrofoil moves at a supercritical velocity, the waves caused by the bound vortices cannot follow, and wave-making drag is nil. However, in the transition range near the critical velocity, the rate at which wave-making drag decreases with velocity from a finite value to zero is not given by existing theories. In the present report, an empirical correction factor depending on the ratio of velocity to critical velocity is applied to the equation for the two-dimensional wave-making drag of a flat plate in a medium of infinite depth in order to approximate the decrease of the wave-making drag in a medium of finite depth. In the actual operation of a hydrofoil in open water, this correction factor becomes negligible.

Wave-making drag and induced drag are subtracted from experimental total drag to give values of profile drag. An examination of the resulting profile drag curves and those obtained directly from N.A.C.A. wind-tunnel tests shows:

(1) very close agreement when the hydrofoil and airfoil sections were tested at the same Reynolds numbers,

(2) similar form and reasonable magnitude when the hydrofoil was tested at lower Reynolds numbers.

Since the wave-making drag and induced drag of a hydrofoil are independent of scale effect, it is possible, given the profile drag at a

suitable Reynolds number, to find the fu. scale total drag at that Reynolds number.

It is also shown that the slope of the lift coefficient with angle of attack is a function of submergence, and increases with depth toward a theoretical infinite-depth value depending on the aspect ratio.

INTRODUCTION

This report is a study of the application of the theories of induced downwash angle and of wave-making resistance to the analysis of experimental lift and drag data on hydrofoils. A deeply-submerged hydrofoil acts as an airfoil in an infinite medium, i.e., the effect of the free surface is negligible. In the case of a foil of infinite span, there is no induced downwash angle and thus no induced drag. Therefore, the only observable resistance is the profile or section drag. However, in the case of a deeply-submerged hydrofoil of finite span, trailing vortices occur, causing a downwash angle and thereby modifying the slope of the curve of lift coefficient vs. angle of attack. The induced downwash angle will produce induced (trailing vortex) drag, so that the total drag is the sum of the profile and induced drag components.

A foil traveling near the surface produces waves which, in turn, provide added increments of velocity to the flow around it, further modifying the lift and drag. Modifications caused by the proximity of the bound vortices to the surface occur whether the span is finite or infinite. There are several methods available for evaluating the wave-making (bound vortex) drag. Vavra (Reference 1) represents the foil as a single vortex filament and considers the relation of the lift to the circulation to be the same as at great depth, i.e., the Kutta-Joukowski equation. Kotchin (Reference 2) also represents the foil as a single vortex filament, but considers the effect of the free surface on the relationship between the lift and the circulation. Keldysch and Lavrentiev (Reference 3), in their study of the free surface effects, represent the foil by a lifting surface, i.e., a surface of discontinuity on which sources and vortices of varying strength are placed. These three methods are compared and discussed herein.

In shallow water, there is a maximum velocity for the propagation of waves, termed the critical velocity. If a hydrofoil moves with a supercritical velocity, the waves caused by the bound vortices cannot follow, and wave-making resistance is nil. However, in the transition range near the critical velocity, the rate of decrease of the wave-making drag from a finite value to zero is not given by existing theories. Therefore, an empirical relationship is developed in this report for the value of wave-making drag in the transition range between subcritical and supercritical velocities.

It should be emphasized that the vanishing of the wave-making resistance at supercritical velocities is essentially a result of laboratory conditions; it would occur in full-scale only in shallow water. The evaluation of the wave-making drag of a full-scale hydrofoil under normal conditions of operation therefore depends on the theory developed for a foil in a medium of great depth. In the present analysis of the shallow-water data obtained in a towing tank, the equations resulting from deep-water theory are modified to take into account the depth of the medium.

In this report, the term "wave-making drag" is applied, in lifting line theory, to the effects of the bound vortex in proximity to the free surface (or, in lifting surface theory, to the effects of the distribution of bound vortices). These effects are determined for the infinite span, i.e., for two-dimensional flow with the formation of transverse waves. The term "induced drag" is applied, following aeronautical usage, to the increment of drag caused by a finite span, i.e., caused by the trailing vortices. The trailing vortices also form waves, but of oblique form.

The above nomenclature differs from that recently used by Vavra in Reference 1. The terminology of "bound vortex drag" and "trailing vortex drag" is used by Vavra and Meyer, and in Reference 1 Vavra groups both of these under the name of "wave-making drag," which is defined as including all resistance in excess of the drag of a foil in an infinite two-dimensional medium, i.e., profile drag. In Vavra's notation, then, the drag of the trailing vortices is divided into two parts:

(a) the induced drag of the finite aspect ratio foil in an infinite medium,

(b) an additional increment due to the effect of the surface included as part of the expression for bound vortex drag.

It was felt by the present authors that this terminology might lead to some confusion, and so the terms "wave-making" and "induced" drag as defined in the preceding paragraph are used in this report.

SYMBOLS

The various terms and coefficients used in this report are as follows:

General Symbols

g = acceleration of gravity, 32.17 ft./sec.^{2}
ν = kinematic viscosity
ρ = mass density

Aerodynamic and Hydrodynamic Symbols

A = aspect ratio
A_e = equivalent aspect ratio
b = span of the hydrofoil, ft.
b_e = equivalent span, ft.
C_{D_i} = induced drag coefficient
C_{D_p} = profile drag coefficient
C_{D_T} = total drag coefficient
C_{D_w} = wave-making drag coefficient
C_L = three-dimensional lift coefficient
C_ℓ = two-dimensional lift coefficient
c = chord length, ft.
$Ei(x)$ = exponential integral, $\int_{-\infty}^{x}(e^u/u)du$
F = Froude number, $V/\sqrt{gc}$, based on the chord as characteristic length
H = tank water depth, ft.
h = hydrofoil depth of submersion, ft.
L = total lift force, lb.
L_1 = lift force per unit span, lb./ft.
M = Munk span factor (see equation (2))
P_1, P_2, Q_1, Q_2 = coefficients (see equations (25)-(28))
Re = Reynolds number, Vc/ν
S = planform area, ft.^{2}
V = horizontal velocity of the foil, ft./sec.
V_c = critical velocity, ft./sec.
w = downwash velocity, ft./sec.
α = angle of attack, radians
α_0 = section angle of attack, i.e., angle of attack of a foil of infinite span, radians
α_{L_0} = angle of attack at zero lift, radians

δ = planform factor (see page 10)
Γ = circulation
ϵ = downwash angle, radians
κ = a form of Froude number, $V^2/2gc$
λ = a form of Froude number, $2gh/V^2$, based on submergence as characteristic length
σ = Munk interference factor (see page 8)

HYDROFOIL THEORY

INDUCED DRAG

There are several developments of expressions for trailing vortex drag. Vladimirov (Reference 4) gives a sketchy treatment based on a single horseshoe vortex, and Vavra and Meyer have treated the problem (Reference 1) in the case of the bound vortex line of varying strength and a complete trailing vortex sheet. This latter treatment gives a double integral which is soluble in closed form for only a few limiting cases (see equations (19)-(22) of the present report). The necessary numerical integration for the more general cases has not yet been completed. There is also a study being made at the E.T.T. in which the effect of the trailing vortices is considered, but the results are not yet available. Consequently, in this section of the report, a simplified expression is used which considers the surface disturbance caused by the trailing vortices to be negligible, which is actually the condition at high speeds. This permits the application of a technique widely used in aerodynamics.

The induced downwash angle of airfoils is determined by integrating the vertical velocities induced by the trailing vortices. In the particular case of an elliptic lift distribution, it may be shown that the downwash velocity is uniform along the span and can be computed by momentum theory, using as the virtual mass the mass of a cylinder of fluid having a diameter equal to the span of the airfoil (Sketch A below).

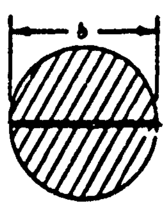

AIRFOIL IN AN
INFINITE MEDIUM

SKETCH A

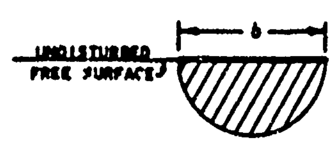

PLANING FOIL

SKETCH B

For a body moving near the water surface, the system can be completed by its reflection from the surface. Thus, for a body planing on the surface of the water, good results are obtained by taking half the cylinder (Sketch B, page 7) as the virtual mass (References 5 and 6).

In the present derivation of the expression for the induced drag coefficient, C_{D_i}, an image span (Sketch C, page 9) is assumed at a distance h (equal to the submergence of the actual foil) above the undisturbed surface. The induced drag is then developed by a procedure similar to that for a biplane in an infinite medium. In biplane theory (Reference 7), the induced drag is found by determining the dimensions of a monoplane equivalent to the biplane (Sketch D, page 9) and then proceeding by monoplane theory.

The equivalent monoplane span, b_e, is given by

$$b_e = Mb \quad . \tag{1}$$

M is the Munk span factor, and is defined as

$$M = \frac{(1 + \xi)\mu}{\sqrt{\mu^2 + 2\mu\xi\sigma + \xi^2}} \quad , \tag{2}$$

where

$\xi = L_a/L_b$, the ratio of the lifts of each span
$\mu = B_a/B_b$, the ratio of the span lengths
σ = the Munk interference factor.

For the hydrofoil, $\mu = \xi = 1$, and the expression for M becomes

$$M = \frac{2}{\sqrt{2(1 + \sigma)}} \quad . \tag{3}$$

The interference factor is determined by numerical integration of the double integral found on page 247 of Reference 7. It is shown plotted against an extended range of h'/b (where h' is the distance between the two spans, equal to $2h$) on Figure 1. For the hydrofoil of rectangular planform, the equivalent aspect ratio, A_e, is given by

$$A_e = \frac{(Mb)^2}{2S} \tag{4}$$

R-438
- 9 -

By using the same method as in Reference 6, the lift is written as

$$L = C_L \frac{\rho}{2} V^2 S = \rho V w J \quad , \qquad (5)$$

where $J = \pi b_e{}^2/8$, the shaded area in Sketch D below.

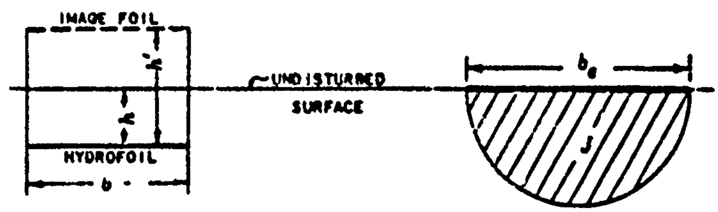

ACTUAL AND IMAGE FOILS

SKETCH C

EQUIVALENT FOIL

SKETCH D

Solving equation (5) for the downwash velocity, w, gives

$$w = \frac{VSC_L}{2J} \quad . \qquad (6)$$

The downwash angle at the lifting line is $\epsilon = w/2V$. Therefore,

$$\epsilon = \frac{SC_L}{4J} \quad . \qquad (7)$$

The induced drag coefficient is given by

$$C_{D_i} = \epsilon C_L = \frac{SC_L{}^2}{4J} \quad . \qquad (8)$$

When the foil has a rectangular planform, $S = bc = c^2 A$. Substituting for S and J in equation (8) gives

$$C_{D_i} = \frac{2C_L{}^2}{\pi M^2 A} \quad . \qquad (9)$$

From equation (4), $A_e = M^2 b^2/2bc = M^2 A/2$ for the rectangular foil. Therefore,

$$C_{D_i} = \frac{C_L{}^2}{\pi A_e} \quad . \qquad (10)$$

In terms of the interference factor,

$$C_{D_i} = \frac{1 + \sigma}{\pi A} C_L^2 \quad . \tag{11}$$

Equation (11) may be obtained in a different way. Equation (28) on page 248 of Reference 7 gives the induced drag of a biplane as the induced drag of each span plus the interference effects of each span on the other, i.e., the induced drag, D_i, is

$$D_i = D_{aa} + 2D_{ab} + D_{bb} = \frac{2}{\pi\rho V^2}\left(\frac{L_a^2}{B_a^2} + 2\sigma\frac{L_a L_b}{B_a B_b} + \frac{L_b^2}{B_b^2}\right) \quad .$$

However, in the case of the hydrofoil, only the induced drag of a single actual span and the interference effect of an assumed image span are considered. Thus,

$$D_i = D_{aa} + D_{ab} = \frac{2}{\pi\rho V^2}\left(\frac{L^2}{b^2} + \sigma\frac{L^2}{b^2}\right) \quad . \tag{12}$$

Therefore,

$$D_i = \frac{2L^2(1 + \sigma)}{\pi\rho V^2 b^2} \quad . \tag{13}$$

Dividing by $(\rho/2)V^2S$ and substituting $C_L(\rho/2)V^2S$ for L give

$$C_{D_i} = \frac{2C_L^2}{\pi M^2 A} = \frac{1 + \sigma}{\pi A} C_L^2 \quad ,$$

which is equation (11).

Equations (10) and (11) hold for the elliptic foil; for the rectangular foil, the induced drag is obtained by multiplying the induced drag coefficient for the elliptic foil by $(1 + \delta)$, where δ is a planform factor. Thus, equations (10) and (11) become

$$C_{D_i} = \frac{(1 + \delta)C_L^2}{\pi A_e} = \frac{(1 + \delta)(1 + \sigma)C_L^2}{\pi A} \quad . \tag{14a}$$

The factors σ and δ are small, so that for low aspect ratios, equation

(14a) may be written as

$$C_{D_i} = \frac{(1 + \sigma + \delta)C_L^2}{\pi A} \qquad (14b)$$

Values of δ over an extended range of A are abstracted from Reference 8 and plotted on Figure 2.

CRITICAL VELOCITY

In Reference 9, Vavra shows analytically that in shallow water, e.g., a towing tank, two entirely different flow regimes exist, one for $V < \sqrt{gH}$, and the other for $V > \sqrt{gH}$, where H is the depth of the water in the tank. $V = \sqrt{gH}$ is termed the critical velocity, which is the maximum velocity of waves in shallow water.

At supercritical velocities, the free transverse waves caused by the bound vortices cannot follow at the speed of the model, and the surface disturbance takes the form of a solitary wave traveling with the model. There is no wave train in the wake, and consequently no energy loss, and no component of wave-making drag. The tests reported in Reference 10 were all made at velocities above the critical, and in the analysis of the data made in the present report (see Figures 11 and 12), the exclusion of a wave-making drag gives results which are closely checked by wind-tunnel tests (Reference 11).

The data of Reference 12 include velocities ranging from subcritical to supercritical, and the problem arises as to how abruptly the wave-making drag ceases to exist at the critical velocity: whether there is a jump discontinuity, or a smooth decrease in the amount of energy transmitted to the wake as V increases toward the critical.

WAVE-MAKING DRAG THEORIES

In Reference 1, Vavra gives the following equation for the two-dimensional wave-making drag, D_w, of a single vortex line in a medium of infinite depth:

$$\frac{D_w}{L} = \frac{gL_1}{\rho V^4} e^{-\lambda} \quad , \qquad (15)$$

where the symbols are those given on page 5. He compares this equation

with the expression obtained by Kotchin in Reference 2,

$$D_v = \frac{\rho g \Gamma^2}{V^2} e^{-\lambda} \quad , \tag{16}$$

and states that with the circulation obtained by the Kutta-Joukowski equation,

$$\Gamma = \frac{L_1}{\rho V} \quad , \tag{17}$$

equations (15) and (16) are identical. However, equation (17) applies only to an infinite medium. Kotchin gives the equation for L_1 in the case of a semi-infinite medium (infinite depth, free surface) as

$$L_1 = \rho V \Gamma - \frac{\rho \Gamma^2}{4\pi h} + \frac{\rho g \Gamma^2}{\pi V^2} e^{-\lambda} Ei(\lambda) \quad , \tag{18a}$$

where $Ei(\lambda) = \int_{-\infty}^{\lambda} (e^u/u)du$. Equation (18a) is thus seen to be the Kutta-Joukowski lift times a factor varying with depth, velocity, and circulation:

$$L_1 = \rho V \Gamma \left[1 - \frac{\Gamma}{4\pi V h} + \frac{g\Gamma}{\pi V^3} e^{-\lambda} Ei(\lambda) \right] \quad . \tag{18b}$$

The actual error involved in using equation (17) in a semi-infinite medium will be a slight one at low values of $V/\sqrt{gh}$, decreasing to zero at $V/\sqrt{gh} \approx 1.57$, and increasing with $V/\sqrt{gh}$ thereafter.

In Reference 13, Vavra gives an expression for the wave-making drag of a vortex line of finite span, b, moving in a fluid of finite depth, with varying circulation around the span (lift variable along the span):

$$D_v = \frac{{L_1}_m{}^2 \lambda^2}{256 \rho V^2} \int_{-\beta}^{\beta} \int_{-\beta}^{\beta} \left\{ \left[1 - \frac{\eta_1{}^2}{\beta^2} \right] \left[1 - \frac{\eta_2{}^2}{\beta^2} \right] \right\}^n \left\{ e^{-\lambda} \left[1 + \frac{i\lambda^2}{4u^2} H_0^{(1)}(iu) \right.\right.$$
$$\left.\left. - \frac{1}{u}\left(\lambda + \frac{v^2}{u^2} \right) H_1^{(1)}(iu) \right] - \frac{v^2}{\pi u^4} \right\} d\eta_1 \, d\eta_2 \quad , \tag{19}^*$$

---

* Again, there is confusion in the nomenclature; in Reference 12, bound vortex drag is called D_v, as in the nomenclature of this report, and in Reference 1, it is termed D_g.

where

$$L_{1_m} = \frac{2L}{h\int_{-\beta}^{\beta}[1-(4\eta^2/b^2)]^n \, d\eta}$$

β = b/h

n = an exponent depending on the distribution of lift along the span (for uniform distribution, $n = 1$; for elliptic distribution, $n = \frac{1}{2}$)

$$u = \frac{\lambda}{2}\sqrt{1 + [(\eta_2 - \eta_1)/4]^2}$$

$$v = \frac{\lambda}{2}\sqrt{1 - [(\eta_2 - \eta_1)/4]^2}$$

$H_0^{(1)}$ and $H_1^{(1)}$ = Hankel functions.

Closed solutions of equation (19) are possible only in three limiting cases:

(a) Very small values of β:

$$\frac{D_g}{L} = \frac{gL_1}{\rho V^4}\left\{\frac{gbe^{-\lambda/2}}{8V^2}\left[iH_0^{(1)}\left(\frac{i\lambda}{2}\right) - \left(1 + \frac{1}{\lambda}\right)H_1^{(1)}\left(\frac{i\lambda}{2}\right)\right] - \frac{4}{\pi\lambda^2}\right\} \tag{20}$$

(b) Very large values of β:

$$\frac{D_g}{L} = \frac{gL_1}{\rho V^4}\, e^{-\lambda}\, \frac{\overline{(L_1^2)}}{(\overline{L_1})^2} \tag{21}$$

where

$\overline{(L_1^2)}$ = mean value of L_1^2 along the span

$(\overline{L_1})^2$ = square of the mean value of L_1 along the span.

The quotient $\overline{(L_1^2)}/(\overline{L_1})^2$ is unity for uniform lift distribution, and 1.08 for elliptic lift distribution.

(c) Very small values of λ:

$$D_g = \frac{2L^2}{\rho V^2 b^2}\left\{\frac{\ln[1 + (b^2/4h^2)]}{8}\right\} \tag{22}$$

If the wave-making drag is obtained from equation (19), the induced drag, D_i, is taken in Reference 1 as that for a foil in an infinite medium, because surface effects are assumed to be accounted for by the following term in equation (19):

$$\int_{\beta}^{\beta} \int_{-\beta}^{\beta} \left\{ \left[1 - \frac{\eta_1^2}{\beta^2} \right] \left[1 - \frac{\eta_2^2}{\beta^2} \right] \right\}^n \frac{v^2}{m s^2} \, d\eta_1 \, d\eta_2 \quad .$$

It will be noted that this term is identical to the interference factor σ given in Reference 7 which is discussed earlier in the present report on page 8.

In Reference 3, Keldysch and Lavrentiev develop general expressions for the lift and wave-making drag of various bodies submerged in a two-dimensional semi-infinite medium. For a hydrofoil, the problem is to find the characteristic function of flow having a given velocity V and a given discontinuity of the tangential and normal velocities along a cambered line representing the foil. By placing on this line sources of intensity $q(s)\,ds$ and vortices of intensity $\gamma(s)\,ds$ which give the same flow pattern as that actually occurring about a thin foil, the desired discontinuity of the normal and tangential velocities is obtained. The boundary conditions due to the free surface are imposed on the sum of the sources and vortices. From the flow pattern thus obtained, expressions for the lift and drag at any angle of attack are formulated. Actually, in Reference 3, the derivation is carried through only for a thin flat plate at an angle of attack α_0, chord c, and submergence h. In the present report, the actual hydrofoil is assumed to be equivalent to the thin flat plate. The zero angle of attack for asymmetric foils is assumed to be the angle of zero lift, α_{L_0}.

The expressions for two-dimensional lift and wave-making drag as developed in Reference 3 are as follows:

$$L_1 = \pi\rho c V^2 \alpha_0 (P_1 - \alpha_0 P_2) \quad . \tag{23}$$

$$D_w = \pi^2 c^2 \alpha_0^2 \rho g (Q_1 - \alpha_0 Q_2) \quad . \tag{24}$$

The dimensionless coefficients P_1, P_2, Q_1, and Q_2 are given as

$$P_1 = 1 - \frac{c^2}{16h^2} + \frac{1}{\kappa}\left[-\frac{\pi e^{-\lambda}}{2} + \frac{\pi^2 e^{-2\lambda}}{4\kappa} - \frac{c}{8h} + \frac{e^{-\lambda} Ei(\lambda)}{8\kappa} \right] \quad , \tag{25}$$

$$P_2 = \frac{c}{2h} - \frac{e^{-\lambda}}{\kappa}\left[Ei(\lambda) + \frac{\pi c}{2h} + \frac{\pi}{8\kappa} - \frac{\pi e^{-\lambda} Ei(\lambda)}{\kappa}\right] \quad , \tag{26}$$

$$Q_1 = e^{-\lambda}\left\{1 - \frac{\pi e^{-\lambda}}{\kappa} - \frac{c^2}{8h^2} + \frac{1}{\kappa}\left[-\frac{c}{4h} - \frac{1}{64\kappa} + \frac{e^{-\lambda}Ei(\lambda)}{4\kappa} + \frac{3\pi^2 e^{-2\lambda}}{4\kappa}\right]\right\}, \tag{27}$$

$$Q_2 = e^{-\lambda}\left\{\frac{c}{2h} - \frac{1}{\kappa}\left[\frac{1}{4} + e^{-\lambda}Ei(\lambda) + \frac{\pi c e^{-\lambda}}{2h} - \frac{\pi e^{-2\lambda}Ei(\lambda)}{\kappa}\right]\right\}, \tag{28}$$

where

$$\lambda = 2gh/V^2$$

$$\kappa = V^2/2gc \quad .$$

P_1, P_2, Q_1, and Q_2 are shown plotted against κ at various submergences on Figures 3, 4, 5, and 6.

There is a certain amount of confusion in the reference material regarding the above expressions. In Reference 3, an additional coefficient of 2 is found in equation (24). It is omitted here since it is not found in Reference 4, which quotes the Keldysch and Lavrentiev results, or in Reference 14, which develops the same expressions independently. On the other hand, Vladimirov, in Reference 4, apparently concentrated his attention on higher speeds and deeper submergences, since he wrote the wave-making drag expression as

$$D_w = \pi^2 a_0^2 \rho g c^2 e^{-2\lambda}\left\{1 - \frac{\pi e^{-\lambda}}{\kappa} + a_0\left[\frac{1}{4\kappa} - \frac{c}{2h} + \frac{e^{-\lambda}Ei(\lambda)}{\kappa}\right]\right\} \quad , \tag{29}$$

omitting the following terms of equations (27) and (28):

$$-\frac{c^2}{8h^2} + \frac{1}{\kappa}\left\{-\frac{c}{4h} - \frac{1}{64\kappa} + \frac{e^{-\lambda}Ei(\lambda)}{4\kappa} + \frac{3\pi^2 e^{-2\lambda}}{4\kappa} + \frac{a_0}{\kappa}\left[-\frac{\pi c e^{-2\lambda}}{2h} + \frac{\pi e^{-2\lambda}Ei(\lambda)}{\kappa}\right]\right\}.$$

The term $1/64\kappa$ is of such negligible magnitude that it may be omitted at all but the very lowest speeds. $Ei(0.3725) = 0$, but $Ei(\lambda)$ rapidly becomes appreciable at values of λ above and below 0.3725. It is easily seen that the other terms will be of sufficient size to be included at moderate speeds and submergences. Therefore, in the present report, the complete expres-

sions, i.e., equations (27) and (28), are used.

In coefficient form, equations (23) and (24) become

$$C_L = 2\pi\alpha_e(P_1 - \alpha_e P_2) \quad , \tag{30}$$

$$C_{D_w} = \frac{\pi^2\alpha_e^{\,2}}{\kappa}(Q_1 - \alpha_e Q_2) \quad . \tag{31}$$

Any comparison of the theoretical results for a finite-span hydrofoil in a finite-depth medium obtained by the formulas of Vavra and those used in the subsequent analysis must necessarily be made on the basis of the sum of the induced and wave-making drag coefficients. The reason for this is that Vavra uses the induced drag of the foil in an infinite medium and corrects for all surface effects in the wave-making drag term, whereas the expressions applied to experimental data in the present report take into account a surface effect in both the induced and wave-making drag terms.

In order to compare the two methods, take the particular case of a hydrofoil under the following conditions: $A = 20$, $c = 2.5$ in., $H = 5.33$ ft., h = one chord, and beam-depth ratio, $\beta = 20$.

Consider first Vavra's method. Since β is large, equation (21) is applicable for determining C_{D_w}. A uniform distribution of lift along the span is assumed. The wave-making drag per unit span is then

$$D_w = \frac{gL_1^{\,2}e^{-\lambda}}{V^4} \quad , \tag{32a}$$

or, in coefficient form,

$$C_{D_w} = \frac{e^{-\lambda}C_L^{\,2}}{4\kappa} \quad . \tag{32b}$$

The induced drag coefficient for a foil in an infinite medium is $(1+\delta)C_L^{\,2}/\pi A$. Therefore,

$$C_{D_w} + C_{D_i} = C_L^{\,2}\left(\frac{e^{-\lambda}}{4\kappa} + \frac{1+\delta}{\pi A}\right) \quad . \tag{33}$$

The second method uses the Keldysch-Lavrentiev formula, equation (31), modified by a factor to take into account the fact that the medium is of

R-438
-17-

finite depth. This factor is discussed further on page 22. The shallow-water wave-making drag coefficient, C_{D_w}', is given by

$$C_{D_w}' = \left[1 - \left(\frac{V}{V_c}\right)\right] C_{D_w} = \left[1 - \left(\frac{V}{V_c}\right)\right] \left[\frac{\pi^2 a_0^2}{\kappa}(Q_1 - a_0 Q_2)\right] . \quad (34)$$

where $V_c = \sqrt{gH}$, the critical velocity. The induced drag is found by equation (14a). The sum of the wave-making and induced drag coefficients in shallow water then becomes

$$C_{D_w}' + C_{D_i} = \left[1 - \left(\frac{V}{V_c}\right)\right] \left[\frac{\pi^2 a_0^2}{\kappa}(Q_1 - a_0 Q_2)\right] + \frac{(1+\sigma)(1+\delta)C_L^2}{\pi A} . \quad (35)$$

The results of equations (33) and (35) are plotted against C_L and Λ on Figure 7. It will be noted that equation (33) consistently gives higher results in this case.

For a semi-infinite medium, i.e., tank depth H very large, it will be seen that in equation (35),

$$\lim_{H\to\infty} \left[1 - \left(\frac{V}{V_c}\right)\right] = 1 \quad .$$

There are three equations for the two-dimensional wave-making drag of the hydrofoil in a semi-infinite fluid: Vavra's (equation (15)), Kotchin's (equation (16)), and that of Keldysch and Lavrentiev (equation 31)) In coefficient form, equation (15) becomes

$$C_{D_w} = \frac{C_L^2}{4\kappa} e^{-\Lambda} \quad . \quad (36)$$

In order to put equation (16) into coefficient form, it is necessary to find an expression for the circulation, Γ. In a design memorandum (Reference 15), Gibbs and Cox, Inc. suggested that the value of Γ around a thin symmetrical foil in an infinite medium be used to approximate the circulation around a hydrofoil. From Reference 7, pages 198-204, this circulation is found to be $\pi a_0 c V$. Substituting $\pi a_0 c V$ for Γ in equation (16) gives

$$C_{D_w} = \frac{\pi^2 a_0^2}{\kappa} e^{-\Lambda} \quad . \quad (37)$$

Replacing Γ by $\pi\alpha_e cV$ in equation (18b) results in

$$L_1 = C_\ell \frac{\rho}{2} V^2 c = \rho V^2 \pi\alpha_e c \left\{1 - \alpha_e \left[\frac{c}{4h} - \frac{gc}{V^2} e^{-\lambda} Ei(\lambda)\right]\right\} ,$$

or

$$\alpha_e = \frac{C_\ell}{2\pi(1 - \alpha_e K)} \qquad (38)$$

where $K = [c/4h] - [(gc/V^2)e^{-\lambda}Ei(\lambda)]$. Substituting equation (38) into (37) gives

$$C_{D_W} = \frac{C_\ell^2 e^{-\lambda}}{4\kappa(1 - \alpha_e K)^2} \qquad (39)$$

In order to put equation (31) into the same form, equation (30) is rearranged:

$$\alpha_e = \frac{C_\ell}{2\pi(P_1 - \alpha_e P_2)} .$$

Substituting for α_e in equation (31) yields

$$C_{D_W} = \frac{C_\ell^2(Q_1 - \alpha_e Q_2)}{4\kappa(P_1 - \alpha_e P_2)^2} \qquad (40)$$

Equations (36), (39), and (40), which are all in the form $(C_\ell^2/4\kappa)R_j$ (where $j = 1,2,3$), are compared in Figure 8, where R_j is plotted against Froude number, $V/\sqrt{gc}$, at various depths.

At the deeper submergences, it is seen that the three equations are in close agreement. However, equations (36) and (39) become less and less accurate as the submergence decreases, since they are based on values of lift derived from the circulation around a single vortex in an infinite medium, and neglect the considerable effect of the proximity to the free surface on the circulation. On page 38 of Reference 14, Kotchin gives an expression for Γ which takes into account the free surface, but it is considered too complicated to evaluate for the purposes of this report. Let it suffice to say, therefore, that equations (36) and (39) give good results at the deeper submergences in a medium of great depth.

Equation (40), which considers a number of sources and vortices distributed along a line of discontinuity, with the free surface as a boundary condition, defines the circulation by the requirement of a finite velocity at the trailing edge. It also has its limitations in proximity to the surface, since at some Froude numbers at shallow submergences, it results in a negative wave-making drag, which is physically impossible. However, at shallower submergences (about 1.5c to 0.75c), the results obtained using equation (40) are more relinble than those obtained using equations (36) and (39).

RELATION BETWEEN LIFT COEFFICIENT AND ANGLE OF ATTACK

If the usual pattern of deriving the lift coefficient slope used in airfoil theory (Reference 7) is followed, the angle of attack of a foil of finite span with respect to the undisturbed surface, α, can be defined as

$$\alpha = \alpha_0 + \epsilon \quad , \tag{41}$$

where

α_0 = the angle of attack exclusive of the induced velocity component, i.e., the angle of attack at infinite aspect ratio, for the same lift coefficient,

ϵ = angle due to the vertical velocity induced at the lifting line as the result of finite span.

Differentiating with respect to the lift coefficient, C_L, gives

$$\frac{d\alpha}{dC_L} = \frac{d\alpha_0}{dC_L} + \frac{d\epsilon}{dC_L} \quad . \tag{42}$$

For a deeply-submerged hydrofoil, $d\alpha_0/dC_L = 1/2\pi$, and, from equation (7),

$$\epsilon = \frac{SC_L}{4J} \quad .$$

As the submergence increases, J approaches $\pi b^2/4$, or,

$$(\epsilon)_{h=\infty} = \frac{SC_L}{\pi b^2} = \frac{C_L}{\pi A} \quad . \tag{43}$$

Consequently,

$$\left(\frac{d\epsilon}{dC_L}\right)_{h=\infty} = \frac{1}{\pi A} \quad ,$$

and

$$\left(\frac{d\alpha}{dC_L}\right)_{h=\infty} = \frac{1}{2\pi} + \frac{1}{\pi A} \quad . \tag{44}$$

Therefore,

$$\left(\frac{dC_L}{d\alpha}\right)_{h=\infty} = 2\pi \frac{A}{A+2} \quad . \tag{45}$$

To obtain the slope of the lift coefficient with angle of attack at infinite aspect ratio, equation (42) is rearranged:

$$\frac{d\alpha_0}{dC_L} = \frac{d\alpha}{dC_L} - \frac{d\epsilon}{dC_L} \quad . \tag{46}$$

The term $d\alpha/dC_L$ may be obtained from experimental data, and from equation (7),

$$\frac{d\epsilon}{dC_L} = \frac{S}{4J} = \frac{1}{\pi A_e} = \frac{1+\sigma}{\pi A} \tag{47}$$

for the elliptic foil. From equation (14a),

$$\frac{d\epsilon}{dC_L} = \frac{1+\delta}{\pi A_e} = \frac{(1+\delta)(1+\sigma)}{\pi A} \tag{48}$$

for the rectangular foil.

ANALYSIS OF EXPERIMENTAL RESULTS

DESCRIPTION OF MODELS AND SOURCES OF TEST DATA

The tests reported in Reference 16 were conducted at the E.T.T. on a wooden model of N.A.C.A. 64_1-A412 section, hereinafter termed Model Ia (chord length = 2½ in.; aspect ratio = 20). The velocity range was from 4.85 to 9.70 ft./sec., and the maximum lift coefficient was 0.62. Reference 10 reports the tests conducted at the N.A.C.A. on a stainless steel model of N.A.C.A. 64_1-A412 section, hereinafter termed Model Ib (chord length = 8 in.; aspect ratio = 10). The velocity range was from 15 to 35 ft./sec., and the maximum lift coefficient was just over 0.50. References 12 and 17 report the results of tests made at the E.T.T. on a symmetrical aluminum model of N.A.C.A. 0012 section, hereinafter termed Model II (chord length = 5 in.; aspect ratio = 6). The velocity range was from 3.5 to 16.0 ft./sec., and the tests were run at two water depths, 5.33 ft. and 3.75 ft., to give a variation of the critical velocity. The maximum lift coefficient was 0.68.

DETERMINATION OF PROFILE DRAG

__MODEL Ia.__ The angle of attack (α)*, lift coefficient (C_L), and total drag coefficient (C_{D_T})** reported for the hydrofoil in Reference 16 are given in columns 4, 5, and 6, respectively, of Table I. The C_{D_T} values of the foil are plotted against C_L^2 in Figure 9, and least squares curves of the form $C_{D_T} = aC_L^2 + b$ are drawn through the points for each Froude number and submergence.

Since the tests of Reference 16 were all made at subcritical velocities, it was originally assumed that the profile drag, C_{D_P}, could be written as

$$C_{D_P} = C_{D_T} - C_{D_i} - C_{D_W} \quad , \tag{49}$$

where

---

* Corrected for ground effect in the present report. All ground effect corrections to angle of attack and total drag are obtained from the equations on page 3 of Reference 16.

** Corrected for strut tare and ground effect in the present report; strut tare corrections are obtained from Figure III-1 of Reference 16.

$$C_{D_i} = \frac{(1+\delta)(1+\sigma)C_L^2}{\pi A} \quad , \quad \text{from equation (14a)}$$

$$C_{D_w} = \frac{\pi^2 \alpha_0^2}{\pi}(Q_1 - \alpha_f Q_2) \quad , \quad \text{from equation (31)} \quad .$$

When the results thus obtained were plotted against C_L^2, it was seen that C_{D_p} decreased with lift. (This was also observed when equation (49) was applied to Model II data at subcritical velocities.) However, in the wind-tunnel tests reported in Reference 11, the profile drag invariably showed an increase with lift for every Reynolds number. It was assumed, therefore, that this should hold true for the range of Reynolds numbers considered in Reference 16. Equation (14a) was derived with the assumption that the surface disturbance is negligible. This assumption is shown to be reasonable from the analysis of the results for Models Ib and II at high (supercritical) Froude numbers, where no wave-making drag exists, since the profile drag is found to increase slightly with lift, as expected. Equation (31) was derived for a two-dimensional foil in a semi-infinite medium, whereas the data analyzed are obtained from tests on a three-dimensional foil in a medium of finite depth. It was assumed, therefore, that although both equations are in error at low Froude numbers, the results of equation (31) contribute by far the greater part of the error. It was decided to apply an empirical correction factor to the wave-making drag term in equation (49) to take into account the fact that there is a critical wave-making velocity. The factor decided upon was $[1 - (V/V_c)]$, where V_c is the critical velocity, $V_c = \sqrt{gH}$. The application of this factor gives a smooth transition to a wave-making drag of zero at $V = V_c$, indicating a steady decrease of the amount of energy transmitted by the bound vortex as the velocity approaches the critical. In the subcritical range, the expression for C_{D_p} then becomes

$$C_{D_p} = C_{D_T} - C_{D_i} - [1 - (V/V_c)]C_{D_w} = C_{D_T} - C_{D_i} - C_{D_w}' \quad . \tag{50}$$

At supercritical velocities $C_{D_w} \equiv 0$.

It should be noted that the use of Vavra's formula, equation (33), will give values of C_{D_p} which decrease with lift, since the $C_{D_i} + C_{D_w}$ results are higher than those obtained by the use of equation (35).

The results of applying equation (50) to the Model Ia data are given in Table I: column 7 lists values of $C_{D_i} + C_{D_w}'$, and column 8 shows C_{D_p} obtained by subtracting column 7 from C_{D_T} (column 6). On Figure 10, C_{D_p} is plotted against C_L^2 and a least squares curve of the form $C_{D_p} = aC_L^2 + b$ is drawn through the points to $C_L^2 = 0$.

Model Ia is an asymmetrical model, and therefore its point of minimum profile drag does not occur at $C_L^2 = 0$, as indicated by the form of the least squares equation adopted. To obtain a parabolic curve with a minimum point at $C_L^2 \neq 0$, the least squares equation should be of the form $C_{D_p} = (aC_L + b)^2$. The point of minimum C_{D_p} found for this foil in Reference 11* is at $C_L^2 = 0.04$. Above this value of C_L, the datum points through which the two curves (i.e., $C_{D_p} = aC_L^2 + b$, and $C_{D_p} = (aC_L + b)^2$) must be drawn can fit either curve closely. But since it is easier to compute the coefficients in the equation $C_{D_p} = aC_L^2 + b$, this is the form used. The least squares curve below $C_L^2 = 0.04$ is shown dotted on Figure 10.

<u>MODEL Ib.</u> Reference 10 gives faired plots of C_L and C_{D_T} vs. velocity at various angles of attack and submergences. Values of C_L and C_{D_T} were taken off these plots at Froude numbers corresponding, insofar as possible, to those reported in Reference 16. The drag and angle of attack were corrected for ground effect, and strut tares** were subtracted from the total drag coefficient. The lift and drag were then cross-faired by plotting them against depth of submersion and angle of attack. C_L and C_{D_T} were then read off at the submergences tested at the E.T.T. on Model Ia. The corrected and cross-faired values of α_0, C_L, and C_{D_T} are given in columns 4, 5, and 6, respectively, of Table II. The C_{D_T} values are plotted against C_L^2 in Figure 11, and least squares curves of the form $C_{D_T} = aC_L^2 + b$ are drawn through the points for each Froude number and depth of submersion.

Since the tests reported in Reference 10 were all run at supercritical velocities, C_{D_p} is found by

$$C_{D_p} = C_{D_T} - C_{D_i} \qquad (51)$$

where C_{D_T} is obtained, as before, from equation (14a).

---

* Reference 11 reports the test conducted on the N.A.C.A. 64_1-412 section, which differs from the N.A.C.A. 64_1-[illegible] section of Reference 16 only by the removal of the trailing edge cusp.

** The strut tare was taken from Figure 7 of Reference 10.

The results of applying equation (51) to the Model Ib data are given in Table II: values of C_{D_i} are listed in column 7 and C_{D_p} in column 8. Figure 12 shows C_{D_p} plotted against C_L^2, with least squares curves of the form $C_{D_p} = aC_L^2 + b$ drawn through the points to $C_L^2 = 0$. This form is adopted for the same reasons given above for Model Ia. The minimum profile drag is also assumed to occur at the same point as for Model Ia, i.e., at $C_L^2 = 0.04$. Below this point, the least squares curve is shown as a dotted line.

<u>MODEL II.</u> Columns 4, 5, and 6 of Table III list the values of α^*, C_L, and $C_{D_T}^{**}$, reported in References 12 and 17. Figure 13 shows C_{D_T} plotted against C_L^2, with least squares curves of the form $C_{D_T} = aC_L^2 + b$ drawn through the points at the various Froude numbers and submergences.

The tests reported in References 12 and 17 range in velocity from the subcritical to the supercritical range, and the profile drag is obtained from equations (50) and (51). The results of the analysis are given in Table III: column 7 shows $C_{D_i} + C_{D_w}'$ (at supercritical velocities, $C_{D_w}' = 0$) and column 8 lists values of C_{D_p} found by subtracting column 7 from column 6 (C_{D_T}). C_{D_p} is plotted against C_L^2 on Figure 14, with least squares curves of the form $C_{D_p} = aC_L^2 + b$ drawn through the points. Model II is a symmetrical foil, and the minimum profile drag point occurs, therefore, at $C_L^2 = 0$.

---

* Corrected for ground effect in the present report.

** Corrected for ground effect and strut tare in the present report. Strut tares were not determined in the tests of References 12 and 17 and are assumed to be 2/3 as great as those given in Figure III-1 of Reference 18.

RESULTS AND DISCUSSION

VARIATION OF PROFILE DRAG WITH LIFT COEFFICIENT AND DEPTH

Figures 10, 12, and 14 show the C_{D_P} results at various velocities for Models Ia, Ib, and II, respectively. These profile drag points are obtained from C_{D_T} data at various submergences. Since profile drag is the drag in an infinite medium, it should show no dependence on the depth of submersion of the hydrofoil. It is seen that, almost invariably, the C_{D_P} points fall close to the least squares lines, with only a normal amount of scatter. The only exceptions are in the case of Model Ia at low speeds (Figure 10), which may be explained by the fact that there is a large spread in the C_{D_T} data. However, on Figure 12, it is seen that there is practically no scatter of the C_{D_P} points, which were obtained from cross-faired C_{D_T} values. This indicates that if all the C_{D_T} values had been cross-faired, the scatter in the C_{D_P} values of Figures 10 and 14 would have been greatly reduced.

With the adoption of the empirical correction to the wave-making drag, it is also seen, on Figures 10 and 14, that there is a small positive slope to the least squares lines drawn through the C_{D_P} points at each Froude number, i.e., the C_{D_P} increases slightly with lift Thus, at lower Re (below the critical velocity), the use of the correction factor gives results which are reasonable when compared with those obtained from wind-tunnel tests at higher Re.

Figure 12 shows the variation of C_{D_P} with lift within the range of Reynolds numbers reported for the wind-tunnel tests of Reference 11. The smooth surface and standard roughness C_{D_P} values of Reference 11 are also plotted on Figure 12. Comparison shows that the C_{D_P} values obtained by applying equation (51) to the C_{D_T} from the towing-tank tests of Reference 10 are slightly higher than the smooth surface C_{D_P} of the wind-tunnel tests and well below the standard roughness C_{D_P}. However, as is mentioned in Reference 10, the surface of the hydrofoil model was slightly pitted during the tests by the salt water in the tank, and therefore was probably somewhat rougher than the smooth airfoil tested in the wind-tunnel.

A very interesting and illuminating result is obtained in the case of the Model II data at V = 12.05 ft./sec. (Figure 14). The C_{D_T} data from which these profile drag points were obtained were taken at two submer-

gences (h = 0.75c and 1.50c) and three tank depths (H = 3.75 ft., 5.33 ft., and 5.83 ft.). Although at H = 5.33 ft. and H = 5.83 ft., the velocity is subcritical and equation (50) applies, and at H = 3.75 ft. the velocity is supercritical and equation (51) applies, it may be seen that the points obtained in each case fall very close to the least squares line drawn through all of them.

DEPENDENCE OF PROFILE DRAG ON REYNOLDS NUMBER

The values of minimum C_{D_p} for the three hydrofoils considered are plotted against Reynolds number on Figure 15. (For Models Ia and Ib, the minimum C_{D_p} occurs at C_L^2 = 0.04; for Model II, the minimum C_{D_p} is at C_L^2 = 0.) The following curves are also plotted for comparison:

(a) Blasius laminar line
(b) Prandtl transition line
(c) Schoenherr mean line
(d) Smooth surface C_{D_p} for N.A.C.A. 64_1-412 and N.A.C.A. 0012 sections
(e) Standard roughness C_{D_p} for N.A.C.A. 64_1-412 and N.A.C.A. 0012 sections.

The slope of the Model Ia minimum C_{D_p} points is greater than that of the Blasius laminar line, but the general shape of the curve indicates that the flow was laminar, with separation causing a high drag.

The section shape of Models Ia and Ib was designed to give laminar flow even at high Reynolds numbers, under favorable conditions. Examination of the Model Ib data on Figure 15 indicates that the flow was probably at least partly laminar at the lower Reynolds numbers. As Re increases, the data fall very close to the transition line.

The line drawn through the Model II points is exactly parallel to the Schoenherr mean line, which indicates that the flow around the foil was turbulent. However, the line is displaced slightly above the Schoenherr line. This may be due to roughness of the model surface, separation of the flow, or a combination of both.

SLOPE OF LIFT COEFFICIENT WITH ANGLE OF ATTACK

The angles of attack (corrected for ground effect) and lift coefficients from the tests of References 10, 12, 16, and 17 are given in

columns 4 and 5, respectively, of Tables I - III.* These are plotted with α as abscissa and C_L as ordinate on Figures 16, 17, and 18 for Models Ia, Ib, and II, respectively, and least squares curves of the form $C_L = m\alpha + n$ are drawn through the points. Also shown on these figures is the theoretical lift coefficient at infinite depth, $(C_L)_{h=\infty}$, which is obtained by integrating equation (45):

$$(C_L)_{h=\infty} = 2\pi\alpha \frac{A}{A+2} + K \quad . \tag{52}$$

where K is a constant determined by α at zero lift, α_{L_0}. For Models Ia and Ib, $\alpha_{L_0} = -0.05$[illegible] radian; for Model II, $\alpha_{L_0} = 0$ radian.

An examination of the curves on Figures 16, 17, and 18 shows that the slopes increase with depth toward the theoretical value obtained from equation (52).

* In some of the runs of Reference 13 (see Table III), it is noted that an error was made in the measurement of angle of attack, α. The error was -0.3[illegible]°, and on Figure 18 the correct α is used.

CONCLUDING REMARKS

It should be possible to apply the expressions given in this report to the prediction of the lift and drag of a full-scale hydrofoil. In the previous sections, theories of induced and wave-making resistance, modified for laboratory conditions, were applied to towing-tank data. The results obtained in regard to profile drag are consistent with wind-tunnel results, and in the cases where direct comparison is possible, they are found to agree very closely with wind-tunnel results. It therefore appears that the initial hypothesis that the total drag of a hydrofoil may be divided into three components (induced, wave-making, and profile drag) is verified, and can be accepted as a physical fact.

Induced drag is a function of aspect ratio, depth-to-span ratio, and lift coefficient; wave-making drag depends on Froude number, depth-to-chord ratio, and lift coefficient (circulation). Therefore, the Froude Law of Comparison holds, i.e., these components of drag are independent of scale effect.

Thus, for a full-scale hydrofoil, equation (14a) on page 10 may be used to predict induced drag.

$$C_{D_i} = \frac{(1 + \delta)(1 + \sigma)C_L^2}{\pi A} \quad ,$$

and equation (31) on page 16 to predict wave-making drag.

$$C_{D_w} = \frac{\pi^2 a_0^2}{\kappa}(Q_1 - a_0 Q_2)$$

See Figures 5 and 6 for values of Q_1 and Q_2.

The profile drag, however, is a function of the foil shape and Reynolds number. A full-size hydrofoil having a chord length of say 10 ft. may operate, for instance, at a designed $Re \approx 5 \times 10^7$, and C_{D_p} may be determined from wind-tunnel tests of the foil at this Reynolds number.

In the special case of a hydrofoil in shallow water (which is the condition under which towing-tank tests are conducted), it must be remembered that the wave-making drag component vanishes at velocities beyond the critical. The procedures followed in analyzing the test data in

the present report may be considered analogous to those used when reducing raw wind-tunnel data to readily applicable form.

-438
29-

REFERENCES

1. Vavra, M.H. *Review of Wave Drag Theories.* The Hydrofoil Corp., Annapolis, Md., Technical Memorandum No. HM-13, April 1951. CONFIDENTIAL

2. Kotchin, N.E.; Kibel, J.A.; and Rose, N.B. *Theoretical Hydromechanics* Chapter VIII, Art. 19, Moscow, 1948. (Translation by B.V. Korvin-Kroukovsky, unpublished.)

3. Keldysch, M.V., and Lavrentiev, M.A. *On the Motion of an Aerofoil Under the Surface of a Heavy Fluid, i.e., a Liquid.* Science Translation Service, Cambridge, Mass., STS-75, November 1949.

4. Vladimirov, A. *Approximate Hydrodynamic Calculation of a Hydrofoil of Finite Span.* ZAHI Report No. 311; English Translation, Admiralty Document PG/53280/NID, May 1946.

5. Wagner, H. *Planing of Watercraft.* N.A.C.A. TM No. 1139, April 1948.

6. Korvin-Kroukovsky, B.V. *Lift of Planing Surfaces.* Journal of the Institute of Aeronautical Sciences, Vol. 17, No. 9, September 1950.

7. Von Mises, R. *Theory of Flight.* First Edition, McGraw-Hill, New York, 1945.

8. *Hydrofoil Research Craft for Office of Naval Research.* Bath Iron Works Corp., by Gibbs and Cox, Inc., Technical Report No 1. CONFIDENTIAL

9. Vavra, M.H. *Wave Drag of Submerged Foils in Shallow Water.* The Hydrofoil Corp., Annapolis, Md., Technical Memorandum No. HM-3, November 1950. CONFIDENTIAL

10. Wadlin, K.L.; Ramsen, J.A.; and McGehee, J.R. *Tank Tests at Subcavitation Speeds of an Aspect-Ratio-10 Hydrofoil with a Single Strut.* N.A.C.A. TM No. L9K14a. CONFIDENTIAL

11. Loftin, L.K., and Smith, H.A. *Aerodynamic Characteristics of 15 N.A.C.A. Sections at Seven Reynolds Numbers from 0.7×10^6 to 9.0×10^6.* N.A.C.A. TN 1945, October 1949.

12. Sutherland, W.H. *Letter Report on Tests of 5" Chord Aspect Ratio 6 Hydrofoil Model.* Experimental Towing Tank Report No. 414, June 1951. CONFIDENTIAL

13. Vavra, M.H. *Wave Drag of Submerged Foils.* The Hydrofoil Corp., Annapolis, Md., Memo No. HM-1, October 4, 1950. CONFIDENTIAL

14. Kotchin, N.E. *On the Wave-Making Resistance and Lift of Bodies Submerged in Water.* Transactions of the Conference on the Theory of Wave Resistance, U.S.S.R., Moscow, 1937; Translation by A.I.(T) Air Ministry, R.T.P. No. 666, March 1938, The Society of Naval Architects and Marine Engineers Technical and Research Bulletin No. 1-8, August 1951.

15. Michel, W.H. *Comparison of Wave Drag Theories.* Gibbs and Cox, Inc., Design Memorandum, March 1, 1951. CONFIDENTIAL

16. Sutherland, W.H. *Letter Report on Extension of Single and Tandem Foil Tests of 2½" Chord Aspect Ratio 20 Hydrofoil.* Experimental Towing Tank Report No. 410, June 1951. CONFIDENTIAL

17. Kaplan, P. *Letter Report on Extension of Single and Tandem Foil Tests of 2½" Chord Aspect Ratio 20 Hydrofoil and 5" Chord Aspect Ratio 6 Hydrofoil.* Experimental Towing Tank Report No. 428, November 1951. CONFIDENTIAL

18. Sutherland, W.H. *Exploratory Model Tests for Engineering Design of a Hydrofoil Vessel.* Experimental Towing Tank Report No. 407, January 1951. CONFIDENTIAL

CONFIDENTIAL

TABLE I

EXPERIMENTAL AND THEORETICAL RESULTS
N.A.C.A. 64_1-A412 (MODEL Ia)

(Experimental Drag Coefficients Are Corrected for Strut Tare and Ground Effect)

(1) F, $V/\sqrt{gc}$	(2) Avg. V, ft./sec.	(3) Re, Vc/ν	(4) α,* deg.	(5) C_L	(6) C_{D_T}	(7) $C_{D_i} + C_{D_W}'$	(8) C_{D_P} = (6) - (7)
CHORD LENGTH = 2½ IN.			TANK WATER DEPTH = 5.96 FT.			DEPTH = 1 CHORD	
1.87	4.85	0.96×10^5	0	.149	.0252	.0020	.0232
			0	.141	.0239	.0020	.0219
			0	.160	.0288	.0026	.0262
			2.01	.289	.0359	.0085	.0274
			2.01	.308	.0302	.0097	.0205
			2.01	.323	.0332	.0106	.0226
			4.01	.451	.0472	.0208	.0264
2.82	7.30	1.44×10^5	0.01	.253	.0208	.0034	.0174
			2.01	.403	.0287	.0087	.0200
			2.01	.406	.0315	.0090	.0225
			2.01	.630	.0296	.0091	.0205
			4.01	.542	.0386	.0160	.0226
3.28	8.50	1.68×10^5	0.01	.244	.0187	.0027	.0160
			0.01	.261	.0189	.0030	.0159
			2.01	.428	.0258	.0082	.0176
			4.01	.558	.0333	.0140	.0193
3.75	9.79	1.92×10^5	0	.231	.0171	.0022	.0149
			0.01	.259	.0170	.0025	.0145
			2.01	.423	.0228	.0072	.0156
			2.01	.436	.0241	.0075	.0166
			4.01	.576	.0307	.0132	.0175
CHORD LENGTH = 2½ IN.			TANK WATER DEPTH = 5.96 FT.			DEPTH = 1.5 CHORDS	
1.87	4.85	0.96×10^5	0	.183	.0257	.0023	.0234
			2.01	.350	.0391	.0093	.0298
			4.01	.514	.0501	.0193	.0308
2.82	7.30	1.44×10^5	0.01	.273	.0230	.0037	.0193
			2.01	.437	.0311	.0096	.0215
			4.01	.578	.0382	.0160	.0216
3.28	8.50	1.68×10^5		.284	.0202	.0035	.0167
				.495	.0261	.0105	.0156
			4.01	.604	.0342	.0156	.0186
3.75	9.70	1.92×10^5	0.01	.288	.0178	.0031	.0147
			2.01	.459	.0237	.0079	.0158
CHORD LENGTH = 2½ IN.			TANK WATER DEPTH = 5.96 FT.			DEPTH = 1.8 CHORDS	
1.87	4.85	0.96×10^5	0	.180	.0285	.0020	.0265
			0	.196	.0261	.0024	.0237
			2.01	.381	.0346	.0092	.0254
			2.01	.396	.0308	.0099	.0209
			4.01	.559	.0405	.0197	.0208
2.82	7.30	1.44×10^5	0.01	.278	.0208	.0036	.0172
			2.01	.460	.0282	.0108	.0182
			4.01	.592	.0369	.0166	.0203
			4.01	.603	.0336	.0172	.0164
			4.01	.606	.0355	.0173	.0182
3.28	8.50	1.68×10^5	0.01	.28	.0192	.0033	.0159
			0.01	.29	.0187	.0034	.0153
			2.01	.472	.0261	.0091	.0170
			4.01	.618	.0329	.0157	.0172
3.75	9.70	1.92×10^5	0.01	.284	.0172	.0028	.0144
			0.01	.292	.0173	.0030	.0143
			2.01	.478	.0231	.0083	.0148

* Corrected for ground effect

CONFIDENTIAL

TABLE II

EXPERIMENTAL AND THEORETICAL RESULTS
N.A.C.A. 64_1-A412 (MODEL Ib)

(Experimental Drag Coefficients Are Corrected for Strut Tare and Ground Effect)

(1) F, $V/\sqrt{gc}$	(2) Avg. V, ft./sec.	(3) Re, Vc/ν	(4) α,* deg.	(5) C_L**	(6) C_{D_T}**	(7) $C_{D_i} + C_{D_W}'$	(8) C_{D_P} = (6) - (7)
CHORD LENGTH = 8 IN.		TANK WATER DEPTH = 6.00 FT.				DEPTH = 1 CHORD	
3.24	15.03	0.95×10^6	0	.226	.0103	.0026	.0077
			0.5	.265	.0115	.0036	.0079
			1.0	.305	.0128	.0048	.0080
			1.5	.344	.0143	.0061	.0082
			2.0	.383	.0160	.0075	.0085
			2.5	.422	.0179	.0091	.0088
			3.0	.462	.0198	.0109	.0089
3.76	17.36	1.10×10^6	0	.226	.0098	.0026	.0072
			0.5	.265	.0110	.0036	.0074
			1.0	.305	.0122	.0048	.0074
			1.5	.344	.0136	.0061	.0075
			2.0	.383	.0152	.0075	.0077
			2.5	.422	.0171	.0091	.0080
			3.0	.462	.0190	.0109	.0081
4.64	21.50	1.36×10^6	0	.226	.0096	.0026	.0070
			0.5	.265	.0106	.0036	.0070
			1.0	.305	.0118	.0048	.0070
			1.5	.344	.0132	.0061	.0071
			2.0	.383	.0147	.0075	.0072
			2.5	.422	.0165	.0091	.0074
			3.0	.462	.0183	.0109	.0074
5.41	25.05	1.58×10^6	0	.226	.0096	.0026	.0070
			0.5	.265	.0105	.0036	.0069
			1.0	.305	.0117	.0048	.0069
			1.5	.344	.0130	.0061	.0069
			2.0	.383	.0145	.0075	.0070
			2.5	.422	.0163	.0091	.0072
			3.0	.462	.0181	.0109	.0072
6.48	30.00	1.90×10^6	0	.226	.0096	.0026	.0070
			0.5	.265	.0105	.0036	.0069
			1.0	.305	.0117	.0048	.0069
			1.5	.344	.0130	.0061	.0069
			2.0	.383	.0145	.0075	.0070
			2.5	.422	.0163	.0091	.0072
			3.0	.462	.0181	.0109	.0072
7.56	35.00	2.21×10^6	0	.226	.0094	.0026	.0070
			0.5	.265	.0105	.0036	.0069
			1.0	.305	.0117	.0048	.0069
			1.5	.344	.0130	.0061	.0069
			2.0	.383	.0145	.0075	.0070
			2.5	.422	.0163	.0091	.0072
			3.0	.462	.0181	.0109	.0072
CHORD LENGTH = 8 IN		TANK WATER DEPTH = 6.00 FT.				DEPTH = 1.5 CHORDS	
3.24	15.03	0.95×10^6	0	.234	.0107	.0026	.0081
			0.5	.276	.0118	.0036	.0082
			1.0	.318	.0131	.0048	.0083
			1.5	.359	.0146	.0061	.0085
			2.0	.401	.0164	.0076	.0088
			2.5	.443	.0182	.0093	.0089
			3.0	.485	.0202	.0111	.0091

* Corrected for ground effect

** Taken from cross-faired plots

CONFIDENTIAL

TABLE II (Cont'd.)

(1) F, $V/\sqrt{gc}$	(2) Avg. V, ft./sec.	(3) Re, Vc/ν	(4) α, ° deg.	(5) C_L **	(6) C_{D_T} **	(7) $C_{D_i} + C_{f_p}'$	(8) C_{D_p} = (6) - (7)
CHORD LENGTH = 8 IN.		TANK WATER DEPTH = 5.00 FT.				DEPTH = 1.5 CHORDS	
3.74	17.34	1.10×10^6	0	.234	.0100	.0023	.0077
			0.5	.276	.0111	.0034	.0077
			1.0	.318	.0135	.0054	.0077
			1.5	.359	.0140	.0061	.0079
			2.0	.401	.0137	.0076	.0061
			2.5	.443	.0175	.0098	.0068
			3.0	.485	.0196	.0111	.0085
4.64	21.50	1.36×10^6	0	.234	.0100	.0026	.0074
			0.5	.276	.0110	.0036	.0074
			1.0	.318	.0121	.0048	.0073
			1.5	.359	.0135	.0061	.0074
			2.0	.401	.0152	.0076	.0076
			2.5	.443	.0178	.0098	.0077
			3.0	.485	.0190	.0111	.0079
5.41	25.05	1.58×10^6	0	.234	.0099	.0026	.0073
			0.5	.276	.0108	.0036	.0072
			1.0	.318	.0120	.0048	.0072
			1.5	.359	.0134	.0061	.0073
			2.0	.401	.0150	.0076	.0074
			2.5	.443	.0170	.0098	.0077
			3.0	.485	.0188	.0111	.0077
6.48	30.00	1.90×10^6	0	.234	.0099	.0026	.0073
			0.5	.276	.0108	.0036	.0072
			1.0	.318	.0120	.0048	.0072
			1.5	.259	.0134	.0061	.0073
			2.0	.401	.0150	.0076	.0074
			2.5	.443	.0179	.0098	.0077
			3.0	.485	.0188	.0111	.0077
7.56	35.00	2.21×10^6	0	.234	.0099	.0026	.0072
			0.5	.276	.0108	.0036	.0072
			1.0	.318	.0120	.0048	.0072
			1.5	.359	.0134	.0061	.0073
			2.0	.401	.0158	.0074	.0074
			2.5	.443	.0170 *	.0098	.0067
			3.0	.485	.0188	.0111	.0077
CHORD LENGTH = 8 IN.		TANK WATER DEPTH = 6.00 FT.				DEPTH = 1.8 CHORDS	
3.24	15.00	0.88×10^6	0	.236	.0100	.0026	.0083
			0.5	.270	.0119	.0036	.0084
			1.0	.320	.0132	.0047	.0085
			1.5	.363	.0140	.0060	.0080
			2.0	.405	.0165	.0075	.0090
			2.5	.447	.0183	.0091	.0092
			3.0	.489	.0208	.0100	.0096
3.74	17.30	1.10×10^6	0	.236	.0104	.0026	.0079
			0.5	.278	.0114	.0036	.0079
			1.0	.320	.0126	.0047	.0079
			1.5	.363	.0140	.0060	[illegible]
			2.0	.405	.0156	.0073	[illegible]
			2.5	.447	.0176	.0091	[illegible]
			3.0	.489	.0197	.0100	[illegible]
4.64	21.50	1.36×10^6	0	.236	.0101	.0025	.0076
			0.5	.278	.0110	.0036	.0074
			1.0	.320	.0122	.0047	.0075
			1.5	.363	.0137	.0060	.0077
			2.0	.405	.0153	.0075	.0078
			2.5	.447	.0171	.0091	.0080
			3.0	.490	.0191	.0100	.0085

* Corrected for ground effect

** Taken from cross-faired plots

CONFIDENTIAL

R-438
-35-

TABLE II (Cont'd.)

(1) F. $V/\sqrt{gc}$	(2) Avg. V, ft./sec.	(3) Re, Vc/ν	(4) α,° deg.	(5) C_L**	(6) C_{D_T}**	(7) $C_{D_i}+C_{D_W}$	(8) C_{D_P} = (6) - (7)
CHORD LENGTH = 8 IN.		TANK WATER DEPTH = 6.00 FT.				DEPTH = 1.8 CHORDS	
5.41	25.05	1.58×10^6	0	.236	.0100	.0025	.0075
			0.5	.278	.0109	.0035	.0074
			1.0	.320	.0121	.0047	.0074
			1.5	.363	.0135	.0060	.0075
			2.0	.405	.0151	.0075	.0076
			2.5	.447	.0169	.0091	.0078
			3.0	.489	.0189	.0109	.0080
6.48	30.00	1.90×10^6	0	.236	.0100	.0025	.0075
			0.5	.278	.0109	.0035	.0074
			1.0	.320	.0121	.0047	.0074
			1.5	.363	.0135	.0060	.0075
			2.0	.405	.0151	.0075	.0076
			2.5	.447	.0169	.0091	.0078
			3.0	.489	.0189	.0109	.0080
7.56	35.00	2.21×10^6	0	.236	.0100	.0025	.0075
			0.5	.278	.0109	.0035	.0074
			1.0	.320	.0121	.0047	.0074
			1.5	.363	.0135	.0060	.0075
			2.0	.405	.0151	.0075	.0076
			2.5	.447	.0169	.0091	.0078
			3.0	.489	.0189	.0109	.0080

* Corrected for ground effect

** Taken from cross-faired plots

TABLE III

EXPERIMENTAL AND THEORETICAL RESULTS
N.A.C.A. 0012 (MODEL II)

(Experimental Drag Coefficients Are Corrected for Strut Tare and Ground Effect)

(1) F, $V/\sqrt{gc}$	(2) Avg. V, ft./sec.	(3) Re, Vc/ν	(4) α,** deg.	(5) C_L	(6) C_{D_T}	(7) $C_{D_i} + C_{D_g}'$	(8) C_{D_F} = (6) - (7)
CHORD LENGTH = 5 IN.			TANK DEPTH = 5.33 FT.			DEPTH = 0.25 CHORD	
1.42	5.30	2.06×10^5	-0.01*	-.135	.0131		
			-0.01	-.062	.0152		
			+4.00*	+.086	.0100		
			4.01	.084	.0141		
			8.02*	.216	.0260		
1.69	6.90	2.73×10^5	-0.01	-.065	.0147		
			+4.01*	+.097	.0119		
			4.01	.121	.0165		
			8.03*	.274	.0262		
			8.03*	.290	.0283		
			8.03	.297	.0272		
2.38	8.46	3.42×10^5	-0.01*	-.069	.0115		
			0	-.048	.0114		
			0	-.046	.0114		
			+4.01*	+.139	.0120		
			4.01*	.116	.0112		
			4.01*	.117	.0112		
			8.98*	.307	.0306		
			8.03*	.311	.0345		
2.88	10.30	4.07×10^5	0*	-.064	.0122		
			4.01*	+.149	.0126		
			4.01	.152	.0131		
			8.03	.319	.0236		
			8.03	.319	.0254		
			8.03*	.322	.0243		
			8.03	.371	.0284		
3.29	12.06	4.76×10^5	-0.01'	-.054	.0122		
			-0.01*	-.065	.0112		
			0	-.063	.0109		
			0	-.048	.0109		
			+4.02*	+.165	.0117		
			8.04	.414	.0279		
3.76	13.75	5.42×10^5	-0.01*	-.064	.0109	.0003	.0106
			0*	-.064	.0113	.0003	.0110
			+4.03*	+.176	.0124	.0029	.0095
			8.04	.423	.0260	.0149	.0111
4.24	15.50	6.12×10^5	0*	-.049	.0102	.0002	.0100
			0*	-.049	.0113	.0002	.0111
			0	-.041	.0115	.0003	.0112
			4.02*	+.183	.0133	.0031	.0102
			4.72	.106	.0144	.0033	.0113
CHORD LENGTH = 5 IN.			TANK DEPTH = 5.33 FT.			DEPTH = 0.75 CHORD	
1.42	5.29	2.06×10^5	-0.01#	-.065#	-.0139#		
			-0.01*	-.053	.0120		
			0	-.026	.0109		
			+2.00*	+.056	.0130		
			2.01	.070	.0121		
			4.00*	.187	.0172		
			4.02#	.168#	.0196#		
			4.02#	.196#	.0149#		
			6.03*	.297	.0400		
			6.04	.346	.0353		
			8.04*	.410	.0420		
			8.04#	.416#	.0464#		
			8.04#	.424#	.0486#		

* Measured α in error
** Corrected for ground effect
\# Depth of water in tank = 3.75 ft.

TABLE III (Cont'd.)

(1) F, $V/\sqrt{gc}$	(2) Avg. V, ft./sec.	(3) Re, Vc/ν	(4) α,** deg.	(5) C_L	(6) C_{D_T}	(7) $C_{D_i} + C_{D_W}'$	(8) C_{D_P} = (6) - (7)
CHORD LENGTH = 5 IN.			TANK DEPTH = 5.33 FT.			DEPTH = 0.75 CHORD	
1.89	6.90	2.73×10^5	-2.01*	-.135	.0131	.0025	.0106
			0*	-.026	.0112	.0002	.0110
			0#	-.018#	.0142#	0#	.0142#
			+2.01*	+.061	.0149	.0003	.0146
			4.02*	.210	.0142	.0063	.0079
			4.06#	.210#	.0184#	.0063#	.0121#
			6.08*	.311	.0266	.0157	.0109
			8.05*	.446	.0387	.0283	.0106
			8.12#	.459#	.0470#	.0299#	.0171#
2.30	8.48	3.42×10^5	-2.01*	-.128	.0118	.0015	.0106
			0*	-.010	.0108	.0001	.0107
			0#	-.008#	.0133#	0#	.0133#
			+2.01*	+.061	.0131	.0003	.0128
			4.02*	.232	.0162	.0055	.0107
			4.02*	.233	.0161	.0055	.0107
			4.06#	.233#	.0171#	.0055#	.0116#
			6.03*	.350	.0218	.0106	.0112
			6.08*	.324	.0232	.0106	.0126
			6.04	.377	.0276	.0147	.0129
			6.04	.379	.0265	.0148	.0117
			8.12#	.456#	.0372#	.0218#	.0154#
			8.04*	.461	.0350	.0222	.0126
			8.03*	.460	.0345	.0219	.0126
2.80	10.30	4.07×10^5	-2.01**	-.133	.0117	.0012	.0105
			0*	-.009	.0101	.0001	.0100
			0	+.004	.0132	0	.0132
			0	.004	.0123	0	.0123
			0#	.008#	.0135#	0#	.0135#
			+2.01*	.077	.0117	.0003	.0114
			2.01	.136	.0121	.0012	.0109
			4.02*	.221	.0162	.0043	.0119
			4.02*	.249	.0182	.0064	.0118
			4.07#	.257#	.0208#	.0061#	.0148#
			6.03*	.334	.0206	.0093	.0113
			6.11*	.320	.0215	[illegible]	[illegible]
			6.04	.358	.0249	.0114	.0135
			6.04	.373	.0276	.0134	.0142
			6.04	.367	.0247	.0134	.0113
			6.04	.398	.0271	.0137	.0134
			8.06*	.464	.0332	.0196	.0129
			8.05*	.446	.0341	.0195	.0146
			8.06	.479	.0364	.0206	.0158
			8.06*	.482	.0354	.0208	.0146
			8.06*	.483	.0344	.0209	.0135
			8.05*	.487	.0364	.0212	.0152
			8.06	.487	.0374	.0212	.0162
			8.13#	.500#	.0366#	.0235#	.0131#
2.98	10.90	4.30×10^5	0#	.006#	.0125#	0#	.0125#
			4.07#	.254#	.0197#	.0046#	.0151#
			8.13#	.500#	.0437#	.0324#	.0113#
3.29	12.05	4.76×10^5	-2.02*	-.150	.0121	.0019	.0102
			-2.01*	-.144	.0137	.0017	.0120
			0*	-.019	.0097	.0006	.0091
			0	+.006	.0131	0	.0131
			0	.006	.0129	0	.0129
			0#	.010#	.0133#	0#	.0133#
			+2.01*	.079	.0101	.0006	.0095
			4.03*	.271	.0102	.0060	.0042
			4.07#	.273#	.0199#	.0069#	.0130#
			6.04*	.349	.0217	.0100	.0117
			6.04	.407	.0250	.0136	.0114
			8.06*	.494	.0324	.0188	.0136
			8.06*	.511	.0354	.0214	.0140
			8.06	.531	.0355	.0222	.0133
			8.06*	.533	.0355	.0224	.0131
			8.14#	.510#	.0421#	.0232#	.0189#

* Measured α in error
** Corrected for ground effect
\# Depth of water in tank = 3.75 ft.

TABLE III (Cont'd.)

(1) F, $V/\sqrt{gc}$	(2) Avg. V, ft./sec.	(3) Re, Vc/ν	(4) α, **	(5) C_L	(6) C_{D_T}	(7) $C_{D_i} + C_{D_o}$'	(8) C_{DP} = (6) - (7)
CHORD LENGTH = 5 IN.			TANK DEPTH = 3.33 FT.			DEPTH = 0.75 CHORD	
3.76	12.75	5.43 x 10^5	-2.01°	-.144	.0115	.0016	.0099
			0°	-.041	.0102	.0001	.0101
			0#	+.012#	.0140#	0	.0140#
			+2.01°	.081	.0102	.0005	.0097
			4.03°	.279	.0172	.0062	.0110
			4.07#	.264#	.0181#	.0042#	.0139#
			4.03°	.266	.0162	.0064	.0098
			6.06	.408	.0238	.0132	.0106
			6.06	.437	.0248	.0144	.0104
			6.04	.420	.0241	.0140	.0104
			8.14#	.549#	.0370#	.0239#	.0131#
4.24	15.50	6.12 x 10^5	-2.01°	-.144	.0126	.0016	.0110
			0°	-.004	.0104	.0001	.0103
			0°	-.031	.0099	.0001	.0098
			0	+.005	.0145	0	.0145
			0	.005	.0141	0	.0141
			+2.01°	.008	.0091	.0005	.0086
			2.01°	.022	.0092	.0005	.0087
			2.04	.142	.0132	.0016	.0116
			4.05°	.290	.0152	.0067	.0085
CHORD LENGTH = 5 IN.			TANK DEPTH = 3.75 FT.			DEPTH = 0.75 CHORD	
3.39	12.05	4.76 x 10^5	0	-.078	.0095	0	.0095
			0	-.006	.0099	0	.0099
			0	-.006	.0096	0	.0095
			0	-.005	.0098	0	.0098
			0	+.002	.0094	0	.0094
			2.08	.117	.0124	.0011	.0113
			4.06	.230	.0159	.0042	.0117
			6.09	.332	.0216	.0098	.0118
			8.12	.444	.0307	.0171	.0136
			8.12	.478	.0312	.0176	.0136
3.63	13.20	5.21 x 10^5	0	-.007	.0121	0	.0121
			0	-.007	.0122	0	.0122
			0	-.006	.0119	0	.0119
			2.03	+.123	.0125	.0012	.0113
			4.06	.242	.0161	.0046	.0115
			4.06	.243	.0161	.0046	.0115
			4.06	.243	.0161	.0047	.0114
			6.09	.367	.0228	.0106	.0122
			8.13	.480	.0329	.0189	.0140
3.88	14.10	~5.57 x 10^5	0	-.008	.0121	0	.0121
			2.03	+.127	.0128	.0013	.0115
			4.06	.236	.0159	.0044	.0115
			4.07	.236	.0167	.0053	.0114
			6.09	.344	.0227	.0106	.0121
			6.10	.369	.0227	.0108	.0119
			8.13	.479	.0326	.0189	.0137
			8.13	.496	.0328	.0196	.0132
4.37	16.00	6.33 x 10^5	0	.001	.0110	0	.0110
			2.06	.130	.0123	.0013	.0110
			4.07	.250	.0168	.0053	.0115
			4.07	.246	.0170	.0053	.0117
			6.11	.392	.0247	.0121	.0126
			6.10	.393	.0247	.0121	.0126
CHORD LENGTH = 5 IN.			TANK DEPTH = 5.33 FT.			DEPTH = 1.50 CHORDS	
1.60	5.30	2.05 x 10^5	0	-.005	.0100		
			4.06	+.314	.0244		
			8.07	.570	.0612		
			8.07	.590	.0606		

* Measured α in error
** Corrected for ground effect
\# Depth of water in tank = 3.75 ft.

TABLE III (Cont'd.)

(1) F, $V/\sqrt{gc}$	(2) Avg. V, ft./sec.	(3) Re, Vc/ν	(4) α,*	(5) C_L	(6) C_{D_T}	(7) $C_{D_i} + C_{D_g}$	(8) C_{D_p} = (6) - (7)
CHORD LENGTH = 5 IN.			TANK DEPTH = 5.33 FT.			DEPTH = 1.50 CHORDS	
1.89	6.90	2.73×10^5	0	-.002	.0162	0	.0162
			4.03	+.277	.0228	.0074	.0154
			8.07	.577	.0459	.0335	.0124
			8.07	.580	.0467	.0338	.0129
2.36	8.65	3.42×10^5	0	.001	.0142	0	.0142
			4.03	.272	.0195	.0065	.0130
			8.07	593	.0430	.0309	.0121
2.82	10.30	4.07×10^5	0	.003	.0139	0	.0139
			0	.006	.0125	0	.0125
			4.03	.272	.0183	.0059	.0124
			8.08	.600	.0408	.0282	.0126
3.29	12.05	4.76×10^5	0	.004	.0119	0	.0119
			4.04	.296	.0194	.0062	.0132
			4.04	.299	.0208	.0063	.0145
			8.08	.621	.0410	.0275	.0135
			8.08	.623	.0411	.0277	.0134
3.76	13.75	5.43×10^5	0	.004	.0110	0	.0110
			0	.004	.0116	0	.0116
			4.04	.309	.0204	.0065	.0139
			4.04	.309	.0207	.0065	.0142
4.24	15.50	6.12×10^5	0	-.002	.0125	0	.0125
			0	-.001	.0120	0	.0120
			4.04	+.303	.0219	.0063	.0156
			4.04	.310	.0196	.0066	.0130
CHORD LENGTH = 5 IN.			TANK DEPTH = 5.83 FT.			DEPTH = 1.50 CHORDS	
1.43	5.20	2.06×10^5	0	-.015	.0150	0	.0150
			4.03	+.276	.0227	.0077	.0150
			6.06	438	.0346	.0196	.0150
			6.06	.439	.0358	.0198	.0159
			8.06	561	.0497	.0300	.0197
1.90	6.96	2.75×10^5	0	-.009	.0120	0	.0120
			0	-.006	.0140	0	.0140
			0	-.005	.0129	0	.0129
			2.01	+ 136	.0156	.0019	.0137
			4.02	.259	.0190	.0067	.0123
			4.02	.259	.0194	.0067	.0127
			6.04	.422	.0304	.0179	.0125
			6.04	.426	.0314	.0181	.0133
			6.04	.424	.0323	.0181	.0142
			6.04	.426	.0308	.0182	.0126
			8.06	.550	.0457	.0304	.0153
2.36	8.65	3.42×10^5	0	-.001	.0117	0	.0117
			0	0	.0124	0	.0124
			2.01	+.133	.0136	.0015	.0121
			4.02	.258	.0176	.0059	.0117
			6.04	.392	.0271	.0137	.0134
			8.06	.522	.0396	.0252	.0144
			8.06	.559	.0413	.0278	.0135
			8.06	.559	.0413	.0278	.0135
			8.06	.570	.0410	.0290	.0120
2.82	10.35	4.09×10^5	0	.006	.0110	0	.0110
			0	.016	.0113	0	.0113
			2.01	.138	.0125	.0014	.0111
			4.02	.269	.0179	.0056	.0123
			6.04	.399	.0270	.0126	.0144
			8.06	.551	.0391	.0240	.0151

* Corrected for ground effect

TABLE III (Cont'd.)

(1) F, $V/\sqrt{gc}$	(2) Avg. V, ft./sec.	(3) Re, Vc/ν	(4) α, ° deg.	(5) C_L	(6) C_{D_T}	(7) $C_{D_i} + C_{D_s}'$	(8) C_{D_p} = (6) -
CHORD LENGTH = 5 IN.			TANK DEPTH = 3.83 FT.			DEPTH = 1.50 CHORDS	
3.29	12.06	4.76×10^5	0	.005	.0111	0	.0111
			0	.005	.0115	0	.0115
			2.01	.145	.0131	.0014	.0117
			4.03	.286	.0176	.0067	.0119
			6.06	.432	.0268	.0128	.0140
			8.06	.565	.0407	.0232	.0155
			8.06	.566	.0479	.0234	.0[illegible]45

* Corrected for ground effect

FIGURE 1
MUNK INTERFERENCE FACTOR, σ

$$\sigma = \frac{b^2}{2\pi (h')^2} \int_{-1}^{1}\int_{-1}^{1} \sqrt{(1-\eta_1^2)(1-\eta_2^2)} \left\{ \frac{1-(b/2h')^2(\eta_2-\eta_1)^2}{\left[1+(b/2h')^2(\eta_2-\eta_1)^2\right]^2} \right\} d\eta_1 d\eta_2$$

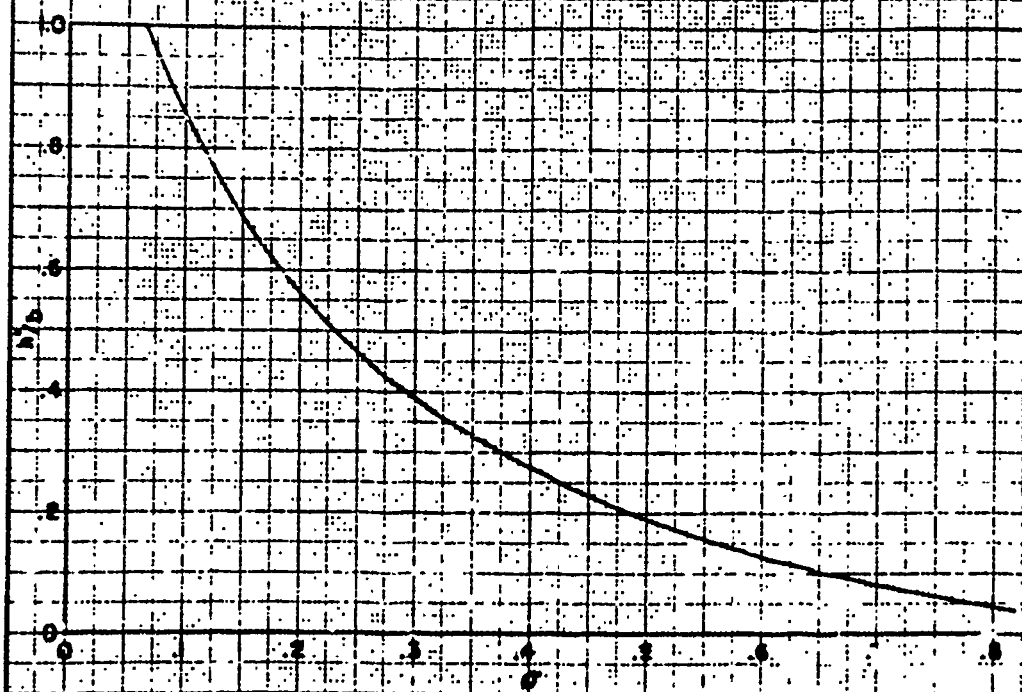

FIGURE 2
PLAN FORM FACTOR, δ
CORRECTION FOR INDUCED DRAG OF RECTANGULAR FOILS

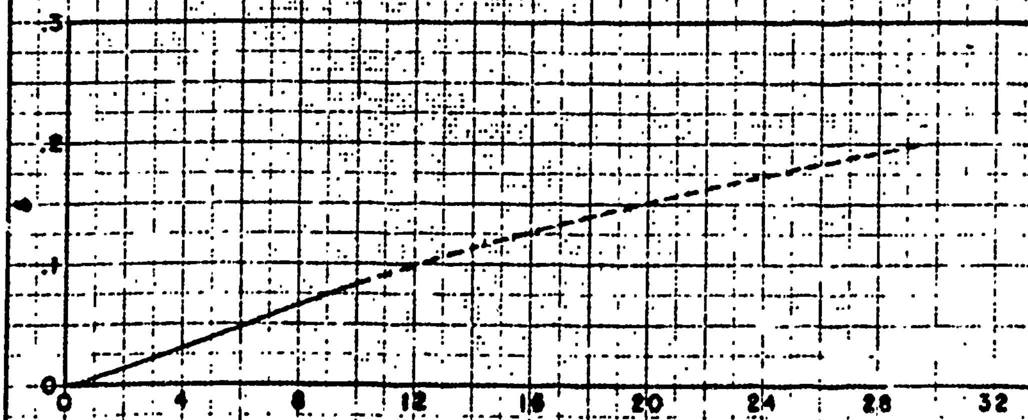

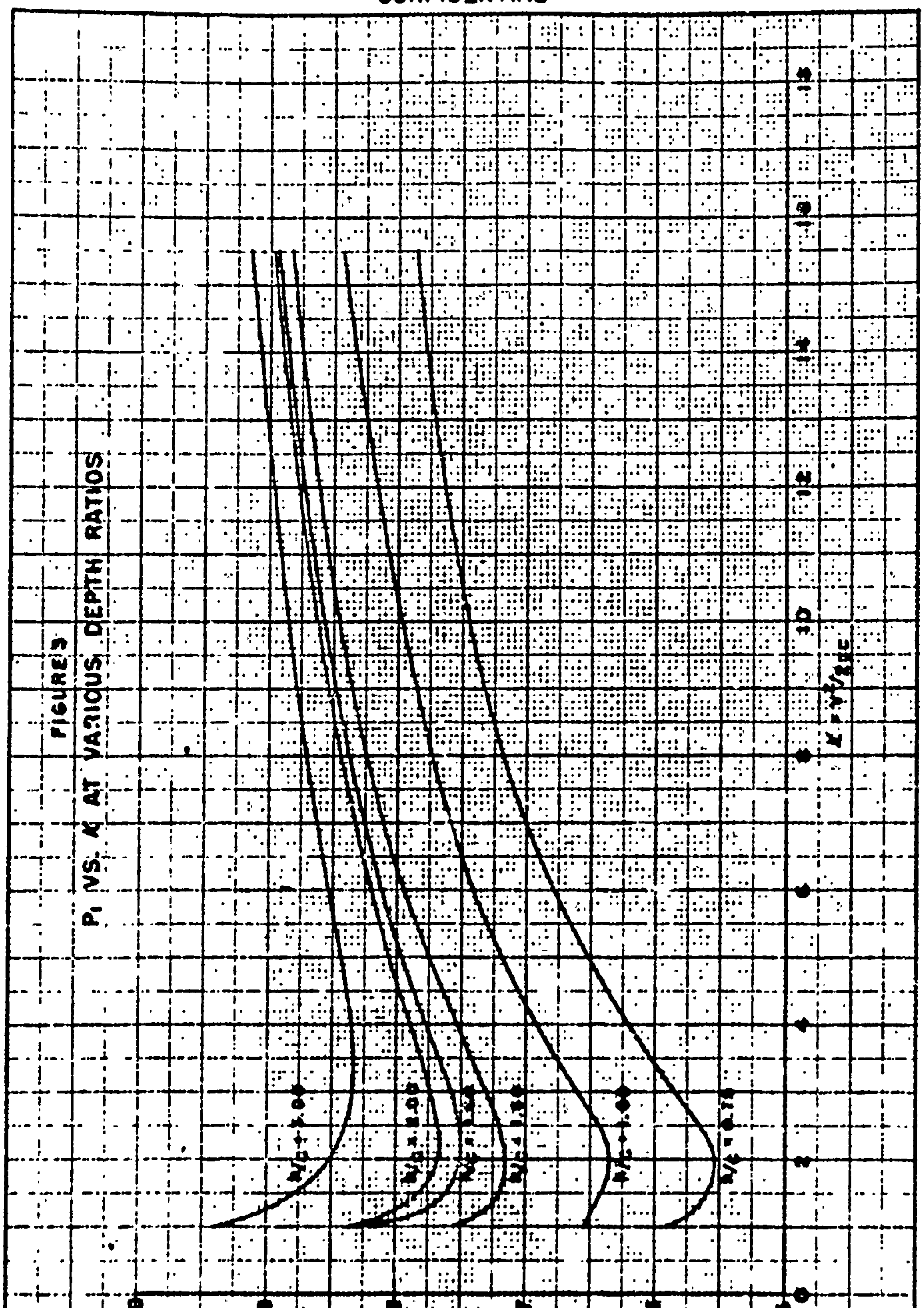

FIGURE 5

P_1 VS. K AT VARIOUS DEPTH RATIOS

CONFIDENTIAL

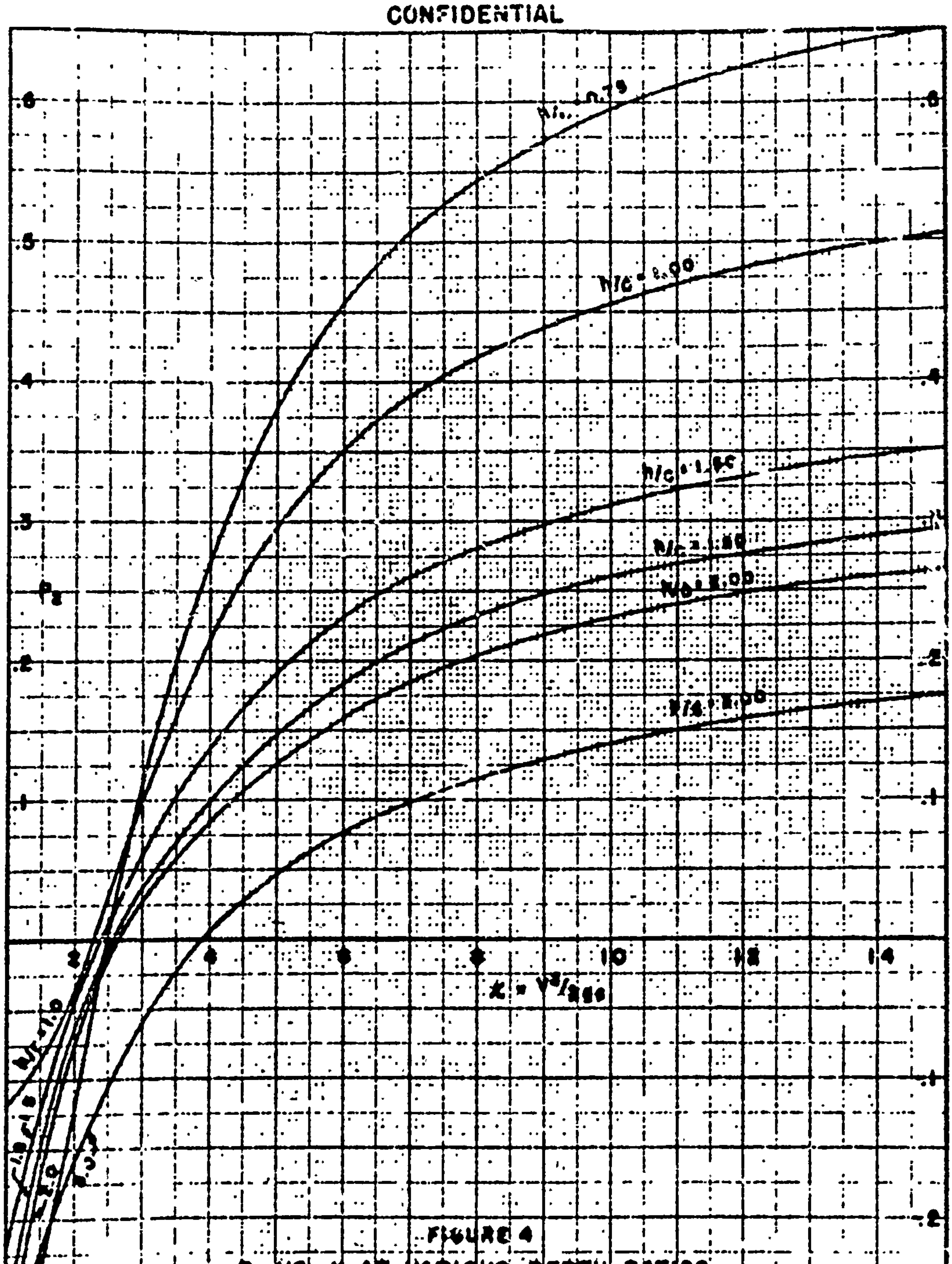

FIGURE 4
P_2 VS. k AT VARIOUS DEPTH RATIOS

CONFIDENTIAL

CONFIDENTIAL

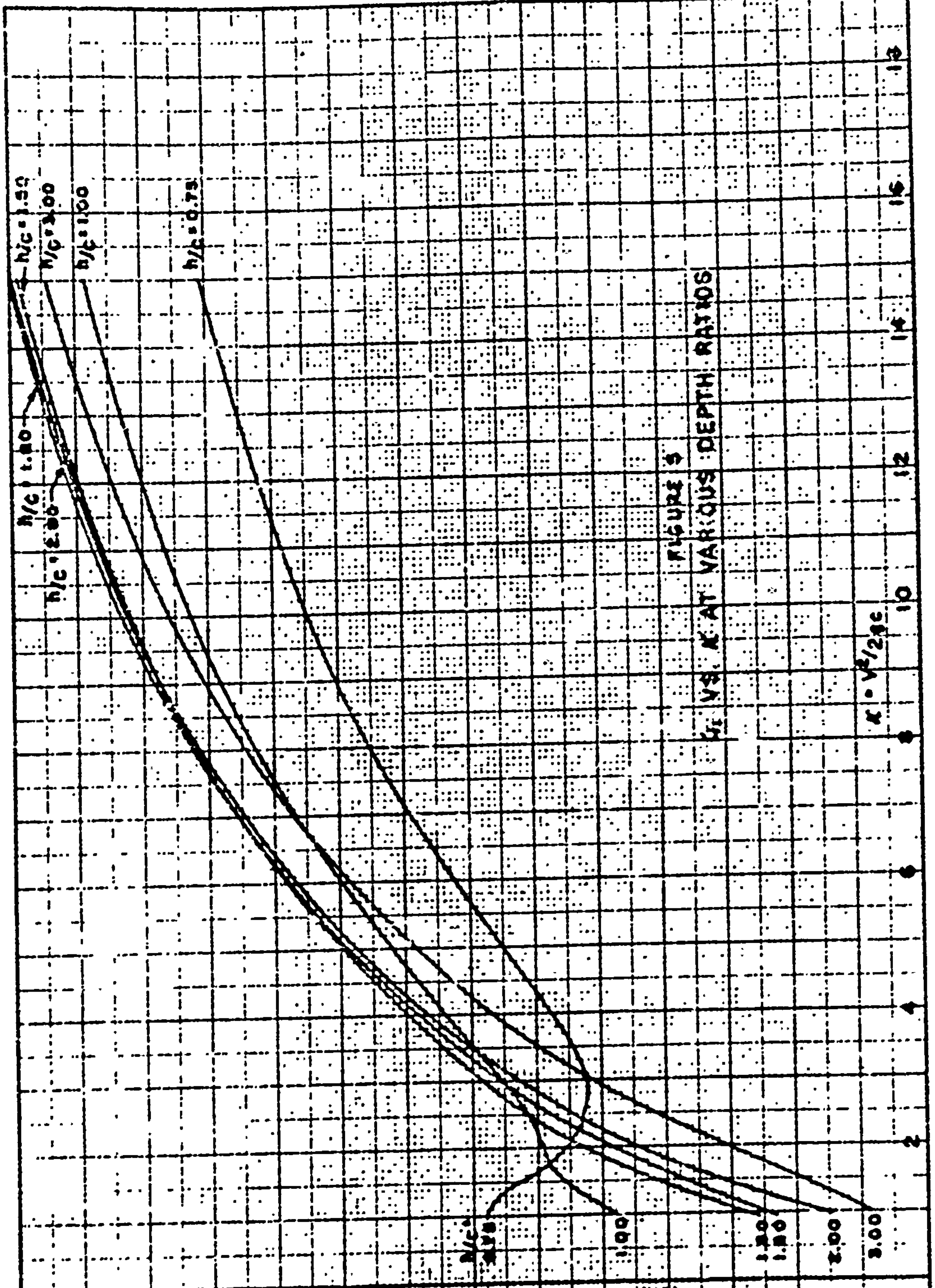

FIGURE 5

VS K AT VARIOUS DEPTH RATIOS

CONFIDENTIAL

CONFIDENTIAL

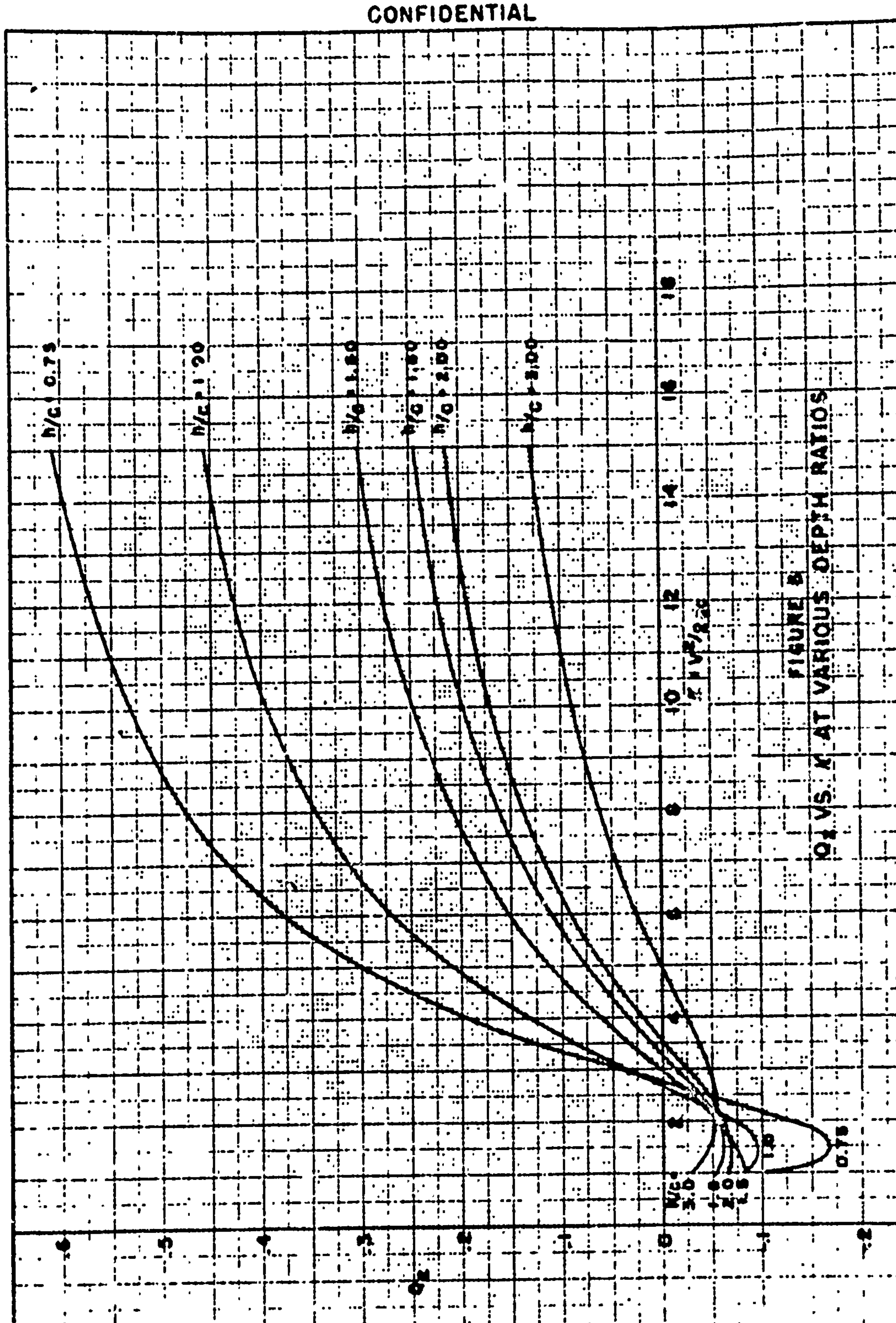

FIGURE 8

Q_2 VS. K AT VARIOUS DEPTH RATIOS

CONFIDENTIAL

CONFIDENTIAL

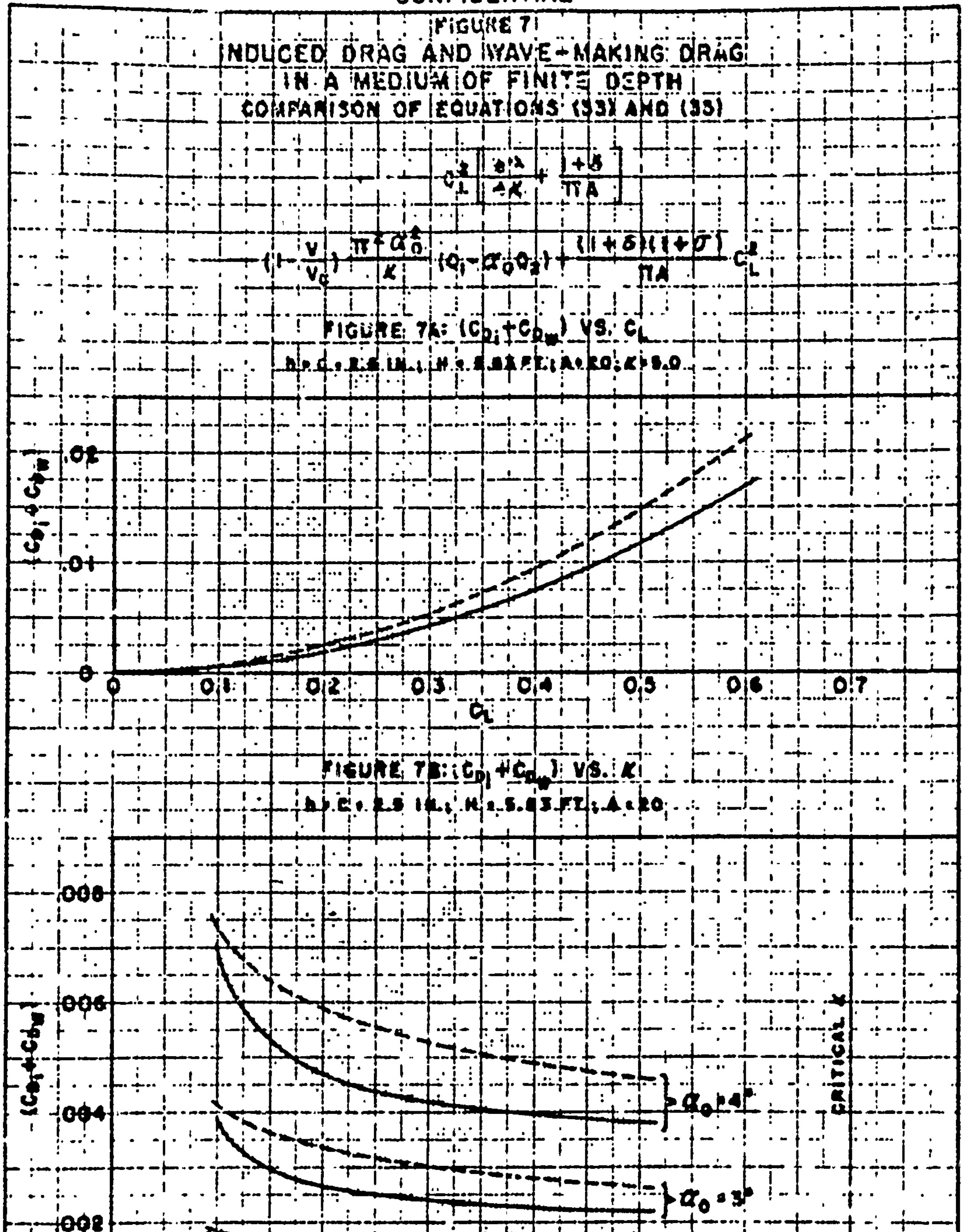

CONFIDENTIAL

CONFIDENTIAL

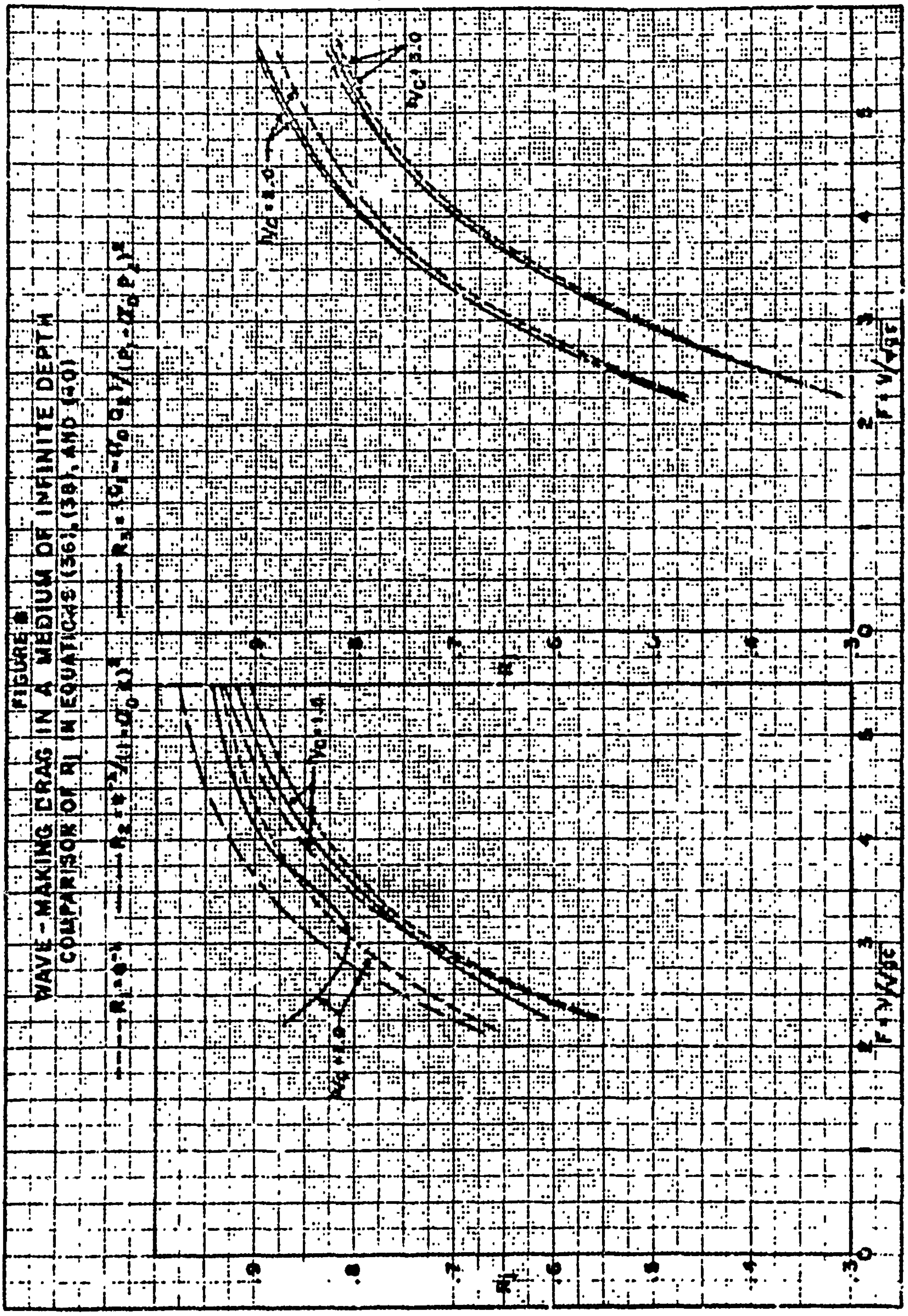

CONFIDENTIAL

FIGURE 9A

COMPUTED INDUCED AND WAVE-MAKING DRAG COMPARED WITH EXPERIMENTAL TOTAL DRAG AT VARIOUS FROUDE NUMBERS

NACA 64$_1$-A412 (MODEL Xa)

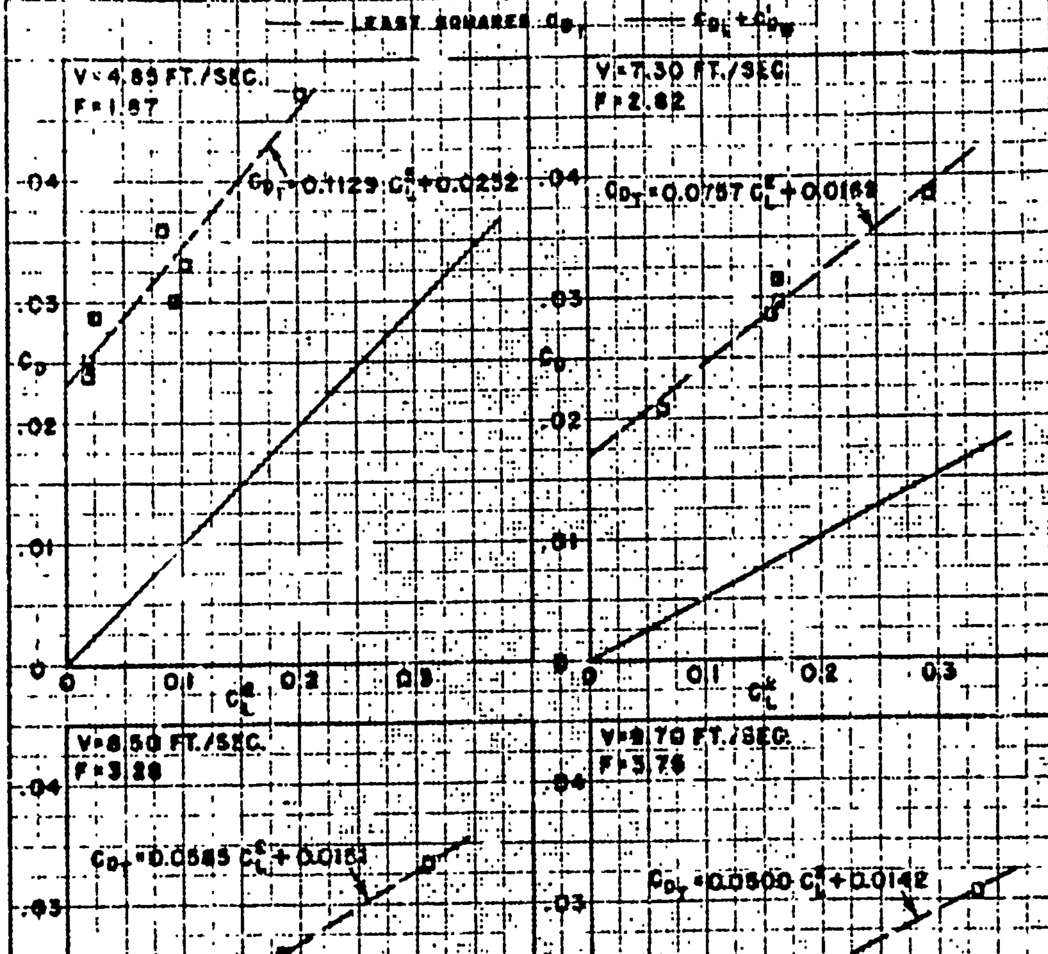

CONFIDENTIAL

FIGURE 98

COMPUTED INDUCED AND WAVE-MAKING DRAG COMPARED WITH EXPERIMENTAL TOTAL DRAG AT VARIOUS FROUDE NUMBERS

NACA 64,-412 (MODEL 2e)

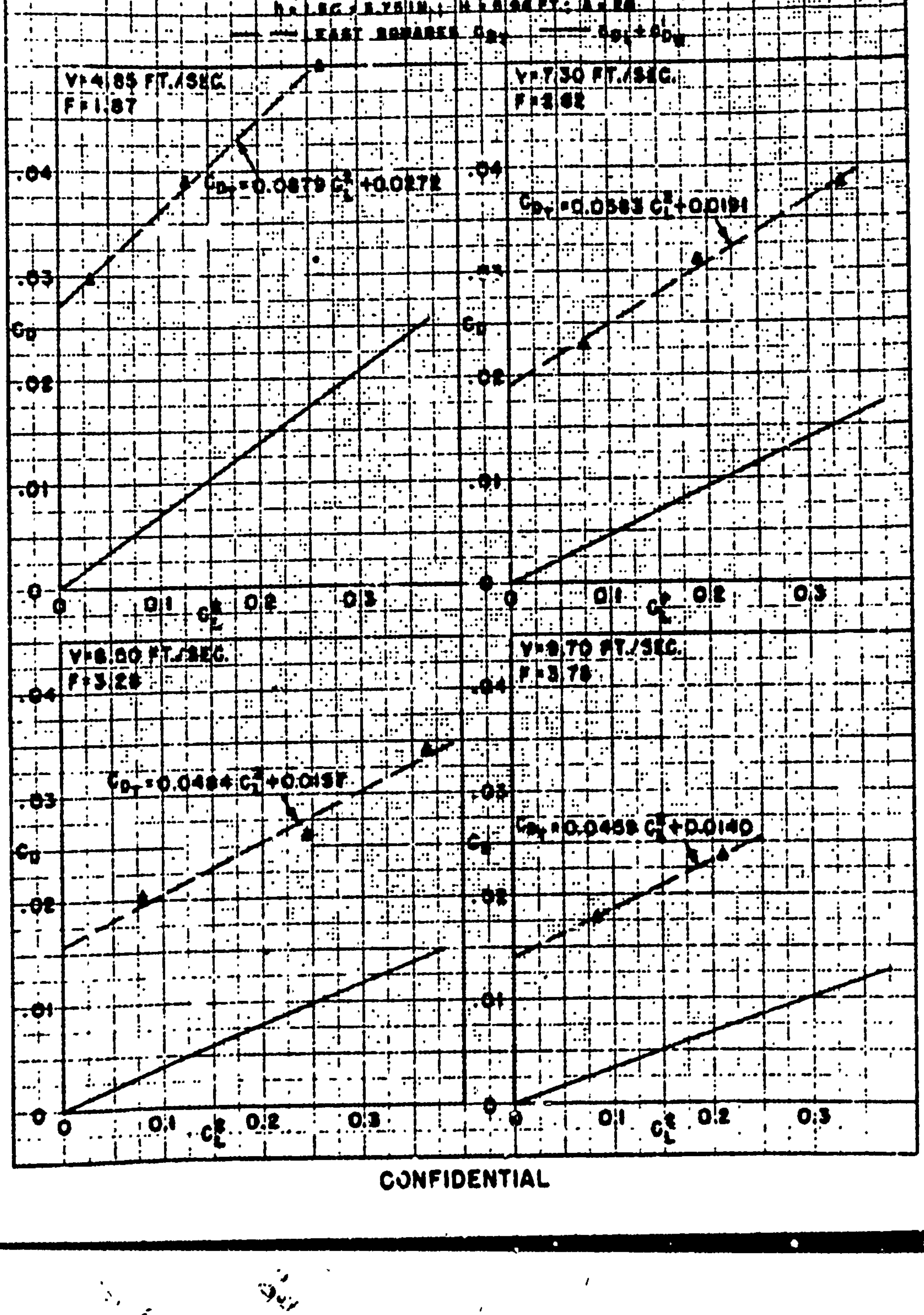

CONFIDENTIAL

CONFIDENTIAL

FIGURE 9C
COMPUTED INDUCED AND WAVE-MAKING DRAG
COMPARED WITH EXPERIMENTAL TOTAL DRAG
AT VARIOUS FROUDE NUMBERS

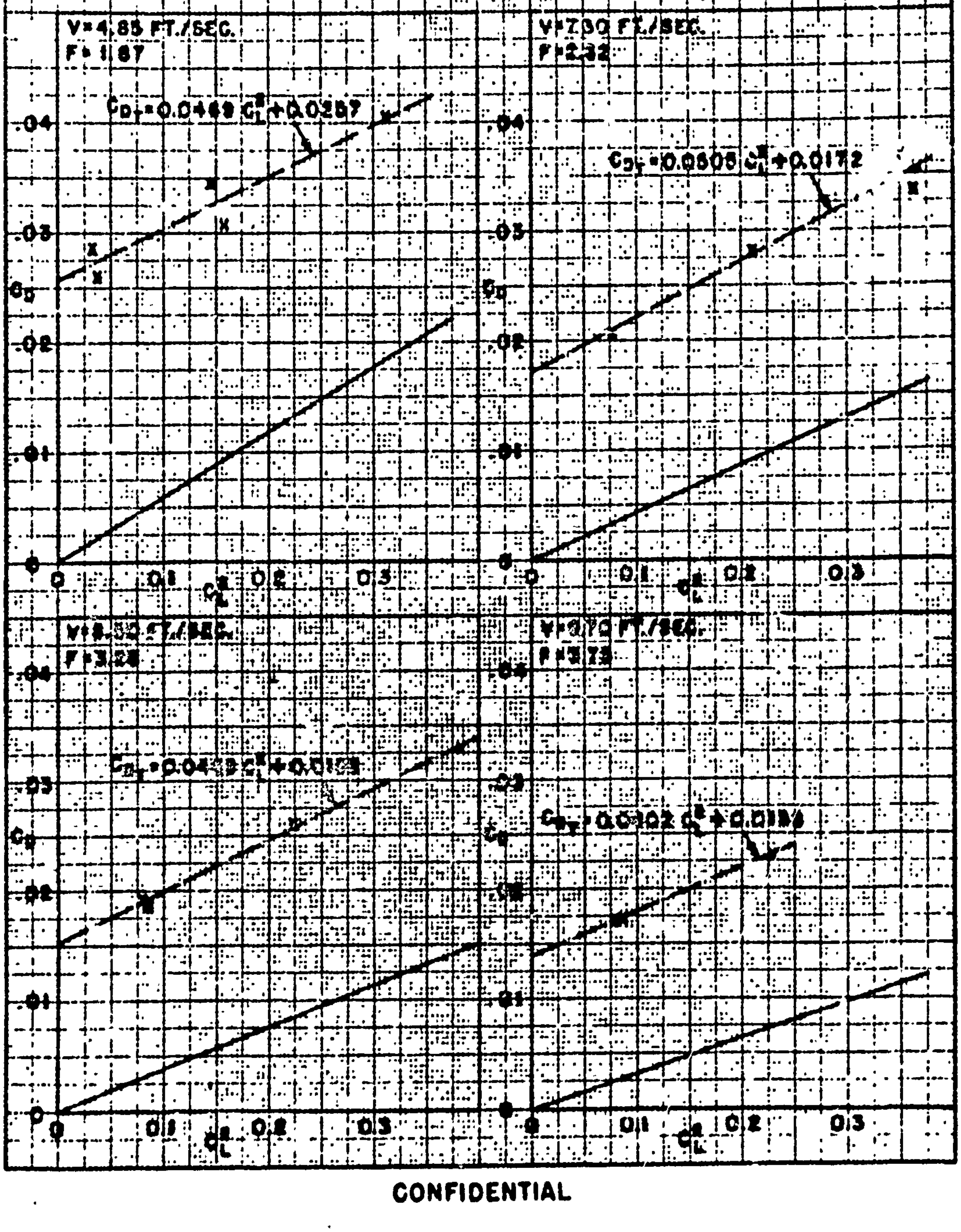

CONFIDENTIAL

CONFIDENTIAL

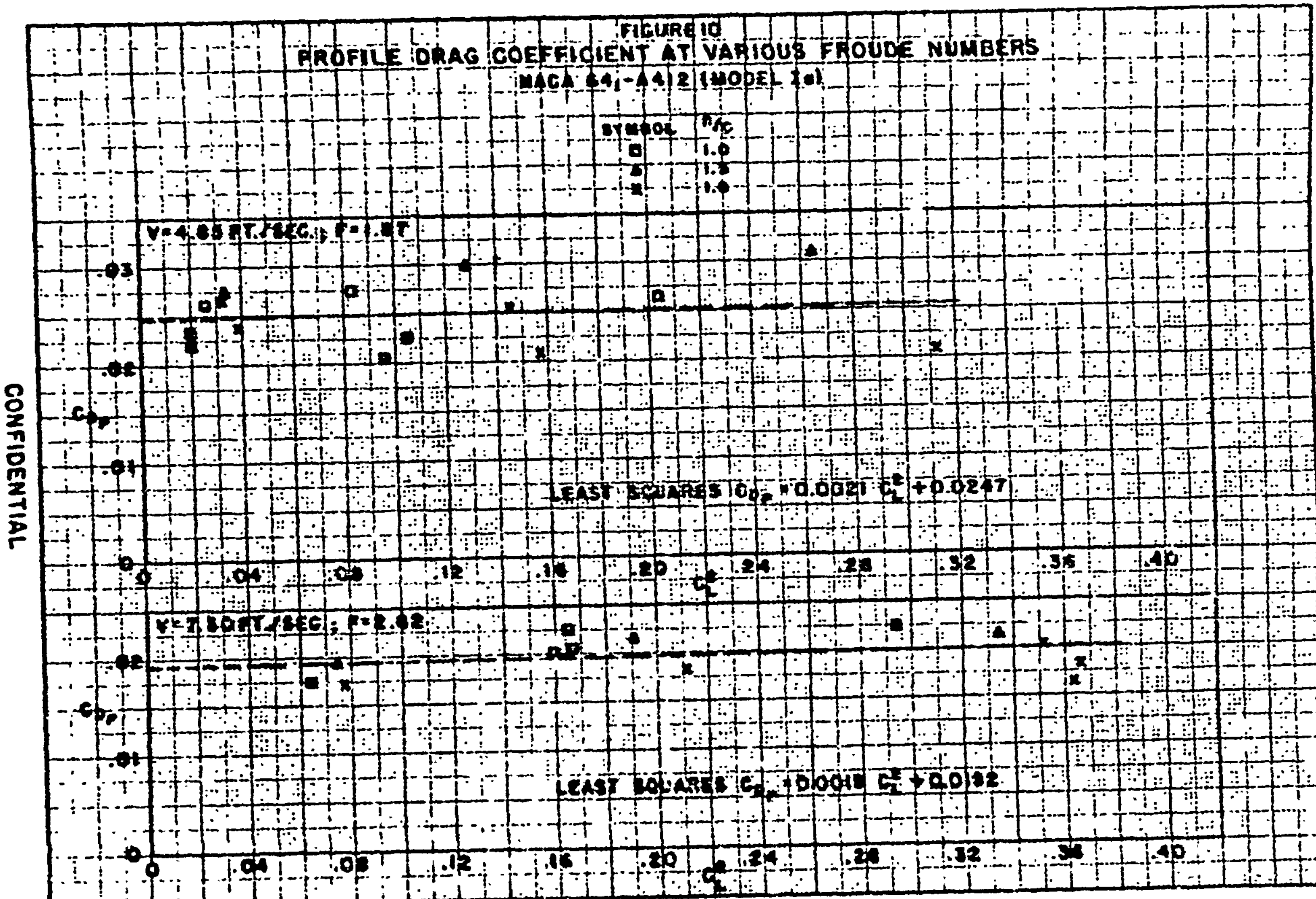

CONFIDENTIAL

CONFIDENTIAL

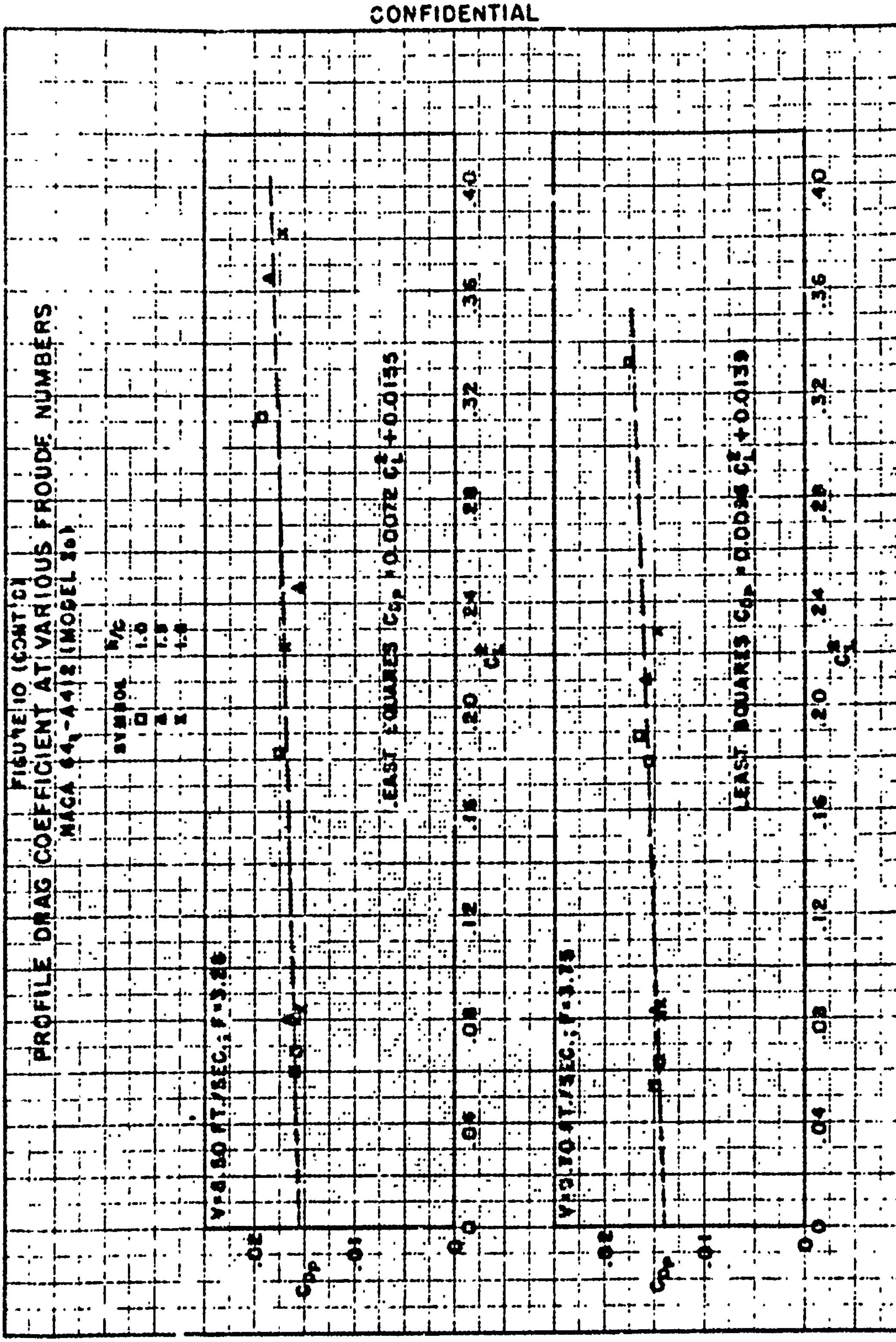

FIGURE 10 (CONT'D)
PROFILE DRAG COEFFICIENT AT VARIOUS FROUDE NUMBERS

CONFIDENTIAL

FIGURE 11A
COMPUTED INDUCED DRAG
COMPARED WITH EXPERIMENTAL TOTAL DRAG
AT VARIOUS FROUDE NUMBERS
NACA 64,-A412 (MODEL Ib)

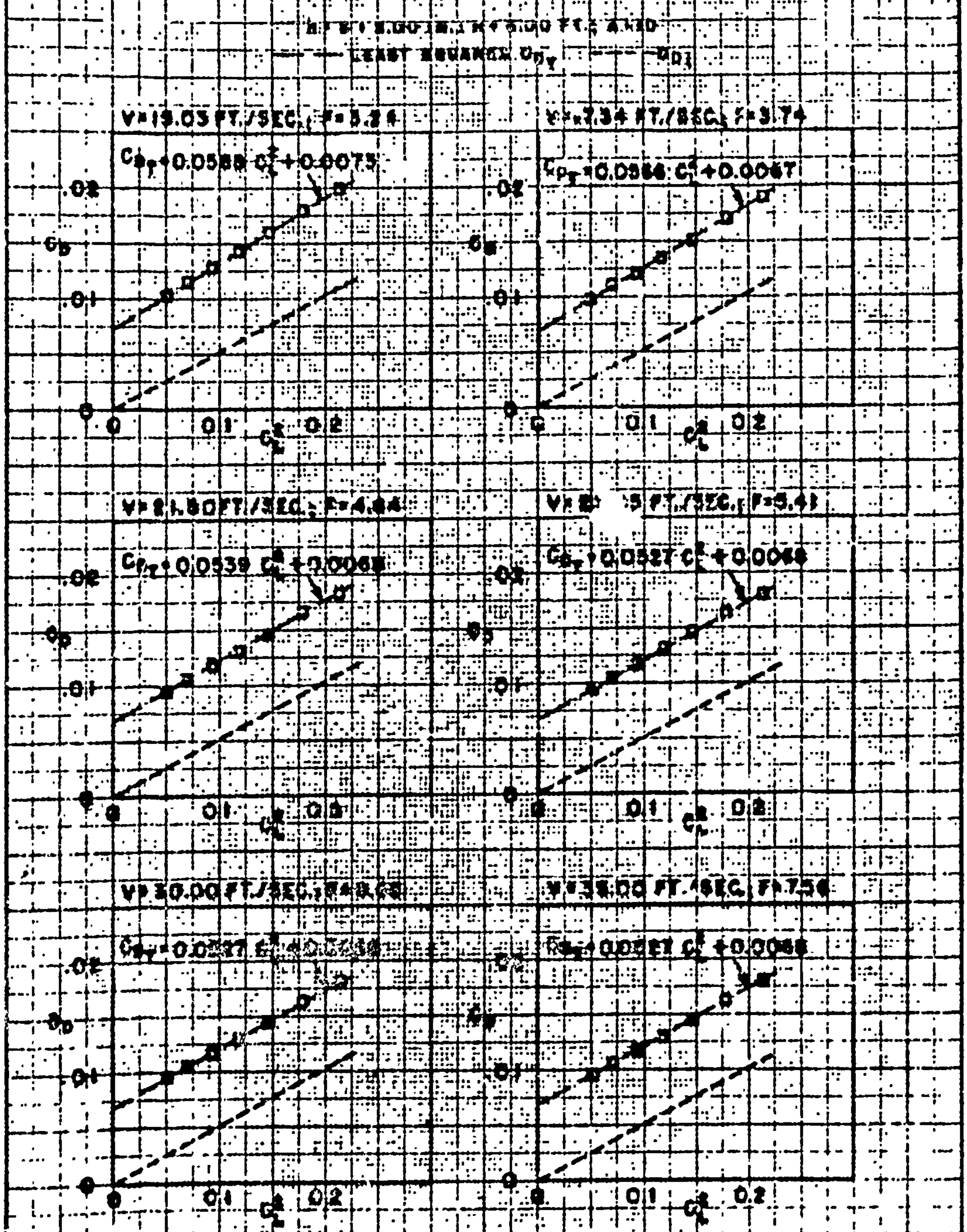

CONFIDENTIAL

FIGURE 11a

COMPUTED INDUCED DRAG
COMPARED WITH EXPERIMENTAL TOTAL DRAG
AT VARIOUS FROUDE NUMBERS
NACA 64(1)-A412 (MODEL 3b)

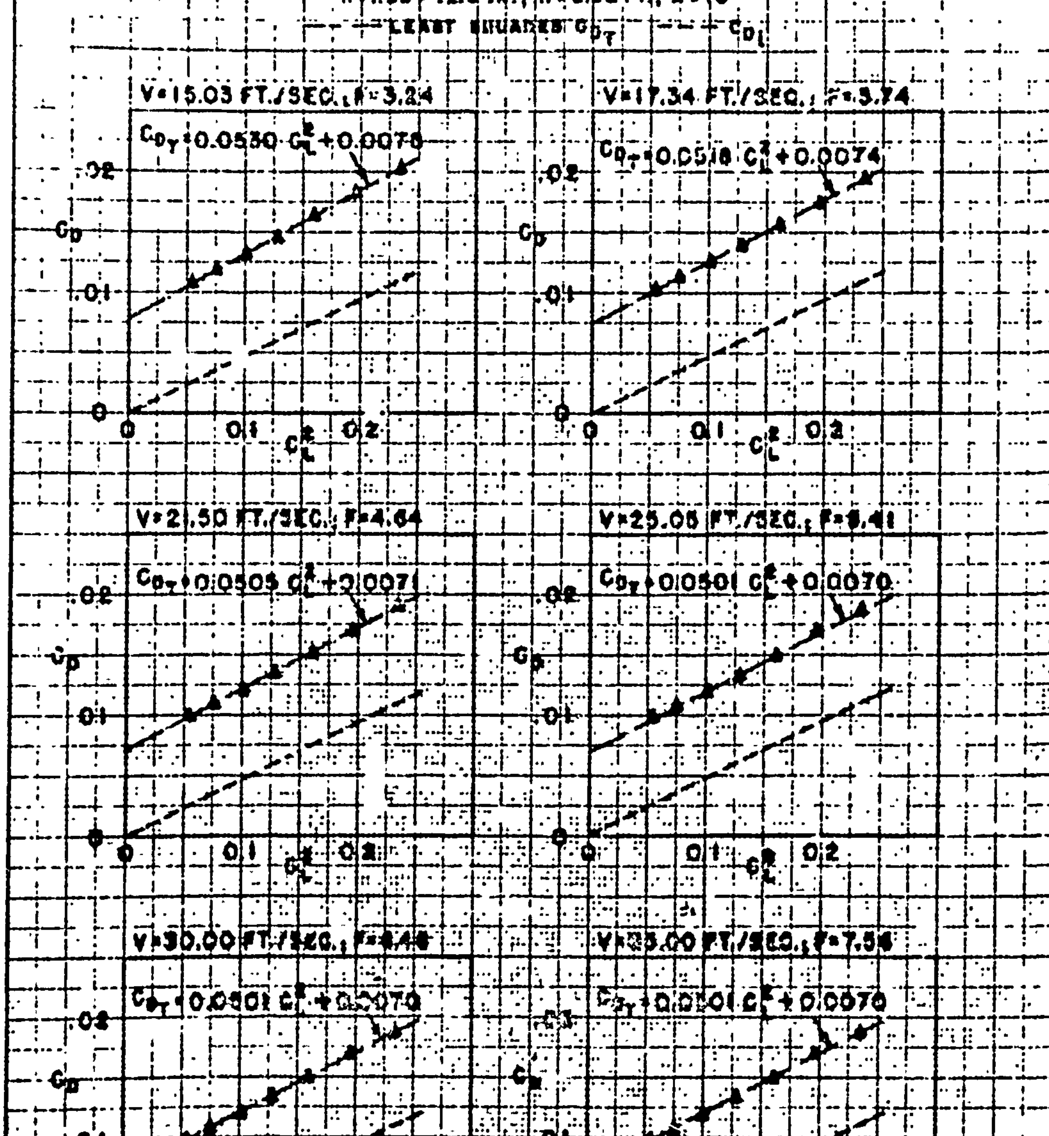

CONFIDENTIAL

CONFIDENTIAL

FIGURE 11C

COMPUTED INDUCED DRAG
COMPARED WITH EXPERIMENTAL TOTAL DRAG
AT VARIOUS FROUDE NUMBERS
NACA 64,-A412 (MODEL X6)

— LEAST SQUARES C_{D_T} — — — C_{D_i}

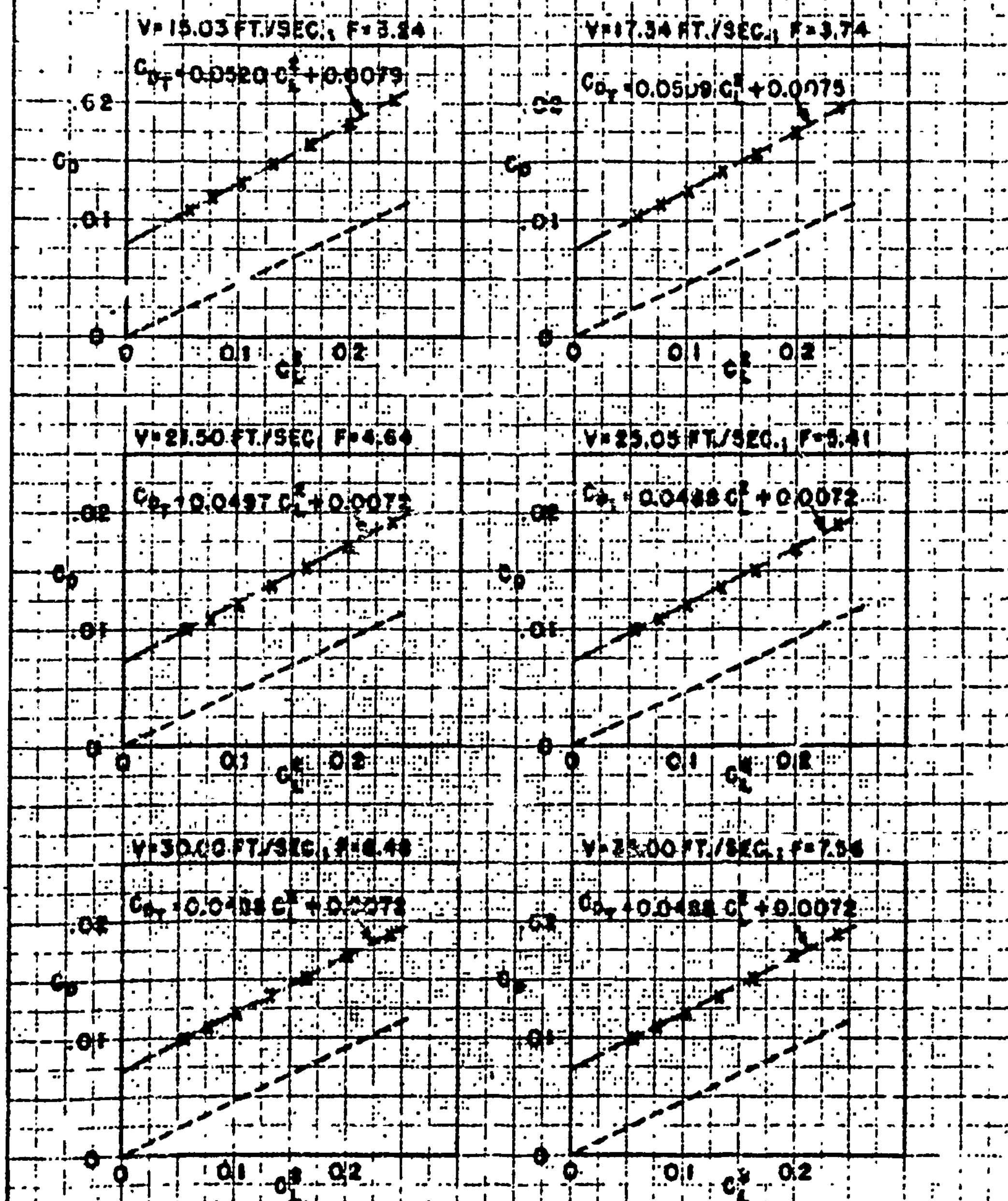

CONFIDENTIAL

CONFIDENTIAL

FIGURE 12

PROFILE DRAG COEFFICIENT AT VARIOUS FROUDE NUMBERS

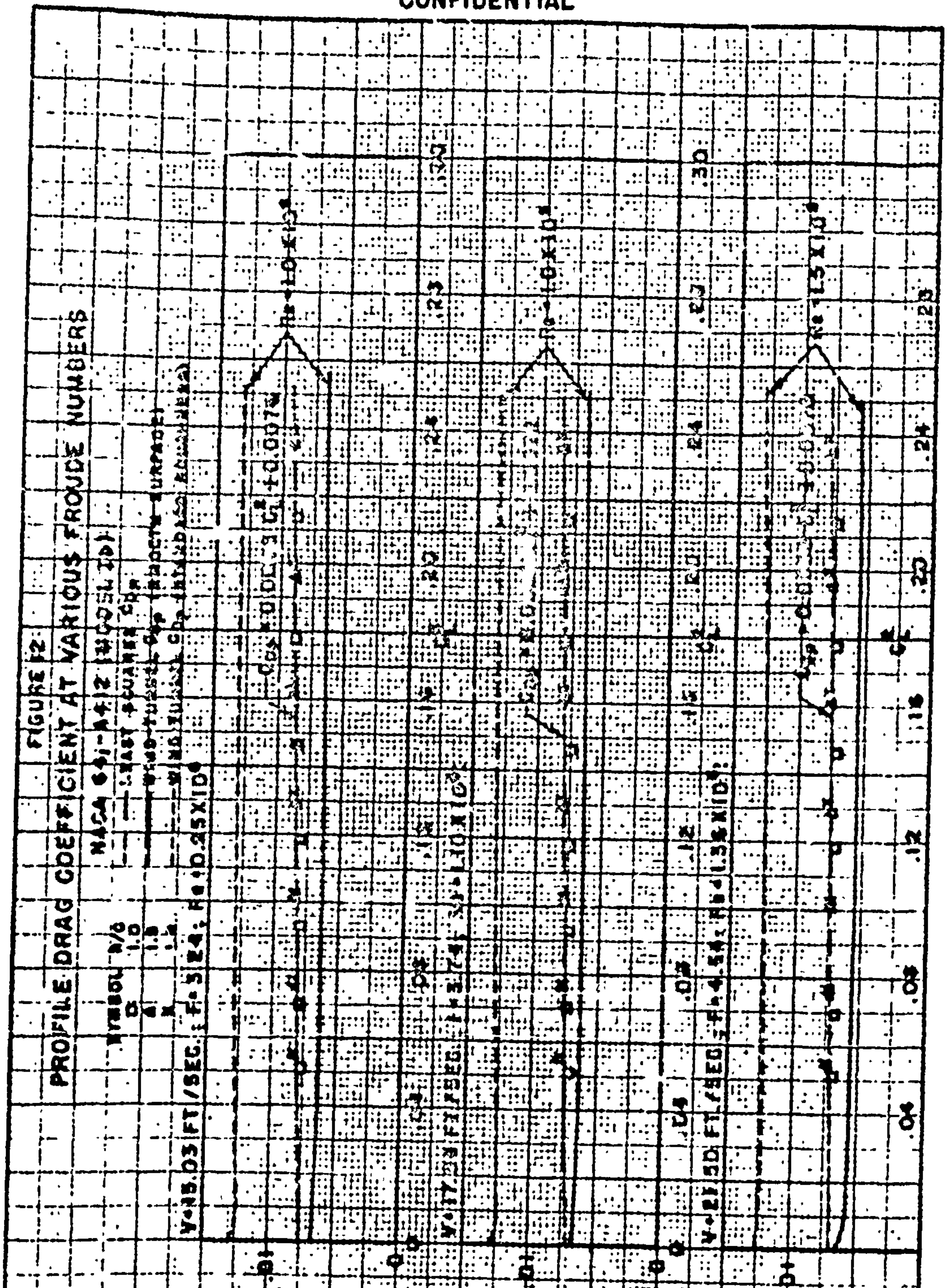

CONFIDENTIAL

CONFIDENTIAL

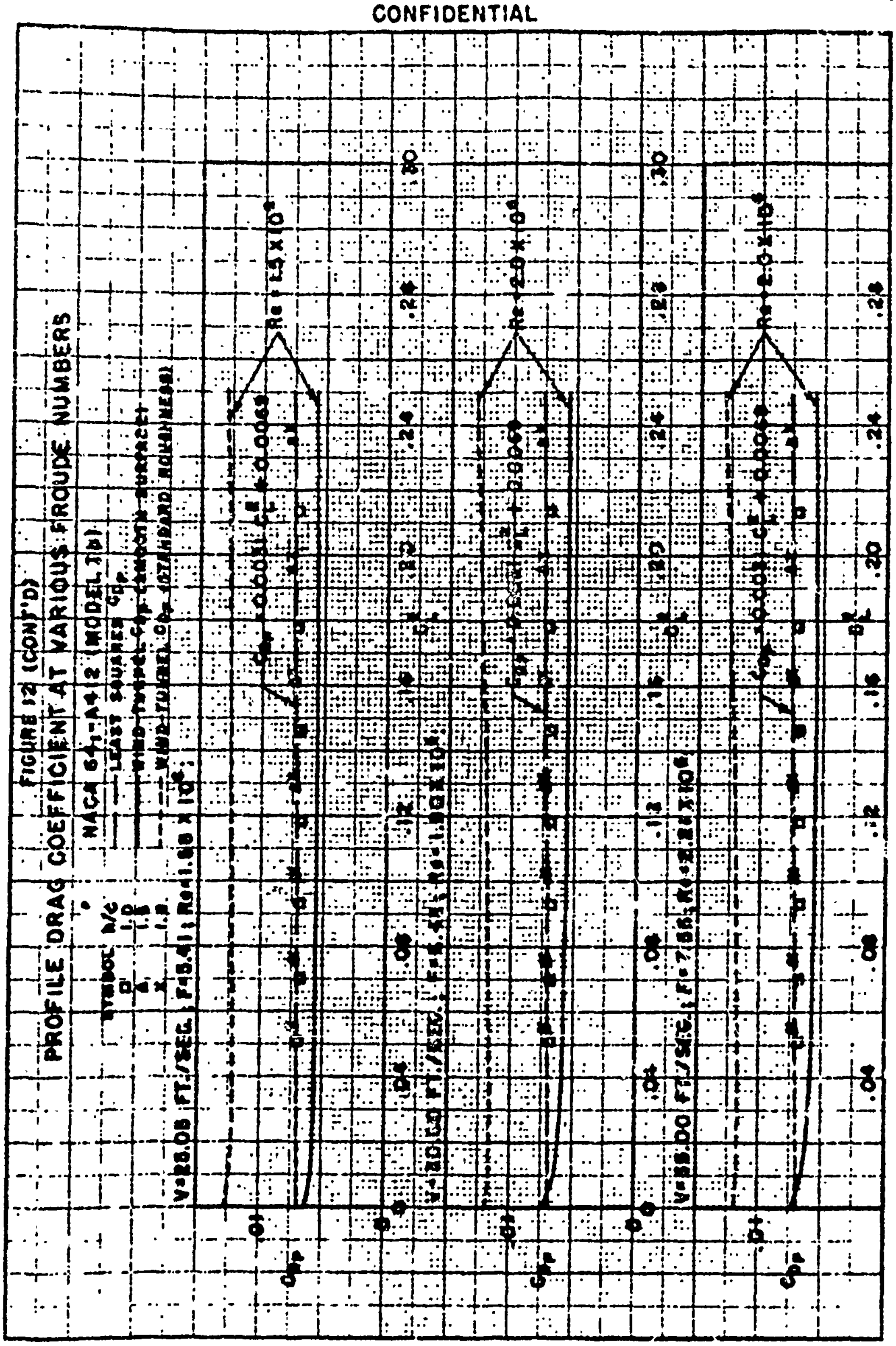

CONFIDENTIAL

FIGURE 15A

EXPERIMENTAL TOTAL DRAG AT VARIOUS FROUDE NUMBERS

NACA 0012 (MODEL II)

h = 0.25C = 1.25 IN.; H = 5.33 FT.; A = 6

—— LEAST SQUARES C_{D_T} — — C_{D_i}

SOLID SYMBOLS INDICATE α IN ERROR

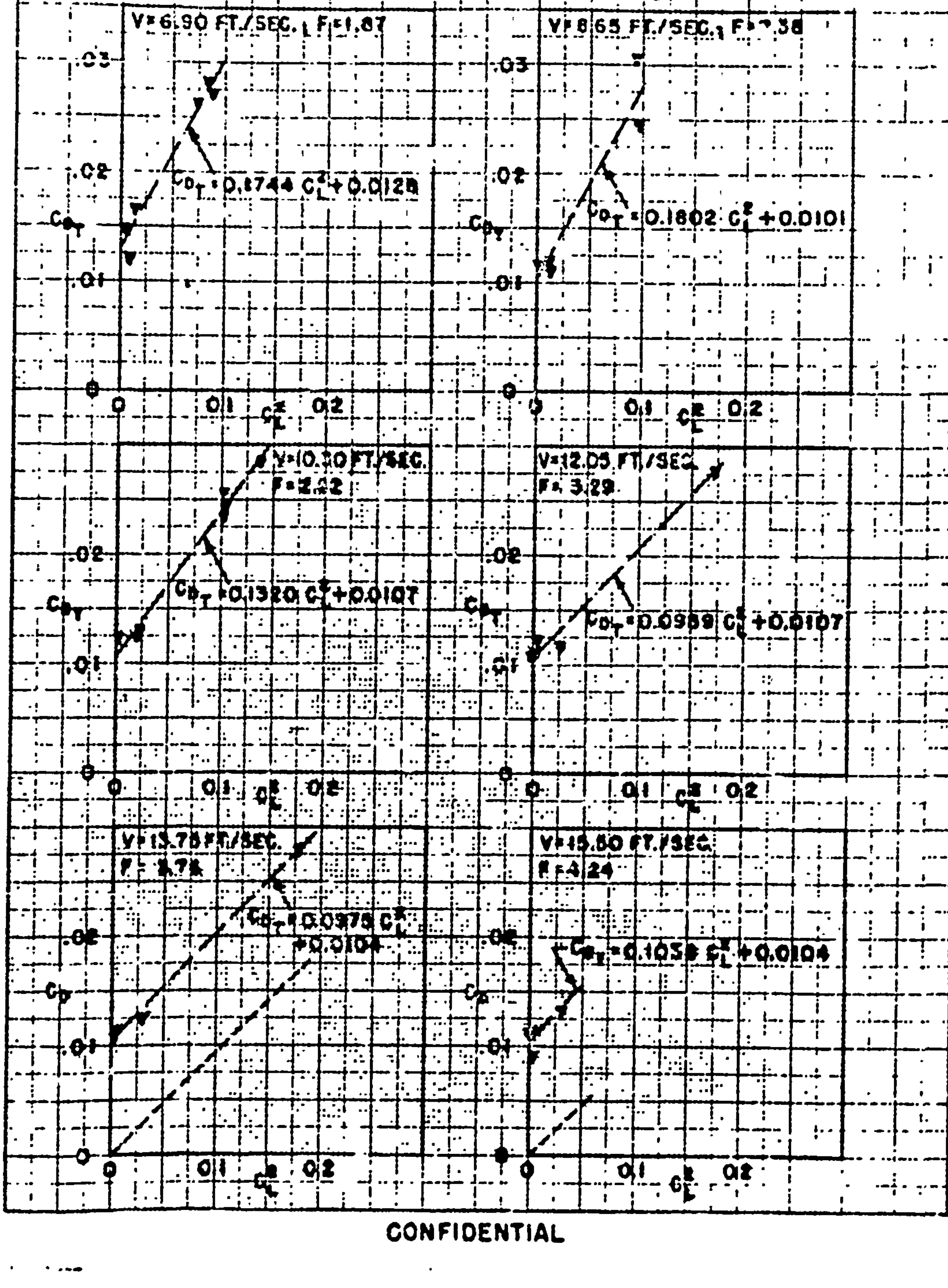

FIGURE 138

COMPUTED INDUCED AND WAVE-MAKING DRAG COMPARED WITH EXPERIMENTAL TOTAL DRAG AT VARIOUS FROUDE NUMBERS

NACA 0012 (MODEL II)

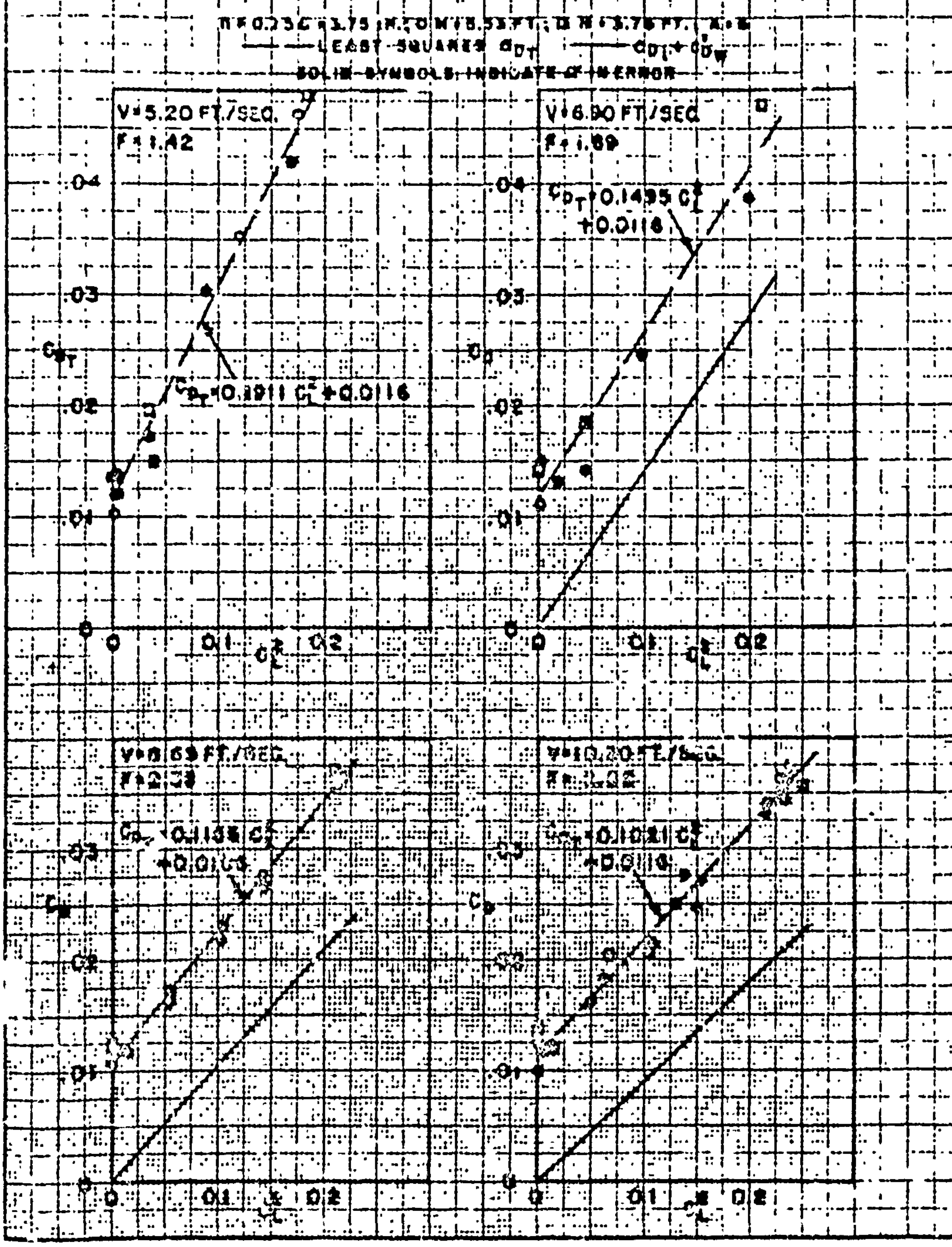

CONFIDENTIAL

FIGURE 138 (CONT'D)

COMPUTED INDUCED AND WAVE-MAKING DRAG COMPARED WITH EXPERIMENTAL TOTAL DRAG AT VARIOUS FROUDE NUMBERS

NACA 0012 (MODEL II)

—— LEAST SQUARES C_{D_T} – – – C_{D_i} —— $C_{D_i} + C_{D_W}$

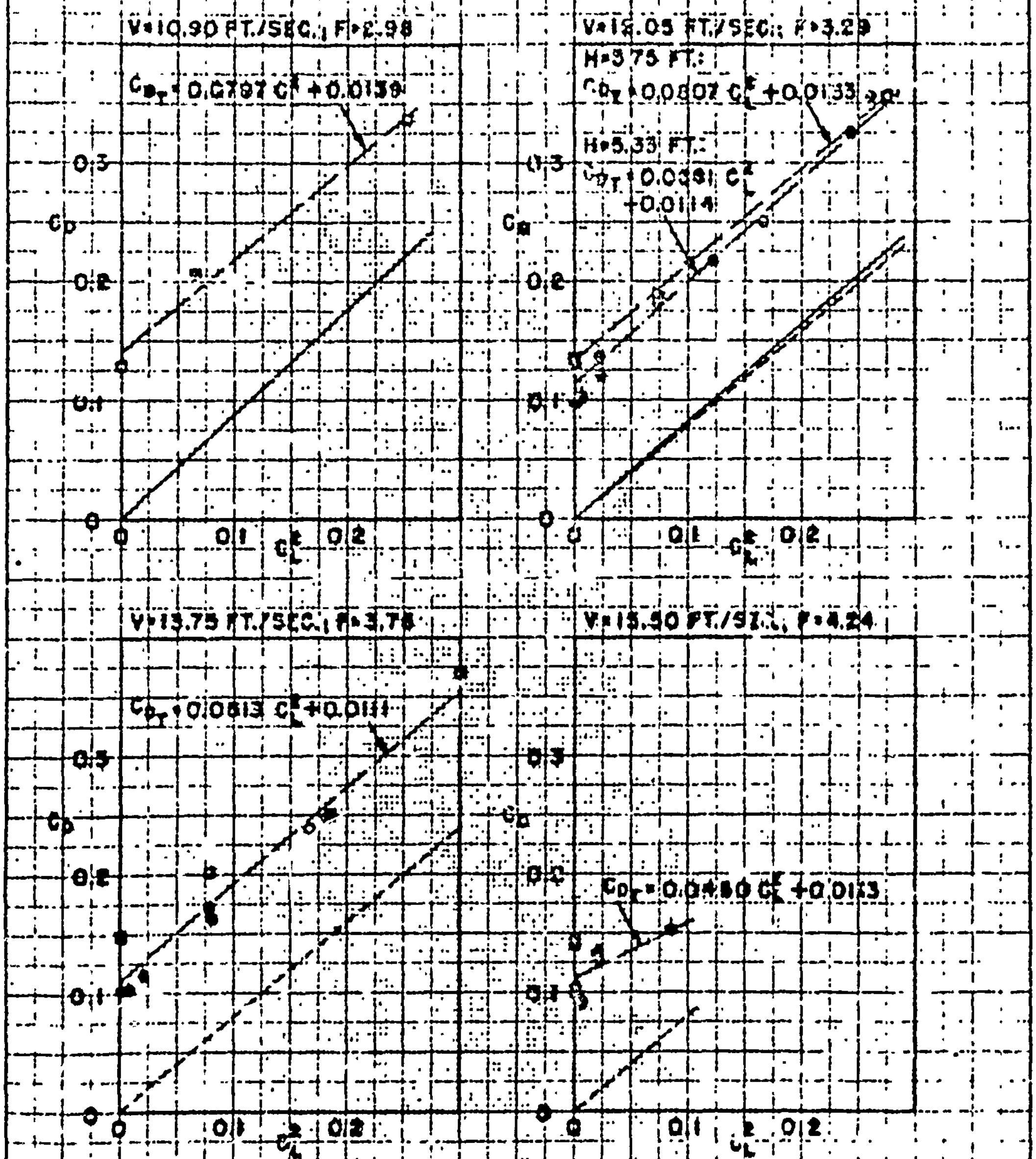

CONFIDENTIAL

FIGURE 13C

COMPUTED INDUCED DRAG COMPARED WITH EXPERIMENTAL TOTAL DRAG AT VARIOUS FROUDE NUMBERS

NACA 0012 (MODEL II)

a = 0.750 . . 5 IN.; H = 3.75 FT.; A = 6

—— LEAST SQUARES C_{D_T} – – – C_{D_i}

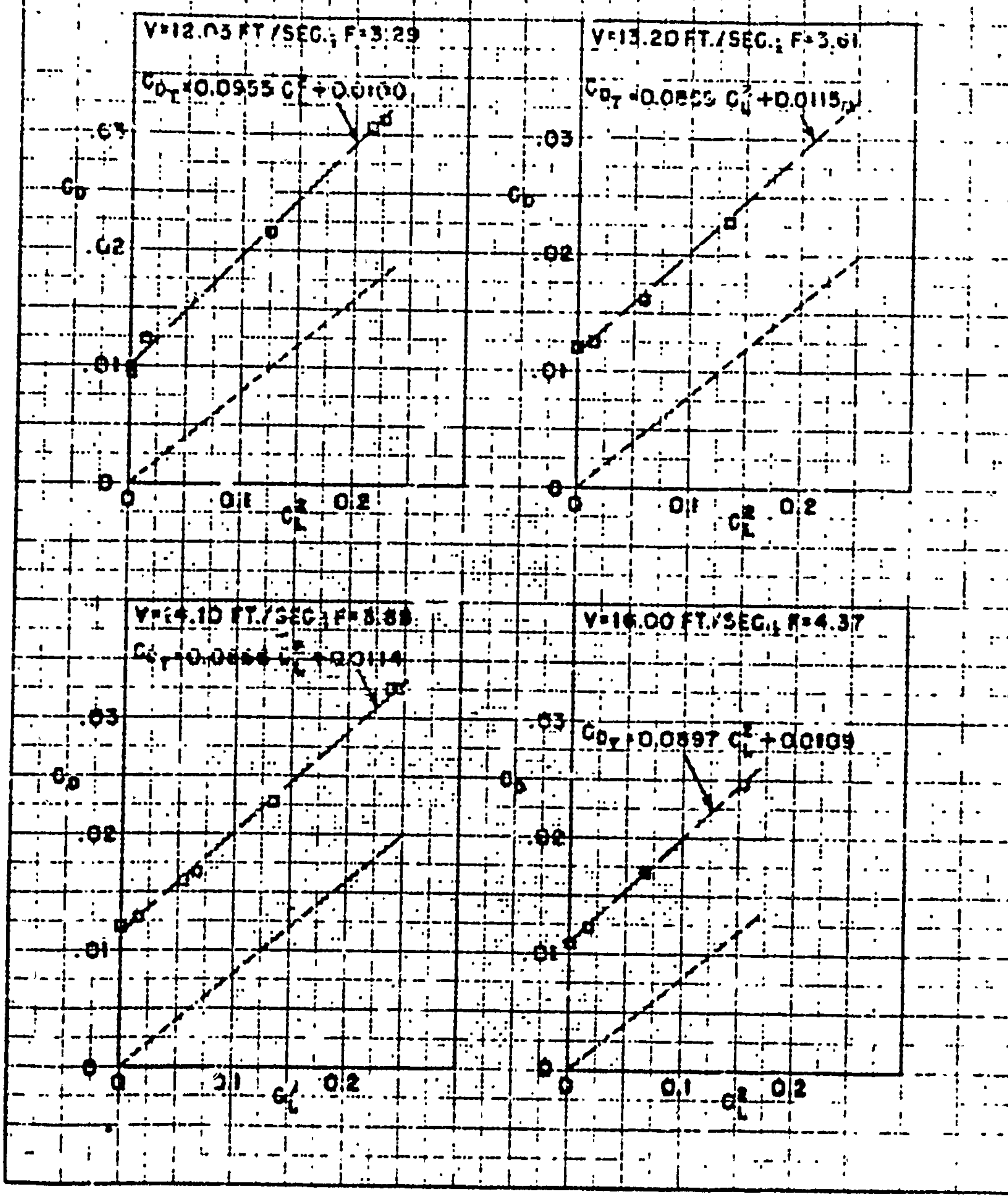

FIGURE 130

COMPUTED INDUCED AND WAVE-MAKING DRAG COMPARED WITH EXPERIMENTAL TOTAL DRAG AT VARIOUS FROUDE NUMBERS

NACA 0012 (MODEL II)

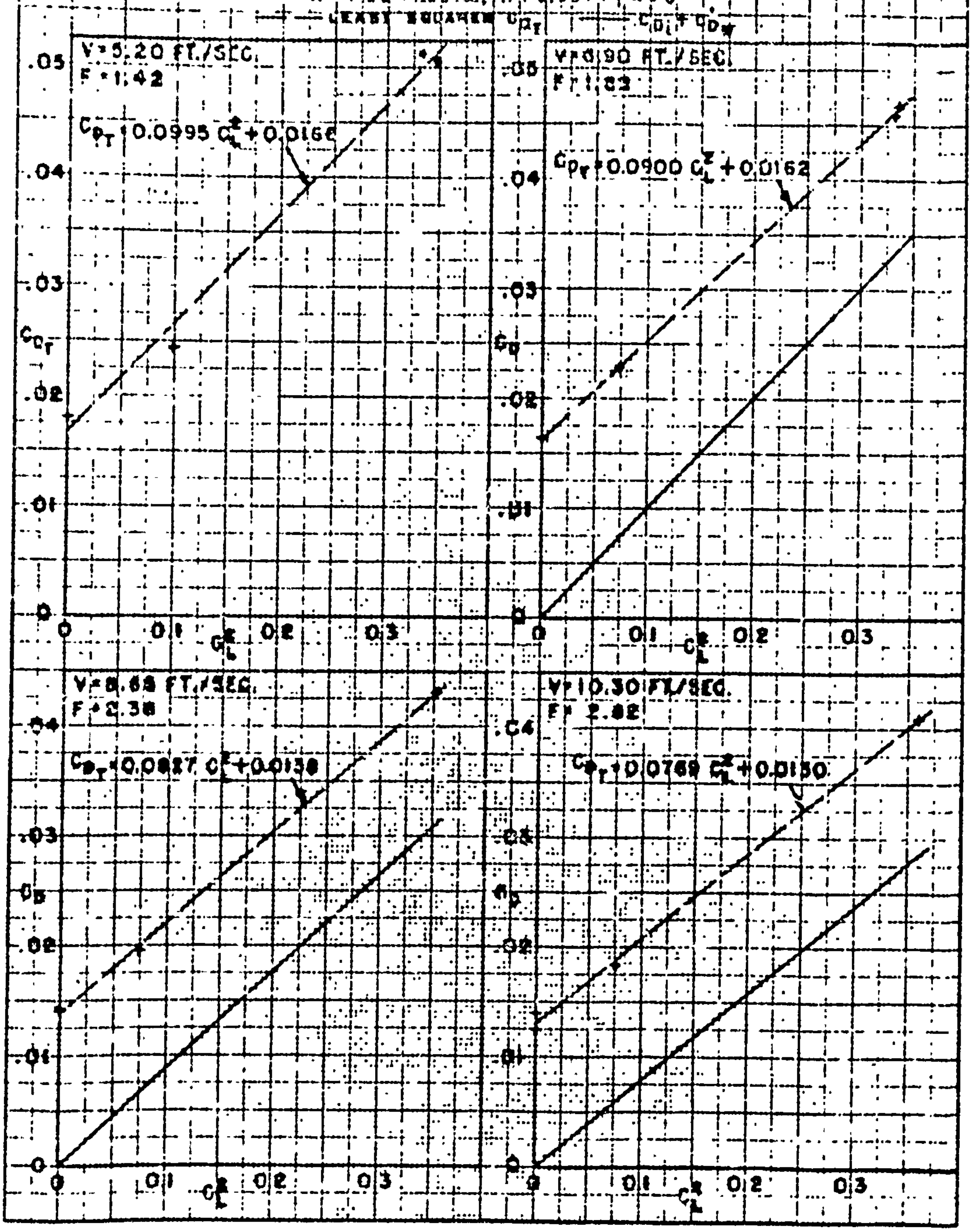

CONFIDENTIAL

FIGURE 13D (CONT'D)
COMPUTED INDUCED AND WAVE DRAG
COMPARED WITH EXPERIMENTAL TOTAL DRAG
AT VARIOUS FROUDE NUMBERS
NACA 0012 (MODEL II)

LEAST SQUARES C_{D_T} — C_{D_i} — $C_{D_i}+C_{D_W}$

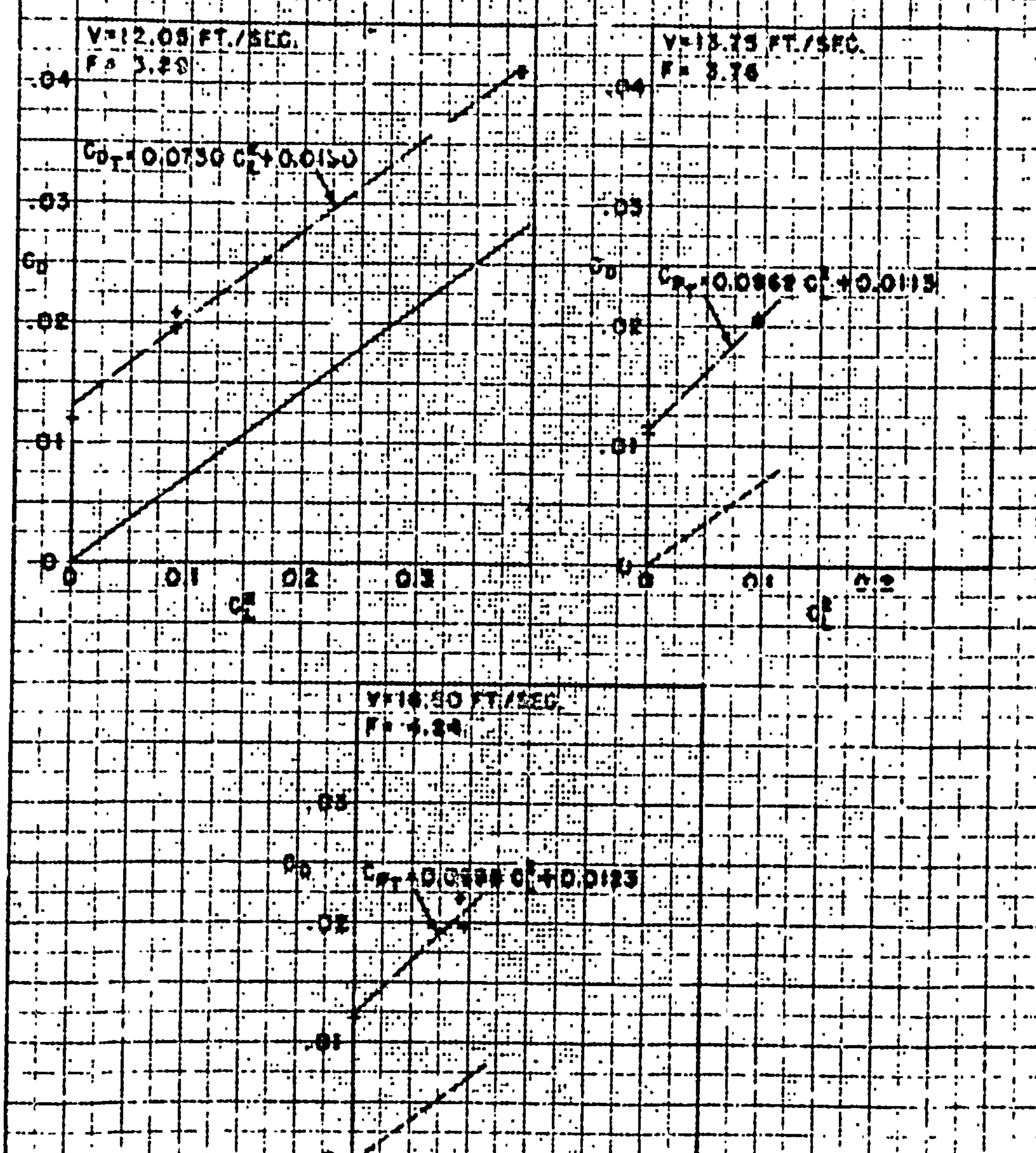

CONFIDENTIAL

CONFIDENTIAL

FIGURE 13E
COMPUTED INDUCED AND WAVE-MAKING DRAG
COMPARED WITH EXPERIMENTAL TOTAL DRAG
AT VARIOUS FROUDE NUMBERS
NACA 0012 (MODEL II)

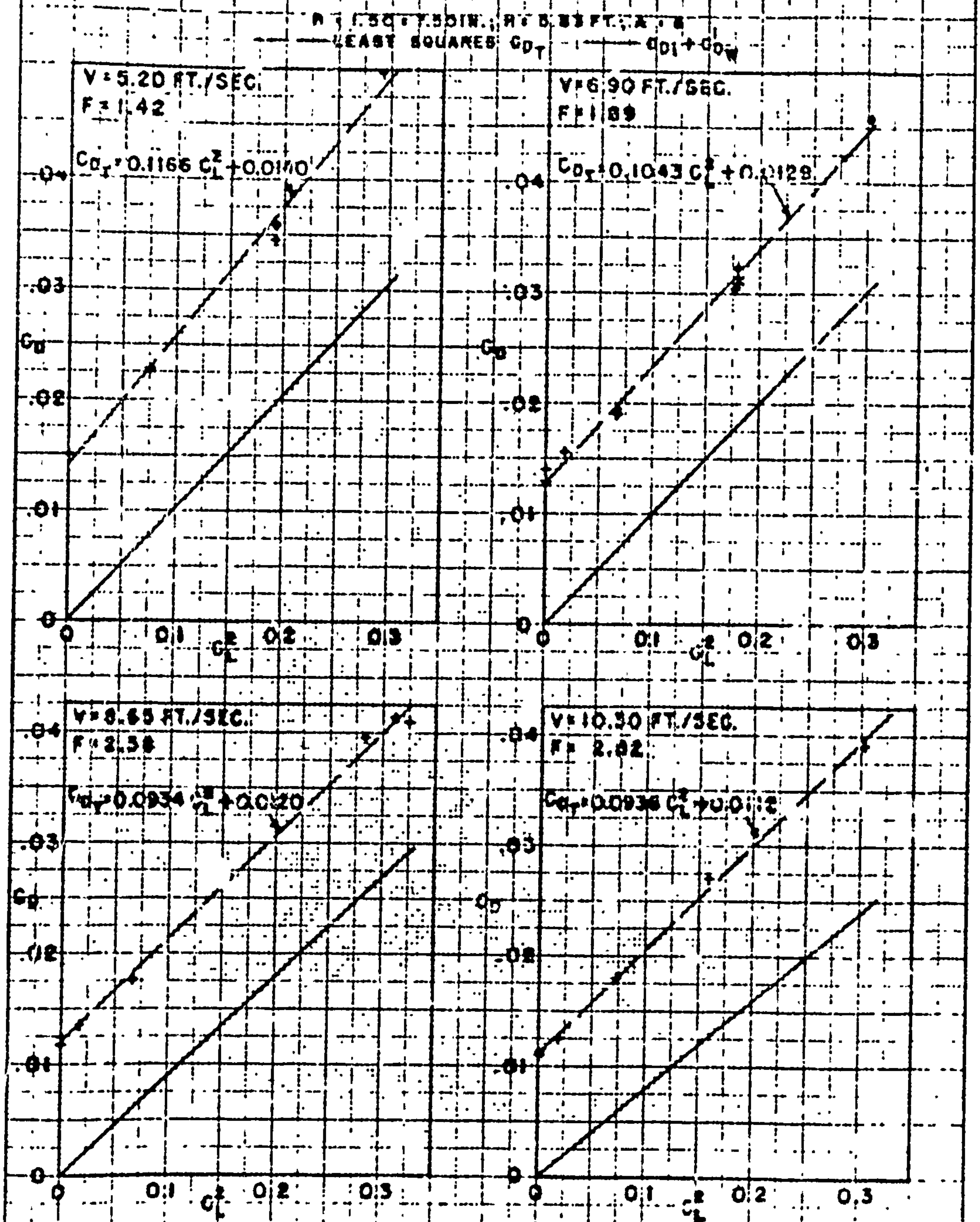

CONFIDENTIAL

CONFIDENTIAL

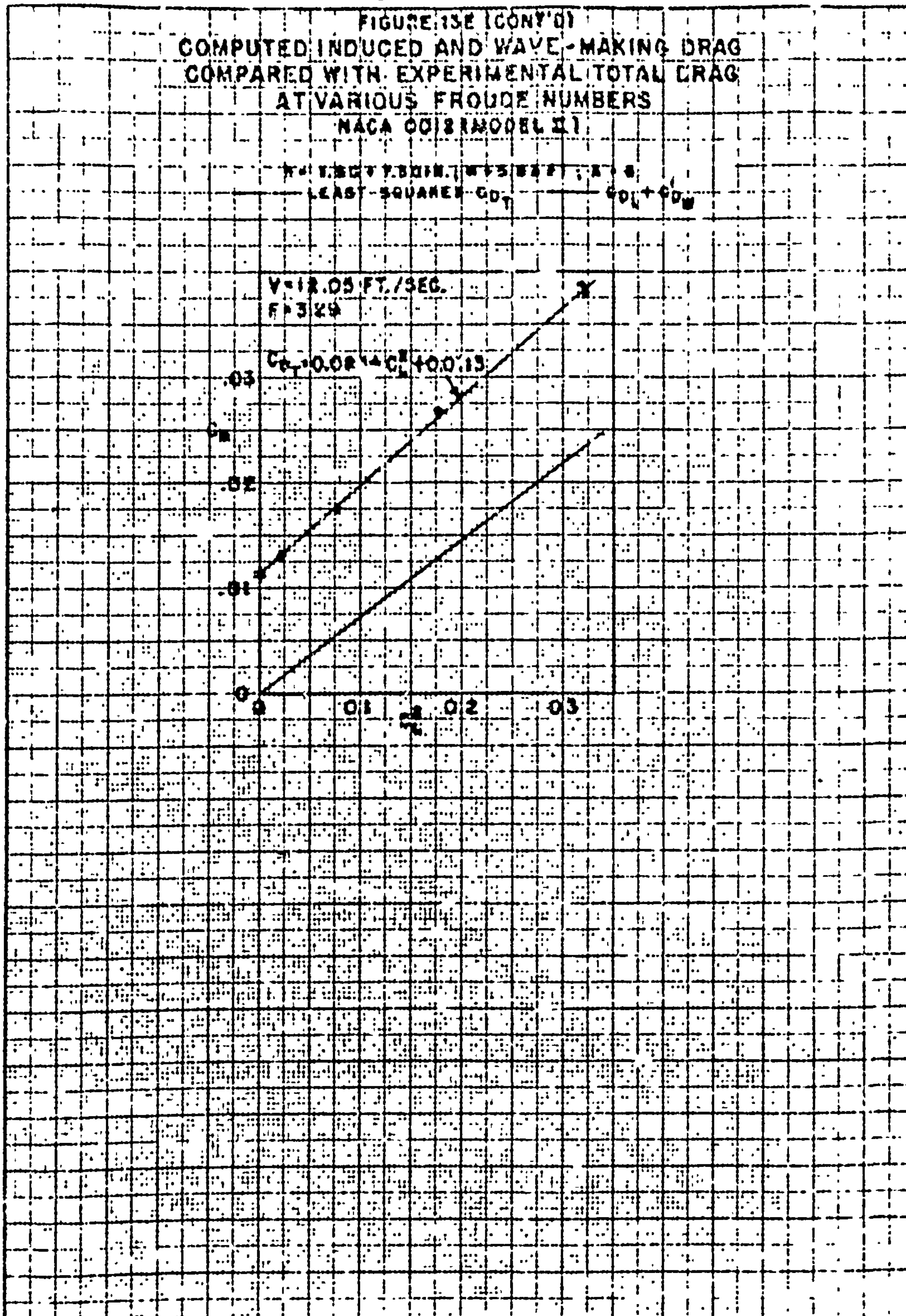

FIGURE 13E (CONT'D)

COMPUTED INDUCED AND WAVE-MAKING DRAG COMPARED WITH EXPERIMENTAL TOTAL DRAG AT VARIOUS FROUDE NUMBERS

NACA 0012 (MODEL II)

LEAST-SQUARES C_{D_T} —— $C_{D_i}+C_{D_W}$

CONFIDENTIAL

CONFIDENTIAL

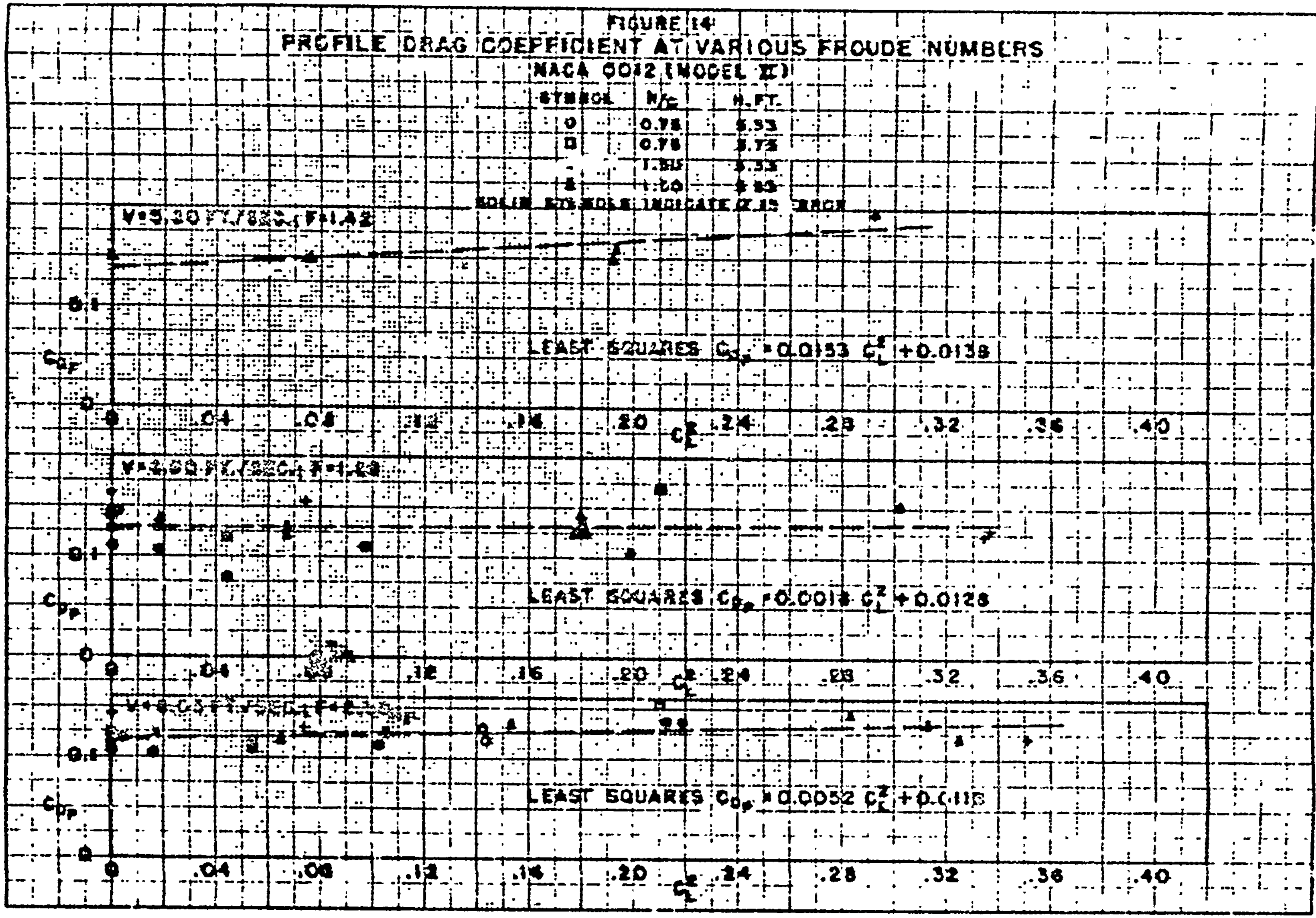

FIGURE 14
PROFILE DRAG COEFFICIENT AT VARIOUS FROUDE NUMBERS

CONFIDENTIAL

CONFIDENTIAL

FIGURE 14 (CONT'D)
PROFILE DRAG COEFFICIENT AT VARIOUS FROUDE NUMBERS
NACA 0012 (MODEL II)

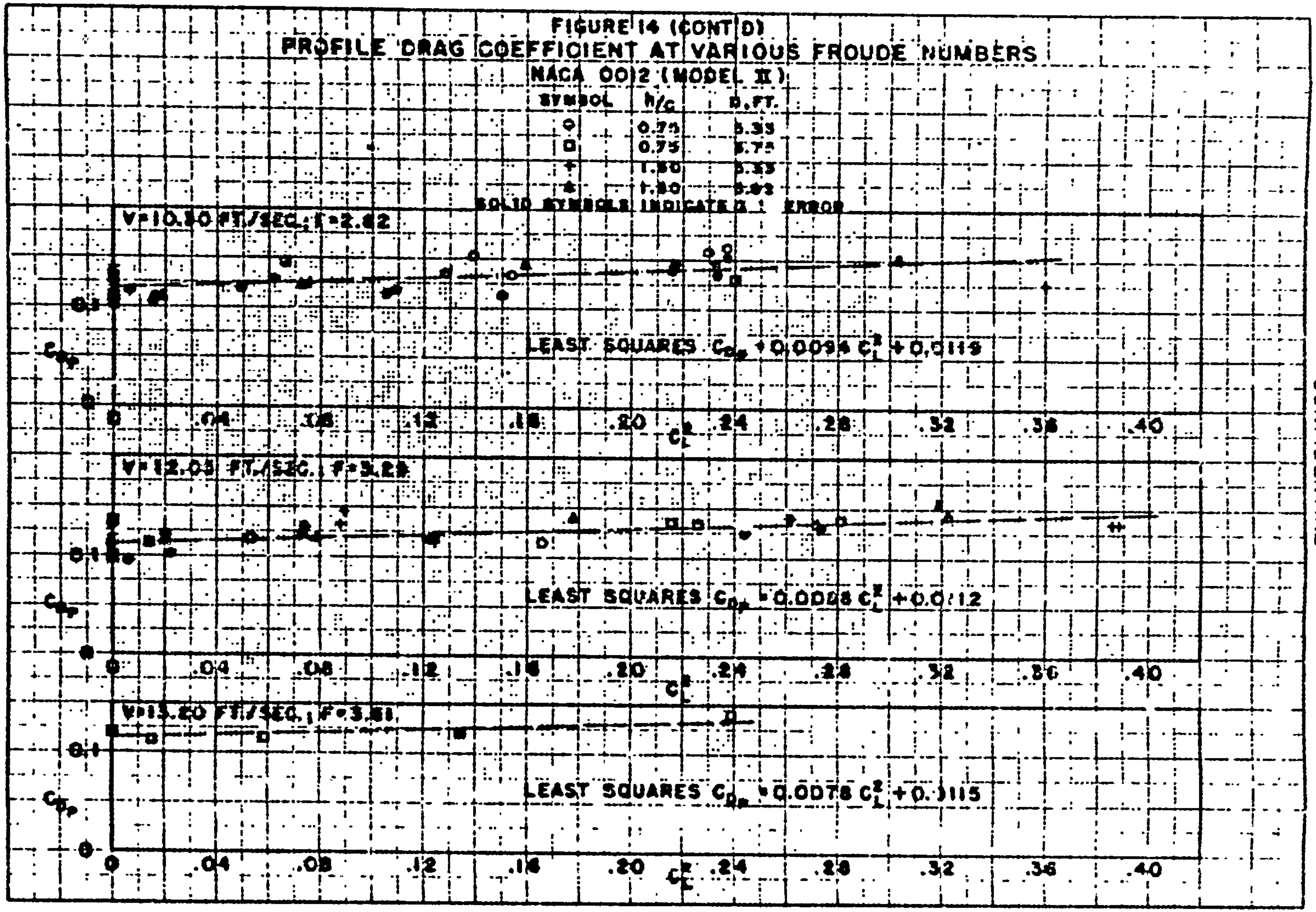

CONFIDENTIAL

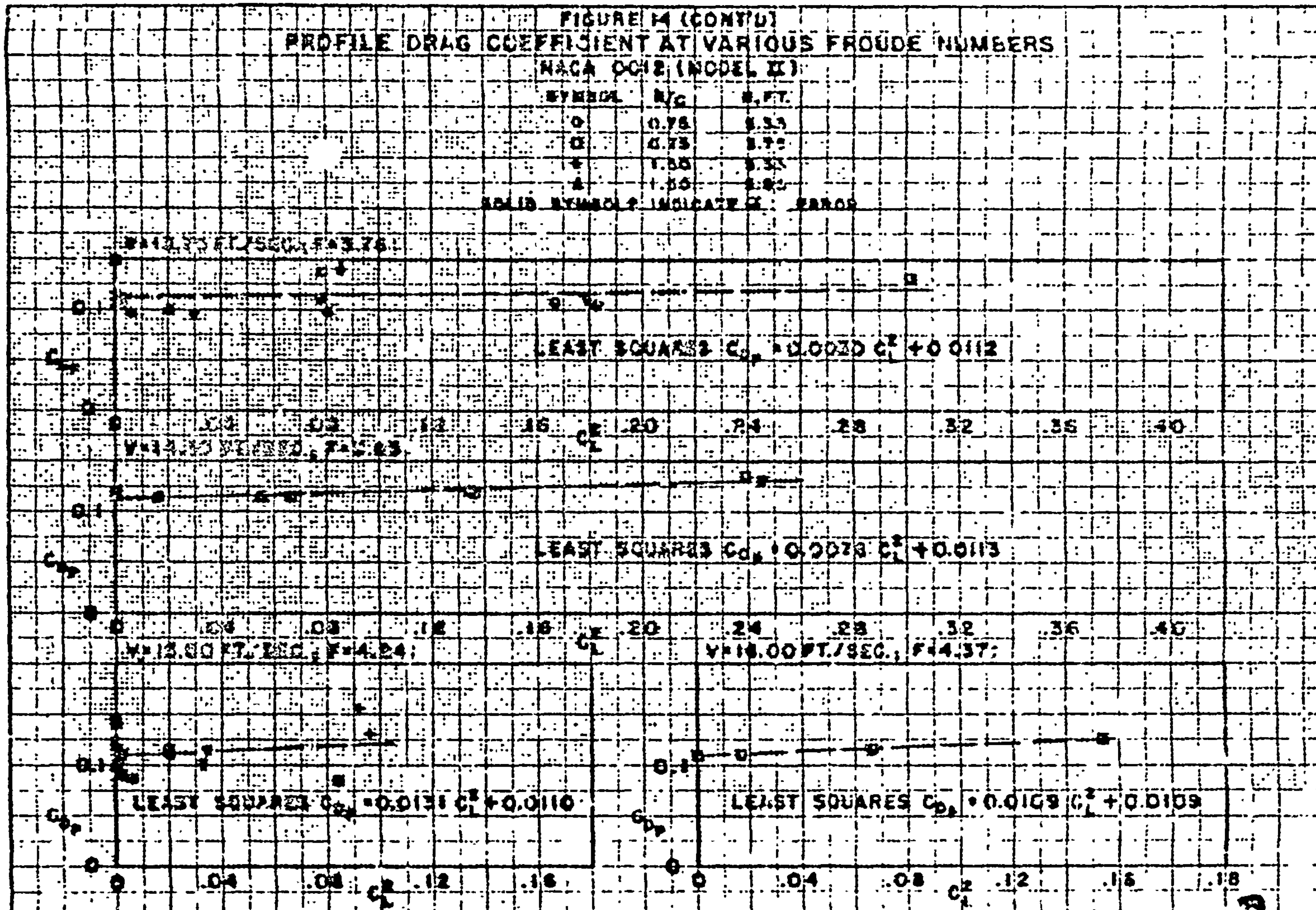

FIGURE 14 (CONT'D)
PROFILE DRAG COEFFICIENT AT VARIOUS FROUDE NUMBERS
NACA 0012 (MODEL II)

FIGURE 15

MINIMUM PROFILE DRAG COEFFICIENT VS. REYNOLDS NUMBER

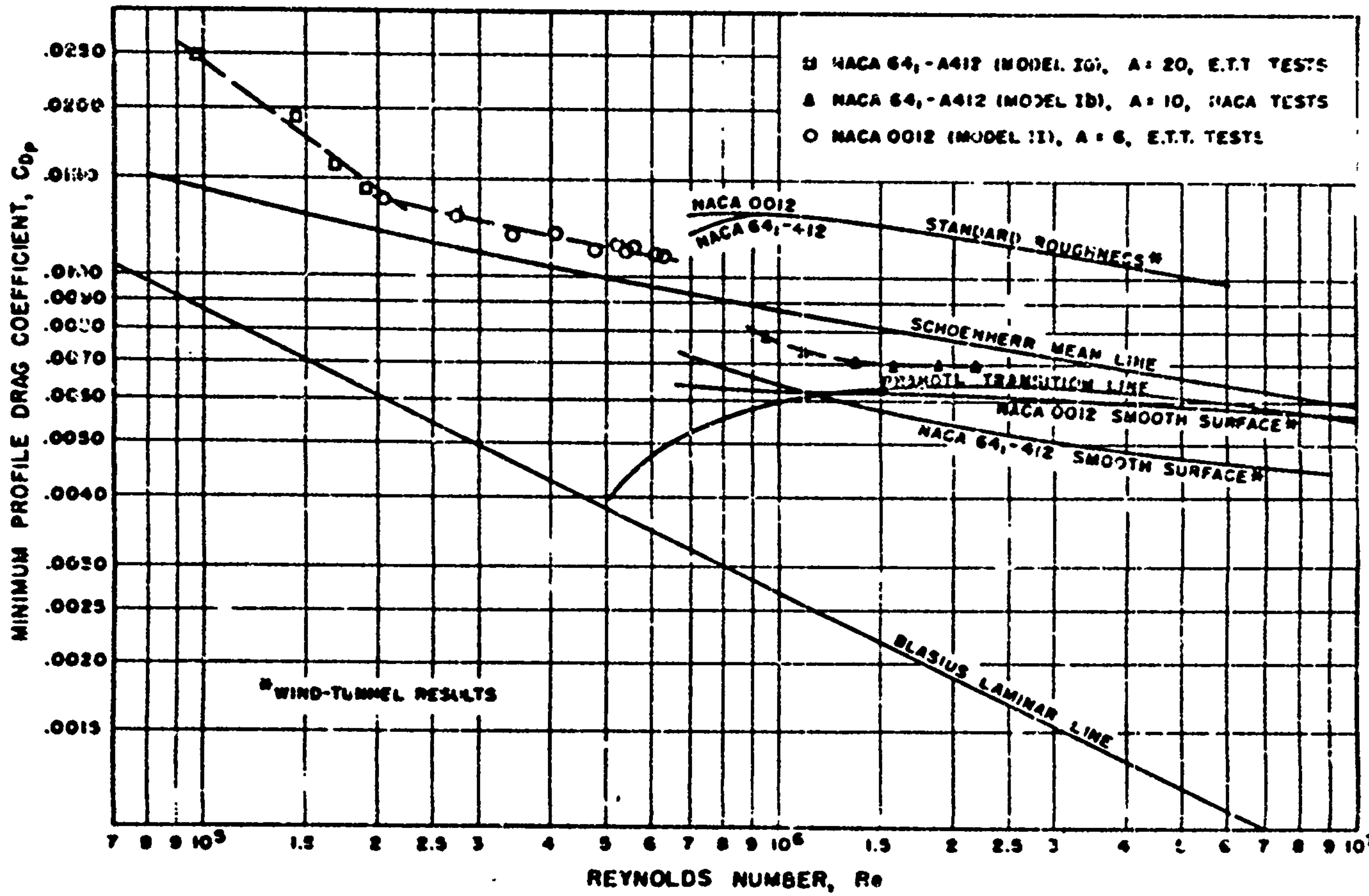

[redacted]

FIGURE 16
LIFT COEFFICIENT VS. ANGLE OF ATTACK
AT VARIOUS FROUDE NUMBERS
NACA 84-A412 (MODEL 1b)

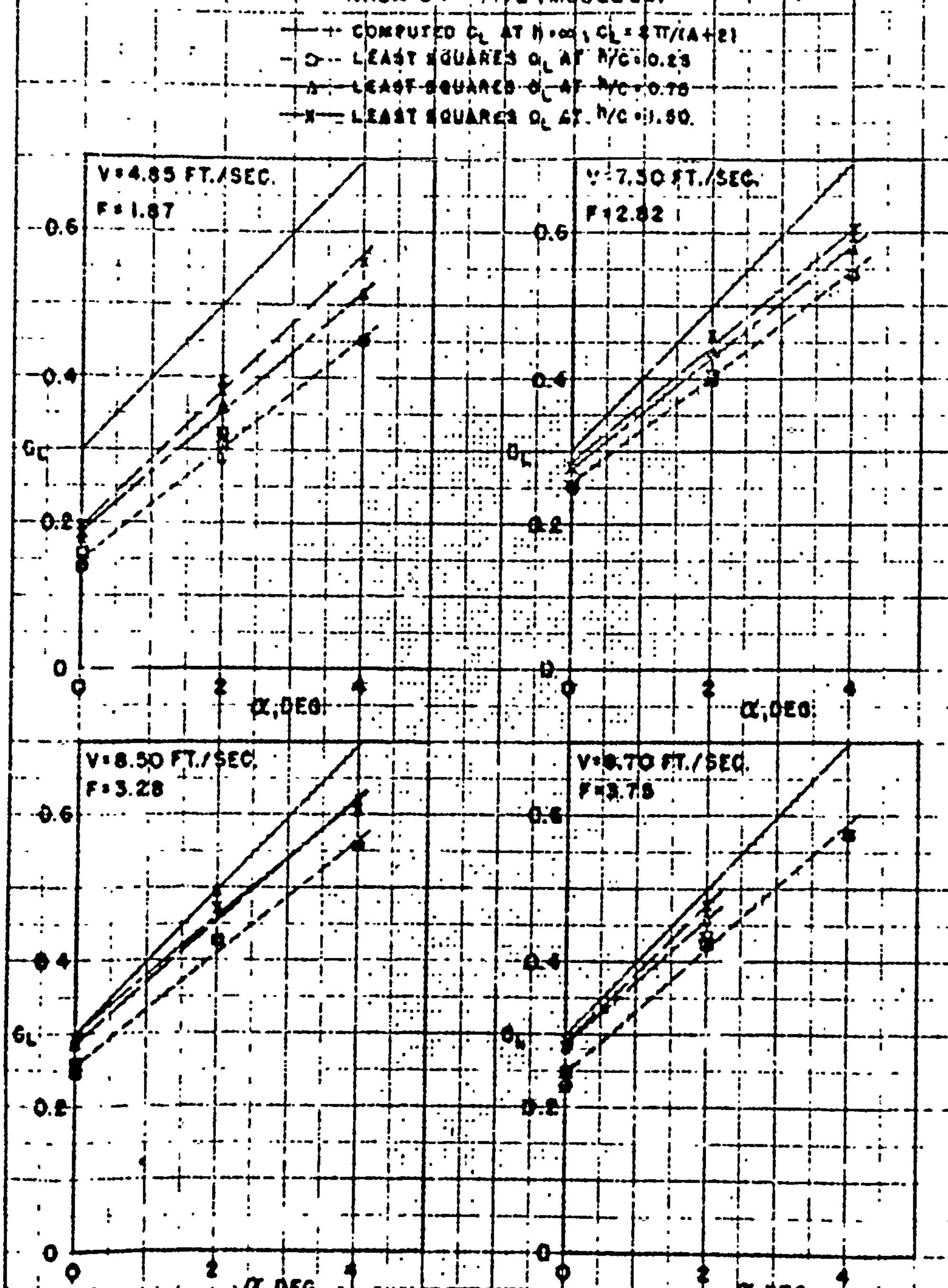

[redacted]

[redacted]

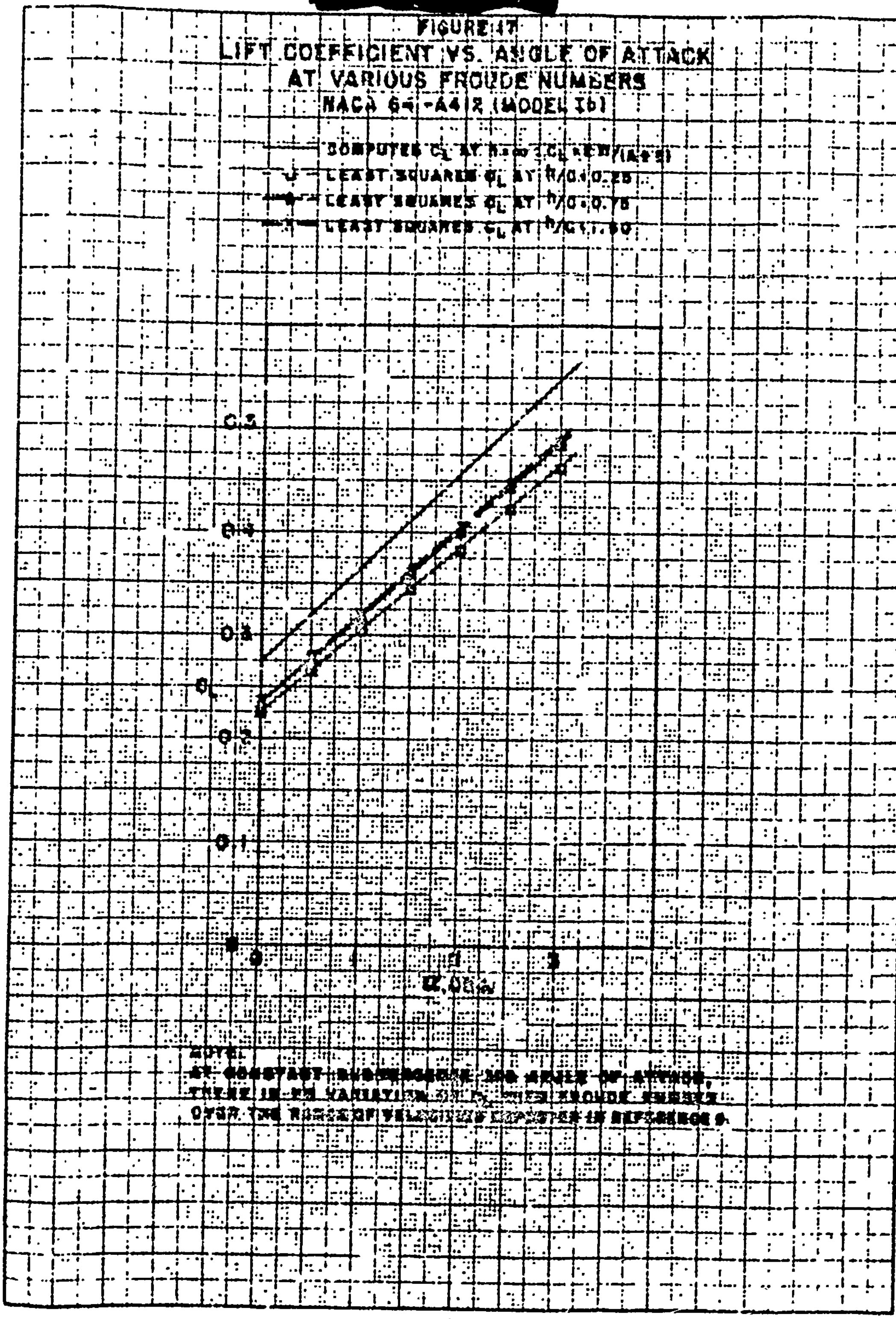

[redacted]

[redacted]

FIGURE 12
LIFT COEFFICIENT VS. ANGLE OF ATTACK
AT VARIOUS FROUDE NUMBERS
NAC 0012 (MODEL II)

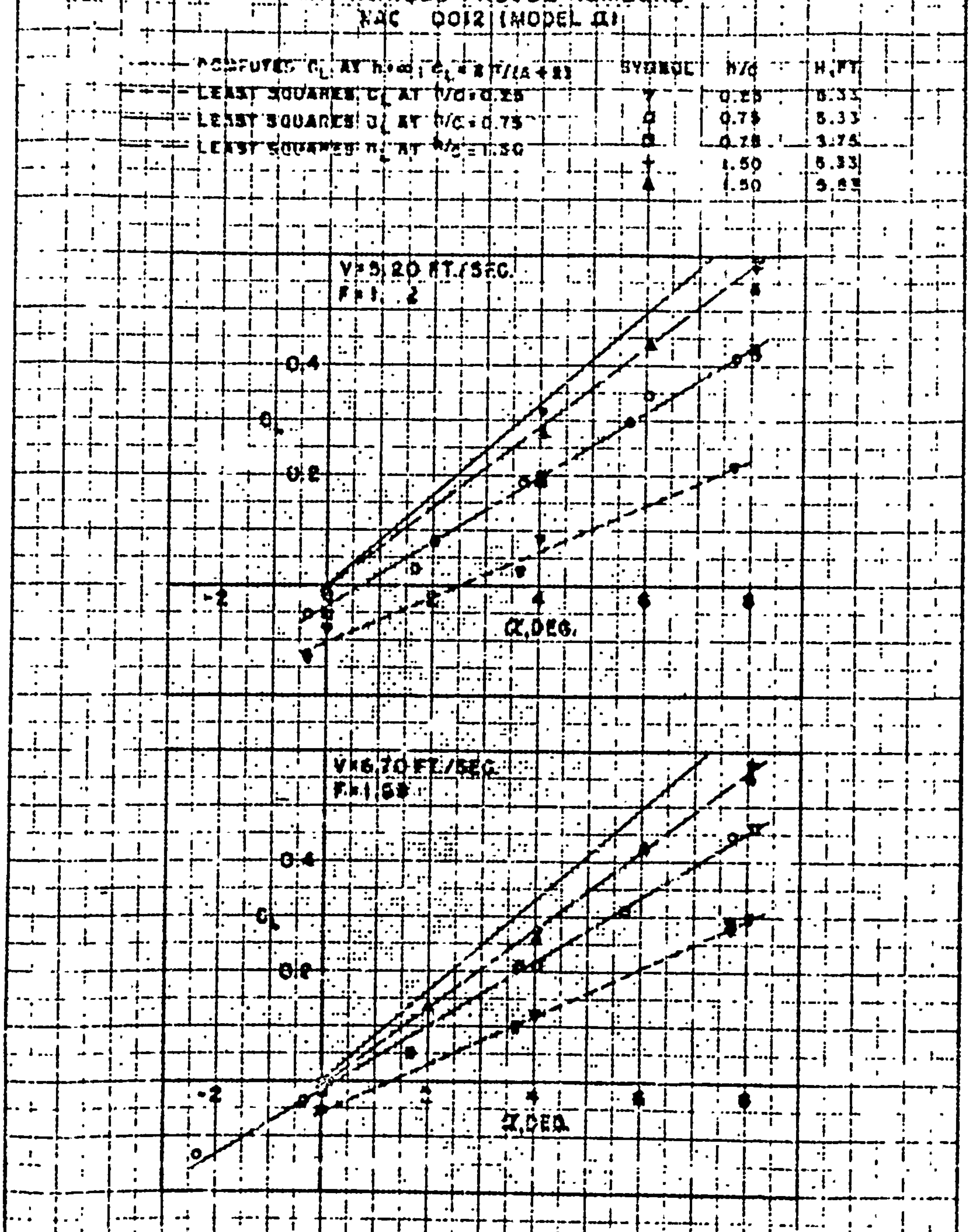

[redacted]

[redacted] SECURITY INFORMATION

FIGURE 18 (CONT'D)
LIFT COEFFICIENT VS. ANGLE OF ATTACK
AT VARIOUS FROUDE NUMBERS
NACA 0012 (MODEL II)

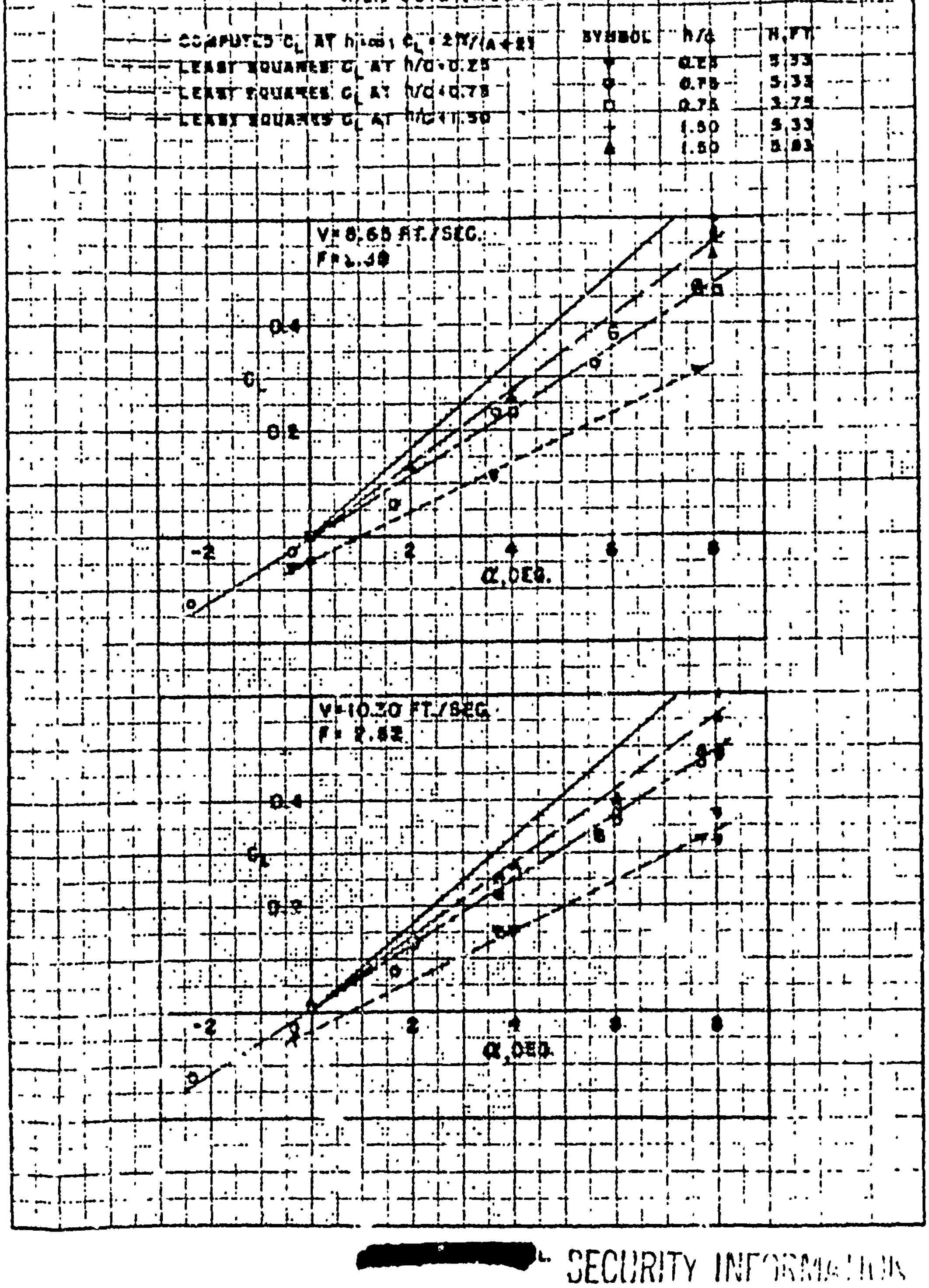

[redacted] SECURITY INFORMATION

FIGURE 18 (CONT'D)
LIFT COEFFICIENT VS. ANGLE OF ATTACK
AT VARIOUS FROUDE NUMBERS
NACA 0012 (MODEL II)